
Theses and Dissertations

Spring 2013

Electric field lines and voltage potentials associated with graphene nanoribbon

Joel Kelly Dale
University of Iowa

Follow this and additional works at: <https://ir.uiowa.edu/etd>



Part of the [Electrical and Computer Engineering Commons](#)

Copyright 2013 Joel Kelly Dale

This thesis is available at Iowa Research Online: <https://ir.uiowa.edu/etd/2471>

Recommended Citation

Dale, Joel Kelly. "Electric field lines and voltage potentials associated with graphene nanoribbon." MS (Master of Science) thesis, University of Iowa, 2013.
<https://doi.org/10.17077/etd.qnuap32p>

Follow this and additional works at: <https://ir.uiowa.edu/etd>



Part of the [Electrical and Computer Engineering Commons](#)

ELECTRIC FIELD LINES AND VOLTAGE POTENTIALS ASSOCIATED
WITH GRAPHENE NANORIBBON

by

Joel Kelly Dale

A thesis submitted in partial fulfillment
of the requirements for the Master of Science degree in Electrical and Computer
Engineering in the Graduate College of
The University of Iowa

May 2013

Thesis Supervisor: Professor David R. Andersen

Copyright by
JOEL KELLY DALE
2013
All Rights Reserved

Graduate College
The University of Iowa
Iowa City, Iowa

CERTIFICATE OF APPROVAL

MASTER'S THESIS

This is to certify that the Master's thesis of

Joel Kelly Dale

has been approved by the Examining Committee
for the thesis requirement for the Master of Science degree in
Electrical and Computer Engineering at the May 2013 graduation.

Thesis Committee: _____

David R. Andersen, Thesis Supervisor

Soura Dasgupta

Hassan Raza

Six years ago, it didn't exist at all, and next year we know that Samsung is planning to release their first mobile-phone screens made of graphene

Dr Novoselov

Nobel Prize in Physics 2010

TABLE OF CONTENTS

LIST OF TABLES	v
LIST OF FIGURES	vi
CHAPTER 1 WHY GRAPHENE?.....	1
CHAPTER 2 THE PROJECT.....	4
CHAPTER 3 THE ALGEBRA AND THE GEOMETRY	8
The Algebra	8
The Geometry	13
CHAPTER 4 COMPUTING THE DATA.....	26
CHAPTER 5 N=8 VISUALIZATIONS	30
Dataset 1	35
CHAPTER 6 N=5 VISUALIZATIONS	48
Dataset 1	52
Dataset 2	65
Dataset 3	72
Dataset 4	80
Dataset 5	88
Dataset 6	97
Dataset 7	104
CHAPTER 7 DIFFERENCES BETWEEN GRAPHENE RIBBONS	113
N=8	114
N=5	121
N=8 vs. N=5	126
CHAPTER 8 SUMMARY	131
APPENDIX A Ψ (PSI) EDITOR IN MATHEMATICA FORMAT	133
APPENDIX B ρ (RHO) EDITOR IN MATHEMATICA FORMAT	135
APPENDIX C THE POISSON SOLVER WITH NOTES ADDED.....	137
APPENDIX D POISSON SOLVER AFTER EXECUTION, WITHOUT NOTES.....	144
APPENDIX E RENDERING CODE	152
APPENDIX F CALCULATED ρ (P) VALUES FROM GIVEN FERMION PROBABILITIES.....	159
acGNR8 ρ Values	159

acGNR5 ρ Values	161
BIBLIOGRAPHY.....	163

LIST OF TABLES

Table 1 - Revised Delta Coefficients – New values for the spacing constants after reducing each one by 3.	15
Table 2 - Total Length Constants – Represented here are the values used to define the problem set.....	20
Table 3 - Delta Coefficients – These are the spacing coefficients used in the computer algorithm to calculate the potentials.....	26
Table 4 – acGNR positions of the ρ values and their associated calculated values for N=8 Dataset 1.....	31
Table 5 – acGNR positions of the ρ values and their associated calculated values for N=8 Dataset 41.....	32
Table 6 – Side by side comparison of the ρ values for N=8 Dataset 1 and N=8 Dataset 41.	33
Table 7 – acGNR positions of the ρ values and their associated calculated values for N=5 Dataset 1.....	48
Table 8 – acGNR positions of the ρ values and their associated calculated values for N=5 Dataset 2.....	49
Table 9 – Side by side comparison of the ρ values for N=5 Dataset 1 and N=5 Dataset 2.	50
Table 10 – acGNR positions of the ρ values and their associated calculated values for N=5 Dataset 2.....	65
Table 11 – acGNR positions of the ρ values and their associated calculated values for N=5 Dataset 3.....	73
Table 12 – acGNR positions of the ρ values and their associated calculated values for N=5 Dataset 4.....	81
Table 13 – acGNR positions of the ρ values and their associated calculated values for N=5 Dataset 5.....	89
Table 14 – acGNR positions of the ρ values and their associated calculated values for N=5 Dataset 6.....	97
Table 15 – acGNR positions of the ρ values and their associated calculated values for N=5 Dataset 7.....	105
Table 16 - Calculated Rho values at position 4 in each respective Dataset of the Brillouin Zone for N=8.....	115
Table 17 – acGNR positions of the ρ values and their associated calculated values for N=5 Dataset 2.....	121

LIST OF FIGURES

Figure 1 - acGNR8 Representation of single line approximation used. The honeycomb structure shows the electrons that were summed together to form the single line.....	12
Figure 2 - Graphene Ribbon with Unique Electron Approximations – This figures illustrates the points across the ribbon where the given electron approximations exist for their respective maximum values	16
Figure 3 - Non-Zero charge densities in graphene nanoribbon. Shown above are the positions in which non-zero values exist for the graphene nanoribbon. The charge density is a maximum in the very middle of the ribbon, and decrease sinusoidally out towards the ends.	18
Figure 4 - acGNR8 with the problem space boxed in around it for initial perspective.	21
Figure 5 – 3D Electric Field Lines for 67x67x67 the array	22
Figure 6 – 3D Electric Field Lines for the 133x133x133 array	23
Figure 7 - Comparison of the 133 array to the 67 array. This picture shows a point by point comparison of the two arrays to see how much the data was changing between the two. A very small difference existed between the two runs. So the 67 array problem space was used as a result.	24
Figure 8 - Comparison between 1×10^{-6} and 1×10^{-7} arrays. This figure shows the amount of change between the resulting potential values when run at 1×10^{-6} and 1×10^{-7} convergence thresholds. The values were only different by .0005 or .05%.....	25
Figure 9 - Plot of the Dataset 1 potentials divided by the Dataset 2 potentials for comparison holding the X axis constant at 50.	34
Figure 10 - Plot of the Dataset 1 potentials divided by the Dataset 2 potentials for comparison holding the Y axis constant at 20.	34
Figure 11 - 3D representation of the potential calculated for Dataset 1.	36
Figure 12 - 3D representation of the field lines calculated from acGNR8 Dataset 1.	37
Figure 13 - 3D representation of the Field Lines and the Potentials associated with acGNR8	38
Figure 14 - 3D representation of 2 full periods of the potentials calculated from Dataset 1	39
Figure 15 - 3D representation of the field lines calculated from the potentials for 2 full periods.	39
Figure 16 - 3D representation of the calculated field lines and potentials from the first dataset.....	40

Figure 17 - 2D representation of the potential of the first dataset, holding the X axis constant at 34.	41
Figure 18 - 2D representation of the field lines of the first dataset, holding the X axis constant at 34.	41
Figure 19 - 2D representation of the field lines and potentials calculated for the scGNR8 Dataset 1.	42
Figure 20 - 2D representation of the potentials calculated along the X and Z axes. This figure also shows the acGNR8 nanoribbon.	43
Figure 21 - 2D representation of the field lines for Dataset 1 holding the Y axis constant. Also shown here is the location of the nanoribbon	43
Figure 22 - 2D representation of the potentials and the field lines for Dataset 1 holding the Y axis constant.	44
Figure 23 - 2D representation of the potentials for Dataset 1 while holding the Z axis constant. The black line running in the Y axis at position 34 is the acGNR8.	45
Figure 24 - 2D representation of the field lines for Dataset 1 while holding the Z axis constant.	46
Figure 25 - 2D representation of the potentials and the field lines for Dataset 1 while holding the Z axis constant at position 34.	47
Figure 26 - Comparison of acGNR5 Dataset 1 potentials divided by Dataset 2 potentials while holding the X axis constant at 50.	51
Figure 27 - Comparison of acGNR5 Dataset 1 potentials divided by Dataset 2 potentials while holding the Y axis constant at 40.	51
Figure 28 - Comparison of acGNR5 Dataset 1 potentials divided by Dataset 2 while holding the Z axis constant at 50.	52
Figure 29 - 3D representation of the potential calculated for Dataset 1.	53
Figure 30 - 3D representation of the field lines calculated from the acGNR5 Dataset 1.	54
Figure 31 - 3D representation of the Field Lines and the Potentials associated with the acGNR5 Dataset 1.	55
Figure 32 - 3D representation of 2 full periods of the potentials calculated from Dataset 1	56
Figure 33 - 3D representation of the field lines calculated from the potentials for 2 full periods.	57
Figure 34 - 3D representation of the calculated field lines and potentials from the first dataset.	58

Figure 35 - 2D representation of the potential of the first dataset, holding the X axis constant at 34.	58
Figure 36 - 2D representation of the field lines of the first dataset, holding the X axis constant at 34.....	59
Figure 37 - 2D representation of the field lines and potentials calculated for the scGNR5 Dataset 1.....	60
Figure 38 - 2D representation of the potentials calculated along the X and Z axes. This figure also shows the acGNR5 nanoribbon.	60
Figure 39 - 2D representation of the field lines for Dataset 1 holding the Y axis constant. Also shown here is the location of the nanoribbon	61
Figure 40 - 2D representation of the potentials and the field lines for Dataset 1 holding the Y axis constant.....	61
Figure 41 - 2D representation of the potentials for Dataset 1 while holding the Z axis constant. The black line running in the Y axis at position 34 is the acGNR5.	62
Figure 42 - 2D representation of the field lines for Dataset 1 while holding the Z axis constant.....	63
Figure 43 - 2D representation of the potentials and the field lines for Dataset 1 while holding the Z axis constant at position 34.	64
Figure 44 - 2D representation of the potential of the 2 dataset, holding the X axis constant at 34.	66
Figure 45 - 2D representation of the field lines of the 2 dataset, holding the X axis constant at 34.	66
Figure 46 - 2D representation of the field lines and potentials calculated for the scGNR5 Dataset 2.....	67
Figure 47 - 2D representation of the potentials calculated along the X and Z axes. This figure also shows the acGNR5 nanoribbon.	68
Figure 48 - 2D representation of the field lines for Dataset 2 holding the Y axis constant. Also shown here is the location of the nanoribbon	68
Figure 49 - 2D representation of the potentials and the field lines for Dataset 2 holding the Y axis constant.....	69
Figure 50 - 2D representation of the potentials for Dataset 2 while holding the Z axis constant. The black line running in the Y axis at position 34 is the acGNR5.	70
Figure 51 - 2D representation of the field lines for Dataset 2 while holding the Z axis constant.....	71

Figure 52 - 2D representation of the potentials and the field lines for Dataset 2 while holding the Z axis constant at position 34.	72
Figure 53 - 2D representation of the potential of the 3rd dataset, holding the X axis constant at 34.	74
Figure 54 - 2D representation of the field lines of the 3rd dataset, holding the X axis constant at 34.....	74
Figure 55 - 2D representation of the field lines and potentials calculated for the scGNR5 Dataset 3.....	75
Figure 56 - 2D representation of the potentials calculated along the X and Z axes. This figure also shows the acGNR5 nanoribbon.	76
Figure 57 - 2D representation of the field lines for Dataset 3 holding the Y axis constant. Also shown here is the location of the nanoribbon	76
Figure 58 - 2D representation of the potentials and the field lines for Dataset 3 holding the Y axis constant.....	77
Figure 59 - 2D representation of the potentials for Dataset 3 while holding the Z axis constant. The black line running in the Y axis at position 34 is the acGNR5.	78
Figure 60 - 2D representation of the field lines for Dataset 3 while holding the Z axis constant.....	79
Figure 61 - 2D representation of the potentials and the field lines for Dataset 3 while holding the Z axis constant at position 34.	80
Figure 62 - 2D representation of the potential of the 4th dataset, holding the X axis constant at 34.	81
Figure 63 - 2D representation of the field lines of the 4th dataset, holding the X axis constant at 34.	82
Figure 64 - 2D representation of the field lines and potentials calculated for the scGNR5 Dataset 4.....	83
Figure 65 - 2D representation of the potentials calculated along the X and Z axes. This figure also shows the acGNR5 nanoribbon.	83
Figure 66 - 2D representation of the field lines for Dataset 4 holding the Y axis constant. Also shown here is the location of the nanoribbon	84
Figure 67 - 2D representation of the potentials and the field lines for Dataset 4 holding the Y axis constant.....	85
Figure 68 - 2D representation of the potentials for Dataset 4 while holding the Z axis constant. The black line running in the Y axis at position 34 is the acGNR5.	86

Figure 69 - 2D representation of the field lines for Dataset 4 while holding the Z axis constant.....	87
Figure 70 - 2D representation of the potentials and the field lines for Dataset 4 while holding the Z axis constant at position 34.	88
Figure 71 - 2D representation of the potential of the 5th dataset, holding the X axis constant at 34.	89
Figure 72 - 2D representation of the field lines of the 5th dataset, holding the X axis constant at 34.	90
Figure 73 - 2D representation of the field lines and potentials calculated for the scGNR5 Dataset 5.....	91
Figure 74 - 2D representation of the potentials calculated along the X and Z axes. This figure also shows the acGNR5 nanoribbon.	91
Figure 75 - 2D representation of the field lines for Dataset 5 holding the Y axis constant. Also shown here is the location of the nanoribbon	92
Figure 76 - 2D representation of the potentials and the field lines for Dataset 5 holding the Y axis constant.....	93
Figure 77 - 2D representation of the potentials for Dataset 5 while holding the Z axis constant. The black line running in the Y axis at position 34 is the acGNR5.	94
Figure 78 - 2D representation of the field lines for Dataset 5 while holding the Z axis constant.....	95
Figure 79 - 2D representation of the potentials and the field lines for Dataset 5 while holding the Z axis constant at position 34.	96
Figure 80 - 2D representation of the potential of the 6th dataset, holding the X axis constant at 34.	98
Figure 81 - 2D representation of the field lines of the 6th dataset, holding the X axis constant at 34.	98
Figure 82 - 2D representation of the field lines and potentials calculated for the scGNR5 Dataset 6.....	99
Figure 83 - 2D representation of the potentials calculated along the X and Z axes. This figure also shows the acGNR5 nanoribbon.	100
Figure 84 - 2D representation of the field lines for Dataset 6 holding the Y axis constant. Also shown here is the location of the nanoribbon	100
Figure 85 - 2D representation of the potentials and the field lines for Dataset 6 holding the Y axis constant.....	101

Figure 86 - 2D representation of the potentials for Dataset 6 while holding the Z axis constant. The black line running in the Y axis at position 34 is the acGNR5.	102
Figure 87 - 2D representation of the field lines for Dataset 6 while holding the Z axis constant.....	103
Figure 88 - 2D representation of the potentials and the field lines for Dataset 6 while holding the Z axis constant at position 34.	104
Figure 89 - 2D representation of the potential of the 7th dataset, holding the X axis constant at 34.	106
Figure 90 - 2D representation of the field lines of the 7th dataset, holding the X axis constant at 34.	106
Figure 91 - 2D representation of the field lines and potentials calculated for the scGNR5 Dataset 7.....	107
Figure 92 - 2D representation of the potentials calculated along the X and Z axes. This figure also shows the acGNR5 nanoribbon.	108
Figure 93 - 2D representation of the field lines for Dataset 7 holding the Y axis constant. Also shown here is the location of the nanoribbon	108
Figure 94 - 2D representation of the potentials and the field lines for Dataset 7 holding the Y axis constant.....	109
Figure 95 - 2D representation of the potentials for Dataset 7 while holding the Z axis constant. The black line running in the Y axis at position 34 is the acGNR5.	110
Figure 96 - 2D representation of the field lines for Dataset 7 while holding the Z axis constant.....	111
Figure 97 - 2D representation of the potentials and the field lines for Dataset 7 while holding the Z axis constant at position 34.	112
Figure 98 - Plot of acGNR8 Dataset 1 divided by acGNR8 Dataset 41, holding the Y axis constant at 20.....	116
Figure 99 – Plot of potentials for the entire set of N=8 Dataset 1 for Y & Z.....	117
Figure 100 - Voltage potentials and electric field lines associated with Dataset 1 holding	118
Figure 101 - Voltage potentials and electric Field Lines associated with Dataset 41 holding	118
Figure 102 - Voltage potentials and electric Field Lines associated with Dataset 1 holding	119
Figure 103 - Voltage potentials and electric field lines associated with Dataset 41 holding	119

Figure 104 - Voltage Potentials and Field Lines in 3D wrt Dataset 1.	120
Figure 105 - Voltage Potentials and Field Lines in 3D wrt Dataset 41.	120
Figure 106 – Plot of potentials for the entire set of N=5 Dataset 1 for Y & Z.	122
Figure 107 - Voltage potentials and electric Field Lines associated with Dataset 1 holding	123
Figure 108 - Voltage potentials and electric Field Lines associated with Dataset 2 holding	123
Figure 109 - Voltage potentials and electric Field Lines associated with Dataset 3 holding	124
Figure 110 - Voltage potentials and electric Field Lines associated with Dataset 4 holding	124
Figure 111 - Voltage Potentials and Field Lines in 3D wrt Dataset 3.	125
Figure 112 - Voltage Potentials and Field Lines in 3D wrt Dataset 4.	125
Figure 113 - Voltage Potentials and Field Lines in 3D wrt Dataset 1 from N=8.	126
Figure 114 - Voltage Potentials and Field Lines in 3D wrt Dataset 4 from N=5.	127
Figure 115 - 2D Y-Z plane slice showing the potential and field lines for acGNR8	127
Figure 116 - 2D Y-Z plane slice showing the potential and field lines for acGNR5	128
Figure 117 - 2D X-Z plane slice showing the potential and field lines for acGNR8.	128
Figure 118 - 2D X-Z plane slice showing the potential and field lines for acGNR5.	129
Figure 119 - 2D plot of N=5 by N=8. This plot shows that rate of change in the voltage potentials between the two acGNR datasets.	130

CHAPTER 1

WHY GRAPHENE?

Graphene can be used to create circuits that could potentially speed electronic components by as much as 100 times [1]. Such blazing speed might also help produce ever-tinier computing devices with more power than your clunky laptop [2]. Graphite is a polymorph of the element carbon [3]. Graphite is made up of tiny sheets of graphene. Graphene sheets stack to form graphite with an interplanar spacing of 0.335 nm, which means that a stack of 3 million sheets would be only one millimeter thick. [1] In 2004, two Russian-born scientists at the University of Manchester used the scotch tape method to create monolayer graphene devices [2]. This nano scale 2 dimensional sheet is graphene. Novoselov and Geim's discovery is now the stuff of scientific legend, with the two men being awarded the Nobel Prize in 2010 [4]. Graphene has exploded on the scene over the past couple of years. "Six years ago, it didn't exist at all, and next year we know that Samsung is planning to release their first mobile-phone screens made of graphene." – Dr Kostya Novoselov [4]. Graphene forms a hexagonal lattice, each vertex tipped with a carbon atom. At the molecular level, it looks like chicken wire [4]. There are two common lattice formations of graphene nanoribbons, armchair and zigzag. These nanoribbons have drastically different electronic properties. Zigzag edges can sustain edge surface states and resonances that are not present in the armchair case Rycerz et al., 2007 [5]. In this work we focused on the armchair graphene nanoribbon formation (acGNR).

Graphene has several notable properties that make it worthy of research. The first of which is its remarkable strength. Graphene has a record breaking strength of 200

times greater than steel, with a tensile strength of 130GPa [1]. Graphene has a Young's modulus of 1000, compared to just that of 150 for silicon [1]. To put it into perspective, if you had a sheet of graphene as thick as a piece of cellophane, it would support the weight of a car. [2] If paper were as stiff as graphene, you could hold a 100-yard-long sheet of it at one end without its breaking or bending. [2]

Another one of graphene's attractive properties is its electronic band gap, or rather, its lack thereof. Graphene is a Zero Gap Semiconductor. So it has high electron mobility at room temperature. Electron transfer is 100 times faster than Silicon [1]. With zero band gap, in the massless Dirac fermion structure, the graphene ribbon is theoretically lossless, making it a perfect semiconductor. Even in the massive Dirac fermion case, the band gap is on the order of 50 meV [6].

This research began, as discussed in Chapter 2, with an armchair graphene nanoribbon unit cell of $N=8$. There were 16 electron probabilities (ψ) provided per unit cell that spanned varying Fermi energy levels. The carbon atoms are separated by 1.42\AA . The unit vector is given as, $a = dx$, where $d = 3\alpha_{cc}$ and $\alpha_{cc} = 1.42\text{\AA}$ is the carbon bond length [5]. Because of the close proximity of the carbon atoms, relative to the plasmon wavelength, the charge density per unit cell can be approximated by a single line allowing us to reduce the charge in 16 atoms down to 8. Poisson's equation, discussed in Chapter 3, was expanded into the 3 dimensional space, allowing us to calculate the potential (ϕ).

Once ϕ was obtained, expanding the electric field gradient equation to support 3 dimensions allowed us to calculate the electric field lines associated with those voltage potentials. This was accomplished using computer algorithms, covered in Chapter 4.

The field lines and potentials were then rendered in both 2 dimensions and 3 dimensions for observation and those graphics are covered in Chapters 5 and 6. Although graphene unit cells of $N=8$ and $N=5$ were used in this research, the algorithms and rendering programs created could easily be adapted to accommodate any size graphene nanoribbon.

CHAPTER 2

THE PROJECT

The end state goal of this project was to produce graphical 2 dimensional and 3 dimensional renderings of the electric field lines and voltage potentials associated with plasmons in graphene nanoribbon. Electron probabilities were provided for two different graphene unit cell structures: $N=8$ and $N=5$. The particular unit cell graphene geometric shape, specific to this research is what is known as the arm-chair graphene nanoribbon (acGNR) representation. Another common graphene structure is the zigzag structure. Our research was specific to the armchair structure, but the zigzag structure is worth mentioning.

The unit cell of the acGNR of atomic width N (acGNRN) contains $2N$ atoms arranged in a honeycomb structure. [5] The unit vector is given as, $a = dx$, where $d = 3\alpha_{cc}$ and $\alpha_{cc} = 1.42\text{\AA}$ is the carbon bond length. This geometry will be revisited later in Chapter 3. The pzTB Hamiltonian of this structure is a $2N \times 2N$ matrix containing only nearest-neighbor couplings. [5] The algorithms and calculations derived as the basis of this research, were done so, working with the $N=8$ armchair nanoribbon structure. However, it should be noted that it is quite straightforward to adjust the algorithms to handle any value of N desired, which was the case for the $N=5$ dataset.

The goal of this research is to produce an electric field profile computer simulation that models the acGNR nanoribbon. Note that electric field is defined as:

The distribution in space of the strength and direction of forces that would be exerted on an electric charge at any point in that space. Electric fields themselves result directly from other electric charges or from changing magnetic fields. The

strength of an electric field at a given point in space near an electrically charged object is proportional to the amount of charge on the object, and inversely proportional to the distance between the point and the object. [8]

As mentioned in the chapter opening, this research began with the probability of the electron, given as an approximation as to where the electron would exist with respect to the sixteen locations lying along the honeycomb $N=8$ structure. The electron approximations will be denoted as ψ (ψ). Taking the sum of the sixteen charge densities $\psi^*\psi$, associated with the nanoribbon, as they lie across the ribbon, results in an expected value of 1. The probability of 1 is expected because only 1 electron may be present in each unit cell. In order to use the electron approximations for computation, the values had to be converted into charge densities. For this paper, the charge densities are denoted as ρ (ρ). Note that, charge density is defined as: The electric charge per unit area or per unit volume of a body or of a region of space. [8] Approximately 35,000 sets of electron approximations were provided, along with their associated propagation (k) vector. Note that, $k = 2\pi / \lambda =$ (scalar) the electron wavenumber along travel direction. [11]. These electron probabilities were provided as complex numbers.

Example: $-0.21425903278600417 - 0.0012253341035276457 * I$.

In preparation for calculating the field and potential, the magnitudes of the charge density had to be obtained. This was accomplished by multiplying the approximation ψ by its complex conjugate. This will be denoted as $(\psi^*\psi)$, where ψ^* represents the complex conjugate.

From the above example given of the complex wave function, multiplying $\psi^*\psi$ yields: 0.045908435. This can be thought of as the probability that the electron would

exist in this location along the nanoribbon. The un-normalized units for charge density (ρ) are given by $\frac{C}{m^3}$. [13]

Once ρ was obtained, the values could be used to calculate the voltage potential. Note that voltage potential is denoted as ϕ (φ) using an expanded version of Poisson's Equation.

$$\nabla^2 \phi = -\frac{\rho}{\epsilon_0} \quad [14]$$

Note that epsilon (ϵ_0) is the permittivity constant of free space. Poisson's Equation can easily be expanded to support all 3-dimensions, which is needed to accommodate the Graphene acGNR environment. This was accomplished using the central difference method explained in Chapter 3. The graphene nanoribbon is 2-dimensional, however, the electric field profile, as a result, is 3-dimensional, therefore requiring Poisson's equation to be expanded to 3-dimensions. As the voltage potentials are calculated, the entire dataset had to be evaluated for convergence by comparing the current calculated values to the last set of calculated values. This is necessary to confirm that the voltage potential calculations have finished contributing to their nearest neighbors, as mentioned previous. This convergence test is nested within the voltage potential iterative loop. For this research, the convergence test threshold ended up being set to 0.000001 or 10^{-7} resolution. The calculation will be explained in detail in Chapter 3.

Once the values had stabilized to the point of passing the convergence threshold, the voltage potential is captured and becomes the basis for computing the electric field. The electric field profile is determined using the following equation:

$$E = -\nabla\phi [15].$$

The un-normalized electric field is measured in units of V/m [13]. Like the Poisson equation referenced previous, the electric field equation must be expanded to 3-dimensional space in order to support the voltage potential dataset. Like Poisson's equation, this is easily done using the gradient method. The electric field is the derivative of the voltage potential with respect to a particular axis. Expanding the above equation to account for each individual axis in 3-dimensional space; yields the following:

$$E(x, y, z) = -\mathbf{i} \frac{\partial V(x,y,z)}{\partial x} - \mathbf{j} \frac{\partial V(x,y,z)}{\partial y} - \mathbf{k} \frac{\partial V(x,y,z)}{\partial z} [15]$$

Where \mathbf{i} , \mathbf{j} , and \mathbf{k} are unit vectors in the x, y, and z direction. The above equation will be expanded in detail in Chapter 3.

Once the electric field profile was computed, both the field lines and voltage potentials could be represented graphically. It should be noted that Wolfram Mathematica 7 [16] was the computer application used to both compute and render the data detailed in this paper. Chapter 3 explains the algebra and the geometry behind the research.

CHAPTER 3
THE ALGEBRA AND THE GEOMETRY

The Algebra

The crux of the problem was to determine field and potential from the probabilities. For this we use Poisson's Equation and the central difference method [14]. An explanation of the Central-Difference Formula follows.

Due to the geometrical make-up of the graphene, and the physical properties of the charge densities, it is understood that each computation point in the nanoribbon couples to its nearest neighbor in terms of the voltage potential. Likewise, that computation point also provides an electrical contribution to its nearest neighbor, and so forth and so on, until the entire set is in equilibrium.

Here is how Poisson's Equation was used to convert the electron densities into voltage potentials. Starting with Poisson's equation itself:

$$\nabla^2 \varphi = -\frac{\rho}{\epsilon_0}$$

The left hand side (lhs) of the equation was expanded to accommodate dimensions: x, y, and z.

$$\frac{\partial^2 \varphi}{\partial x^2} + \frac{\partial^2 \varphi}{\partial y^2} + \frac{\partial^2 \varphi}{\partial z^2}$$

Continuing with the lhs and taking the discrete derivative of $\frac{\partial^2 \varphi}{\partial x^2}$ looks like:

$$\frac{\partial \varphi}{\partial x} = \frac{\Delta \varphi}{\Delta x} = \frac{\varphi_{x1} - \varphi_{x-1}}{\Delta x}$$

The same step needs to be performed on the Y and Z components. In order to use with Poisson's equation, the second derivative is required, and performing that on X looks like:

$$\frac{\partial^2 \varphi}{\partial x^2} = \frac{\left(\frac{\varphi_{x1} - \varphi_{x0}}{\Delta x} - \frac{\varphi_{x0} - \varphi_{x-1}}{\Delta x}\right)}{\Delta x}$$

Again, the same must done for the Y and Z components. Reducing the lhs for X:

$$\frac{\partial^2 \varphi}{\partial x^2} = \frac{\varphi_{x1} - 2\varphi_{x0} + \varphi_{x-1}}{\Delta x^2}$$

Applying this to the entire lhs produces:

$$\frac{\varphi_{x1} - 2\varphi_{x0} + \varphi_{x-1}}{\Delta x^2} + \frac{\varphi_{y1} - 2\varphi_{y0} + \varphi_{y-1}}{\Delta y^2} + \frac{\varphi_{z1} - 2\varphi_{z0} + \varphi_{z-1}}{\Delta z^2}$$

The definition of ρ in Poisson's Equation and defined in Chapter 2, is: $\psi * \psi$

The right hand side (rhs) may be re-written as:

$$-\frac{\psi * \psi}{\epsilon_0}$$

Setting both sides equal to each other results in:

$$\frac{\varphi_{x1} - 2\varphi_{x0} + \varphi_{x-1}}{\Delta x^2} + \frac{\varphi_{y1} - 2\varphi_{y0} + \varphi_{y-1}}{\Delta y^2} + \frac{\varphi_{z1} - 2\varphi_{z0} + \varphi_{z-1}}{\Delta z^2} = -\frac{\psi * \psi}{\epsilon_0}$$

Solving for $\varphi_{(0)}$ in each dimension gives the final equation that forms the basis behind the solver algorithm.

$$\varphi_{(0)x,y,z} = \frac{\Delta x^2 + \Delta y^2 + \Delta z^2}{2} \times \left[\frac{\varphi_{x1} + \varphi_{x-1}}{\Delta x^2} + \frac{\varphi_{y1} + \varphi_{y-1}}{\Delta y^2} + \frac{\varphi_{z1} + \varphi_{z-1}}{\Delta z^2} + \frac{\psi * \psi}{\epsilon_0} \right]$$

Epsilon (ϵ_0) is the permittivity constant of free space:

$$\epsilon_0 = 8.85418782 \times 10^{-12} \frac{s^4 A^2}{m^3 kg}$$

The differential form of Gauss's law will prove useful for the electric field lines and is defined in

Poisson's Equation derived from Gauss's Law using general vector notation.

Note that \mathbf{E} represents vector notation.

$$\nabla \cdot \mathbf{E} = \frac{\rho}{\epsilon_0} \quad (a)$$

This is Gauss's Law in a differential form. Here we have applied a short-hand notation that is common for the vector derivatives by using a vector operator ∇ called the del operator, which in Cartesian coordinates is

$$\nabla \equiv \frac{\partial}{\partial x} i + \frac{\partial}{\partial y} j + \frac{\partial}{\partial z} k$$

The static electric field is a conservative field, which we have expressed as

$$\nabla \times \mathbf{E} = 0$$

This means that the electric field could be represented as the gradient of a scalar electric potential V

$$\mathbf{E} = -\nabla V \quad (b)$$

Recall the vector identity

$$\nabla \times \nabla V = 0$$

Combine (a) with (b) and obtain

$$\nabla^2 V = -\frac{\rho}{\epsilon_0}$$

That we have computed the potential from the charge densities, we use this result to calculate the electric field lines. Reference the equation (b) noted above in Poisson's Equation derivation:

$$\mathbf{E} = -\nabla V$$

As was done with Poisson's Equation, the electric field equation must be expanded to accommodate all three dimensions. Expanding the rhs for the discrete derivative and replacing V with ϕ results in:

$$E_{x,y,z} = -\frac{(\phi_{x2} - \phi_{x1})}{\Delta x} - \frac{(\phi_{y2} - \phi_{y1})}{\Delta y} - \frac{(\phi_{z2} - \phi_{z1})}{\Delta z}$$

Now the 2 major parts of the problem, the voltage potentials and the field lines, have been expanded for discrete use in all 3 dimensions.

All that's missing now is ρ and all parts required for the calculations will have been obtained. ρ was obtained by solving the Schrodinger equation for the nanoribbon. As mentioned in Chapter 2, these probabilities sum to 1 across the nanoribbon unit cell and that fact was used as an accuracy check against the computed ρ values. The wave functions are denoted as ψ . An editor was created in Mathematica to convert the wave functions ψ into the charge densities ρ for insertion into Poisson's equation. Details on that editor can be found in Appendix A.

Note that $\rho = \psi^* \psi$ where ψ^* is the complex conjugate of ψ . Starting with the 16 electron probabilities; and multiplying them by their complex conjugate, then summing horizontally across the unit cell using single line approximation, results in ρ on a set of 8 points.

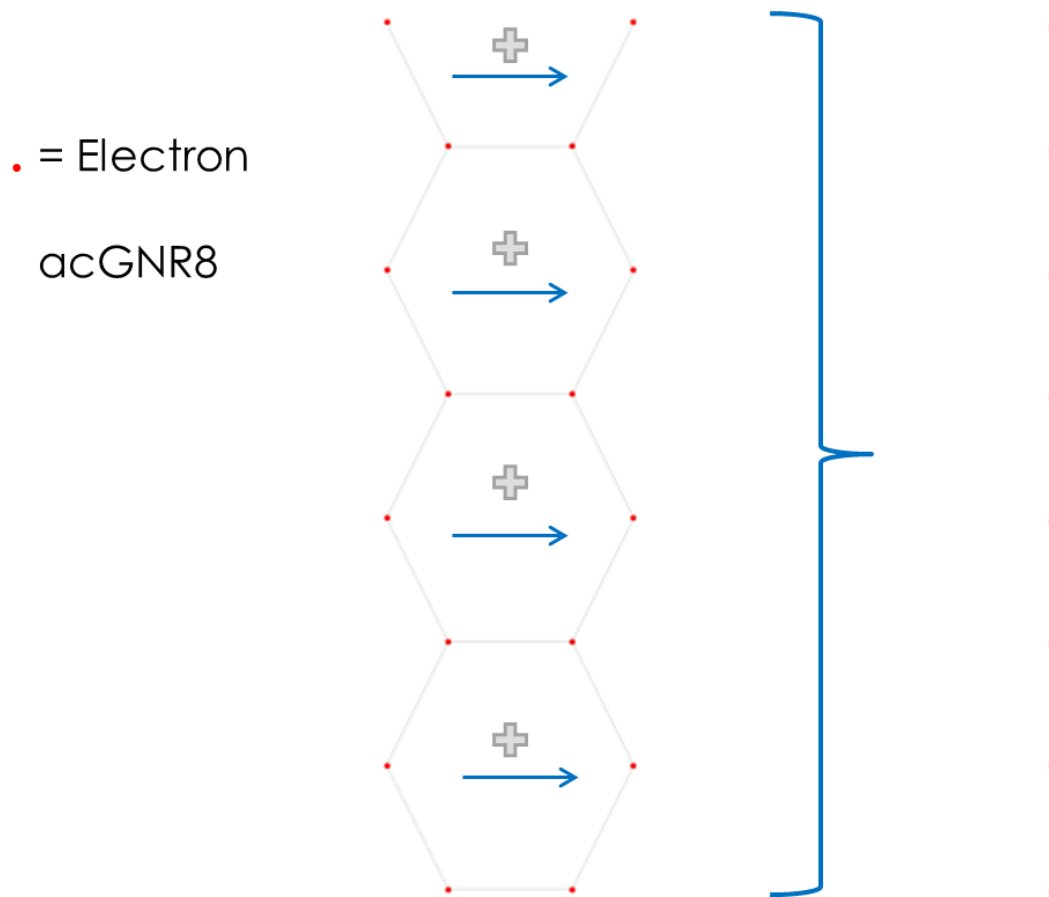


Figure 1 - acGNR8 Representation of single line approximation used. The honeycomb structure shows the electrons that were summed together to form the single line.

The figure above illustrates the electron summing order followed for single line approximation. The red dots on the left represent the p_z orbital electrons. The single line end result is shown on the right. This method was acceptable due to the fact that the plasmon wavelength is infinitely long with respect to the graphene unit cell. Now that all of the components of Poisson's Equation are collected, the data is ready for computation.

More on the calculations will be explained in Chapter 4

The Geometry

As with any technical multidimensional computation, In order to ensure accurate calculations, one must fully understand the geometric make-up of the environment itself. As introduced in the opening; the 2-dimensional graphene nanoribbon exists in a hexagonal shape, referred to as a honeycomb structure.

“Geometry of the Unit Cell: The unit cell of the acGNR of atomic width N (acGNRN) contains $2N$ atoms arranged in a honeycomb structure. The unit vector is given as, $a = dx$, where $d = 3\alpha_{cc}$ and $\alpha_{cc} = 1.42\text{\AA}$ is the carbon bond length. The pzTB Hamiltonian of this structure is a $2N \times 2N$ matrix containing only nearest-neighbor couplings.” [5] The renderings produced from this research were done for the $N=8$ and $N=5$ armchair graphene nanoribbon. Based on the way the algorithms were designed, it is straightforward to extend the calculations for any value of N .

The initial problem set environment was established as a starting point, by representing the graphene ribbon bound inside a transparent 3-dimensional box. The size of the box was adjusted accordingly to allow the field lines to fully develop. The actual electric field profile itself would determine the appropriate problem set parameters. We now consider an armchair nanoribbon with armchair edges along the y direction. The boundary conditions at the edges of the ribbon located at $x=0$ and $x=67$, $\varphi=0$ [19]. Using the voltage potential boundary conditions of $\varphi=0$ at the ends of the nanoribbon, along with the initial threshold convergence setting of 1×10^{-6} . The geometry of the problem set was expanded as needed based on the fringing profile of the electric field lines themselves. Ultimately we determined that a suitable geometry for the problem was an array of points with the nanoribbon embedded in the center.

The convergence test was introduced into the algorithm as a way to ensure that the computations were not exiting prematurely. After one loop of the algorithm, the results were compared to the previous iteration. Every element in the 67x67x67 array was compared to itself in the previous iteration. If that data was different by more than 1×10^{-6} then the algorithm was invoked again. This meant that the nearest neighbor contributions were still taking place at a significant rate. Stopping the computations early would negatively impact the potentials and the field lines. The convergence test looked like the following:

- V_{new} is the newest set of voltage potentials calculated in the Poisson solver.
- V_{old} is the previous set of voltage potentials calculated in the Poisson solver. This will be explained in more detail in Chapter 4.

$$\frac{V_{new} - V_{old}}{V_{old}} > \text{Convergence Threshold}$$

Again the Convergence Threshold was originally set to 1×10^{-6} . This means that the change in each point in the 300,763 element dataset, from one iteration to another, must be less than 0.000001 in order to pass the test.

The resultant electric field rendering, would be compared visually to another electric field rendering made from a larger 133x133x133 array using the same set of ρ data approximations, to confirm that the field lines are essentially identical. It is important, due to the boundary conditions to ensure that the electric field profile is not being artificially clipped by constraining the area of the problem set. The geometry behind the problem set is not arbitrary, but it does not drive the computations. In our

work, the electric profile is visually compared for various problem space geometries and the smallest suitable resolution was chosen. The initial constants behind the 3-dimensional environment were derived as follows:

Δx	$= ((\sqrt{3}/2)/3) * \alpha_{cc}$	0.409918691 Å
Δy	$= (3/3)$	1 Å
Δz	$= (3/3) * \alpha_{cc}$	1.42 Å

Table 1 - Revised Delta Coefficients – New values for the spacing constants after reducing each one by 3.

The orientation of the problem space is represented below. The calculated ρ values are placed along the nanoribbon in the z-direction. The ρ values were scaled using the multiplier $\sin[\frac{\pi}{2} * \frac{z}{34}]$, representing one-half wavelength of a plasmon and distributed along the ribbon in the z direction to fill in the points. Chapter 4 will explain this more in detail. Like the ψ editor, a ρ editor was created in Mathematica to aid in creating the scaled list of the nanoribbon. See Appendix B for details pertaining to the ρ editor. Below is representation of the non-zero charge density values within the nanoribbon.

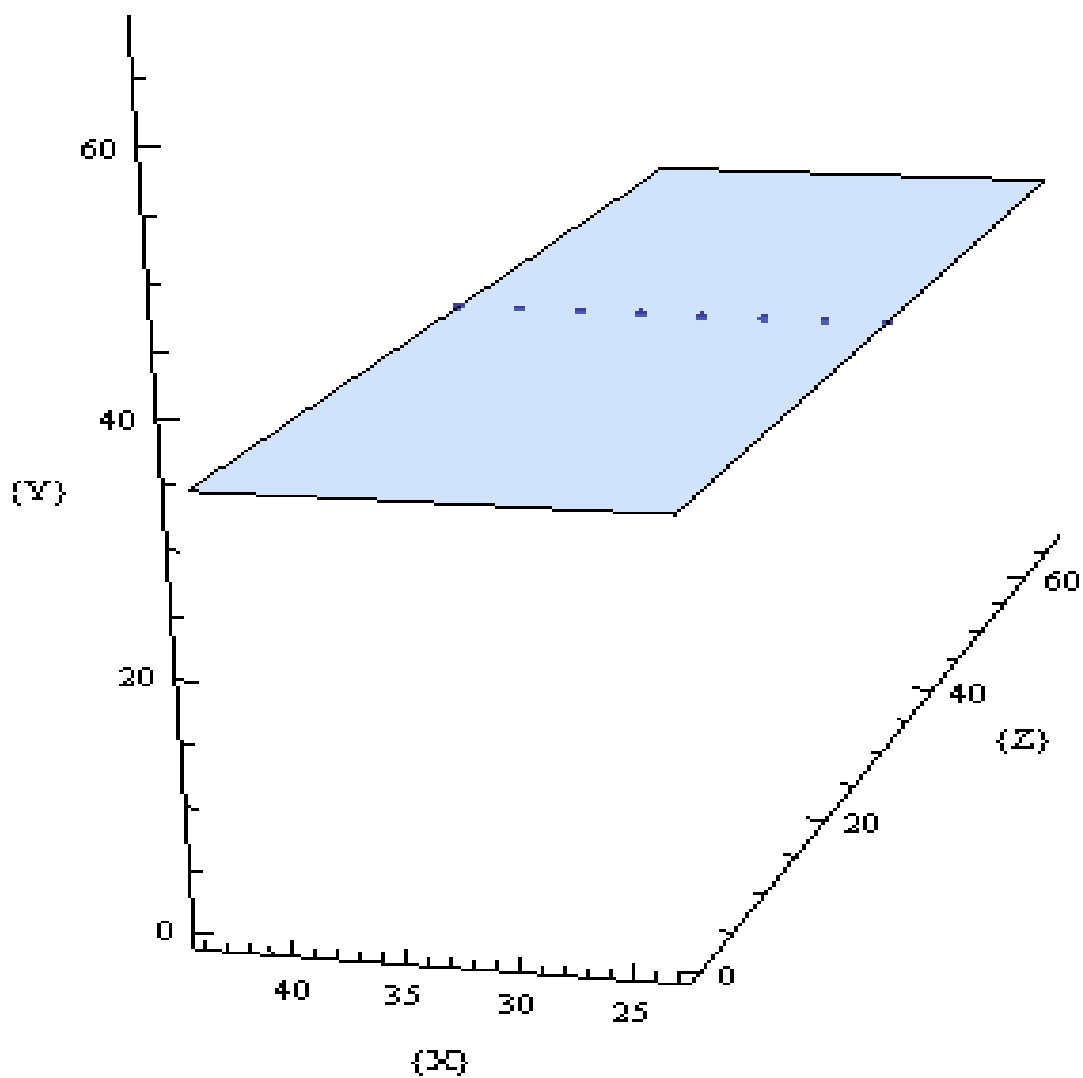


Figure 2 - Graphene Ribbon with unique electron approximations. This figure illustrates the points across the ribbon where the given electron approximations exist for their respective maximum values

The figure above represents the eight electron charge density points at the center of the problem space. This max occurs at both Y_{34} and Z_{34} , and spans from $X_{23} \rightarrow X_{44}$ with 2 zero value points spaced in between each non-zero point.

If you were to sum these eight points, the result would be 1. Applying the scaling factor mentioned previous and filling in the remainder of the points along the Z direction completes the ribbon.

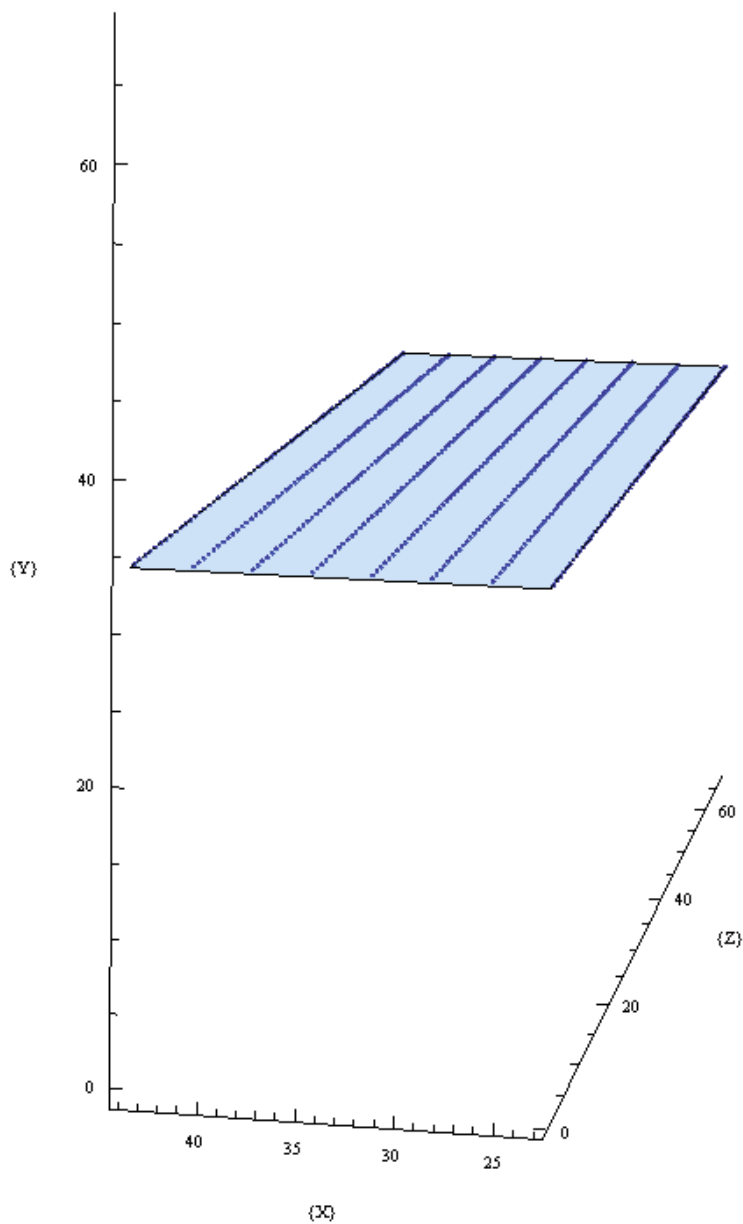


Figure 3 - Non-Zero charge densities in graphene nanoribbon. Shown above are the positions in which non-zero values exist for the graphene nanoribbon. The charge density is a maximum in the very middle of the ribbon, and decrease sinusoidally out towards the ends.

The figure above represents all the non-zero data points placed along the ribbon.

Determining L_X and L_Y was quite trivial. L_Z was fixed due to the formation of the acGNR. Since the goal of the research was to allow the potentials and the field lines to occur naturally, the requirements for the area surrounding the nanoribbon were:

- Do not interfere with the voltage potential and field line fringing
- Problem space small enough so that the algorithms could be run in a realistic duration.

The second requirement exists because expanding the problem space bounding box to $133 \times 133 \times 133$ resulted in algorithm run times of 9 days at a 1×10^{-6} convergence threshold. Running the algorithm for a $267 \times 267 \times 267$ bounded box at a 1×10^{-6} convergence threshold, was terminated after 24 days of runtime. Its estimated based on the increase in run times from $67 \times 67 \times 67$ to $133 \times 133 \times 133$ that the $267 \times 267 \times 267$ element algorithm would take ~90 days to run.

As depicted in the figures above, the problem space consists of a bounded box with the nanoribbon lying in the middle, starting at $1/3 L_X$ and ending at $2/3 L_X$. For the size of $67 \times 67 \times 67$, the acGNR was placed at Y_{34} , and spanned from $X_{23} \rightarrow X_{44}$, and from $Z_0 \rightarrow Z_{67}$.

L_X , L_Y , and L_Z are computed by multiplying Δx , Δy , Δz by 67.

$\Delta x \times 67$	27.4646 Å
$\Delta y \times 67$	67 Å
$\Delta z \times 67$	95.14 Å

Table 2 - Total Length Constants – Represented here are the values used to define the problem set

The space spanned 67 points across all three dimensions, allowing for the potentials and the field lines to fully fringe.

After expanding the problem space to 133x133x133 and comparing those results with the 67x67x67 electric field profile, it was determined that 67x67x67 would allow us to successfully capture the field lines without artificially influencing the profile. An array of this size (67x67x67) results in 300,763 data points. Below are three different figures for perspective and comparison. The first is the 67x67x67 problem space with the acGNR8 hung in the middle. The second is the 67 array, and the third is the 133 array. Notice there is no difference visually between the two profiles.

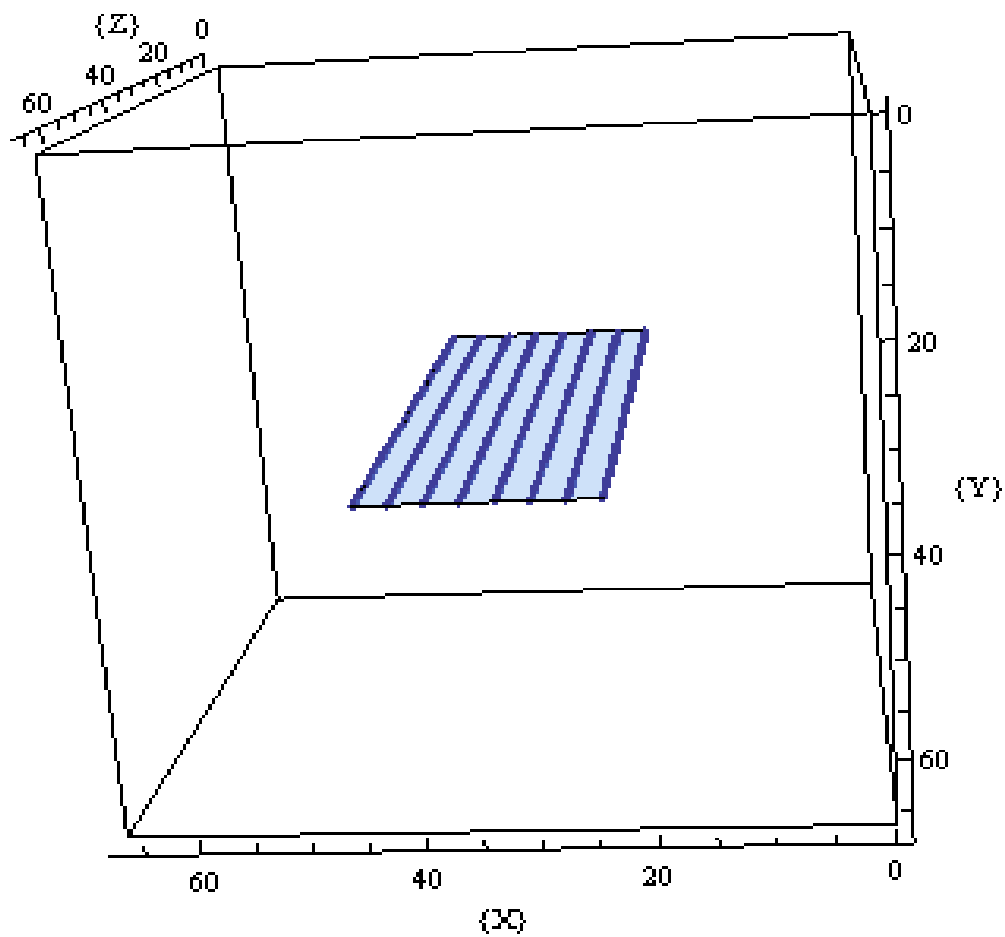


Figure 4 - acGNR8 with the problem space boxed in around it for initial perspective.

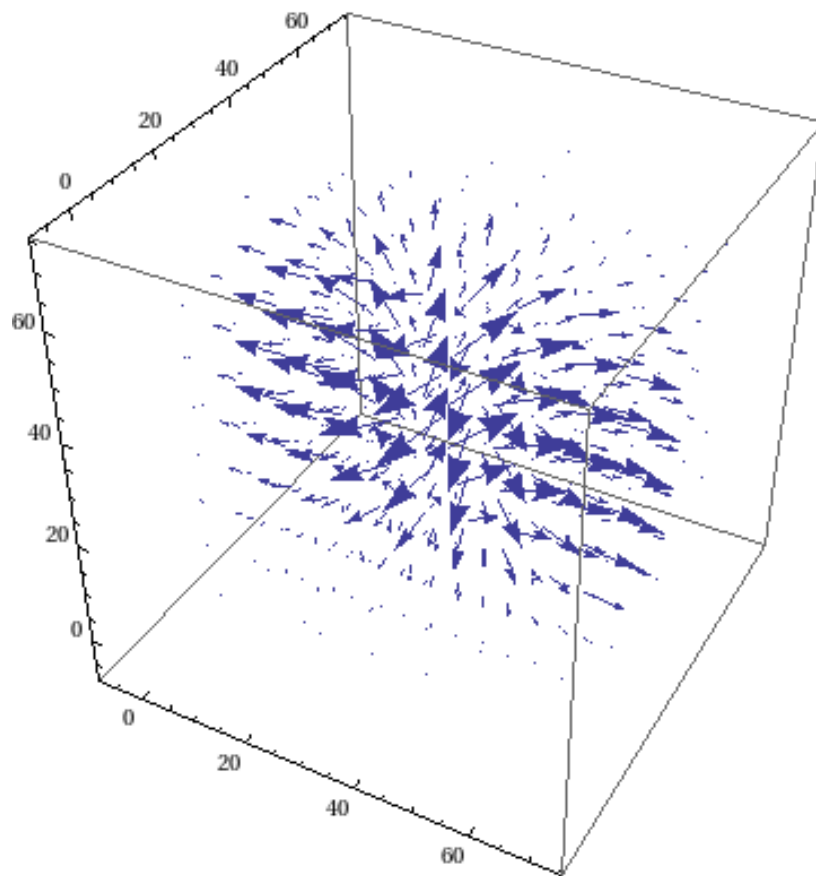


Figure 5 – 3D Electric Field Lines for 67x67x67 the array

These are the field lines produced from the 67x67x67 array.

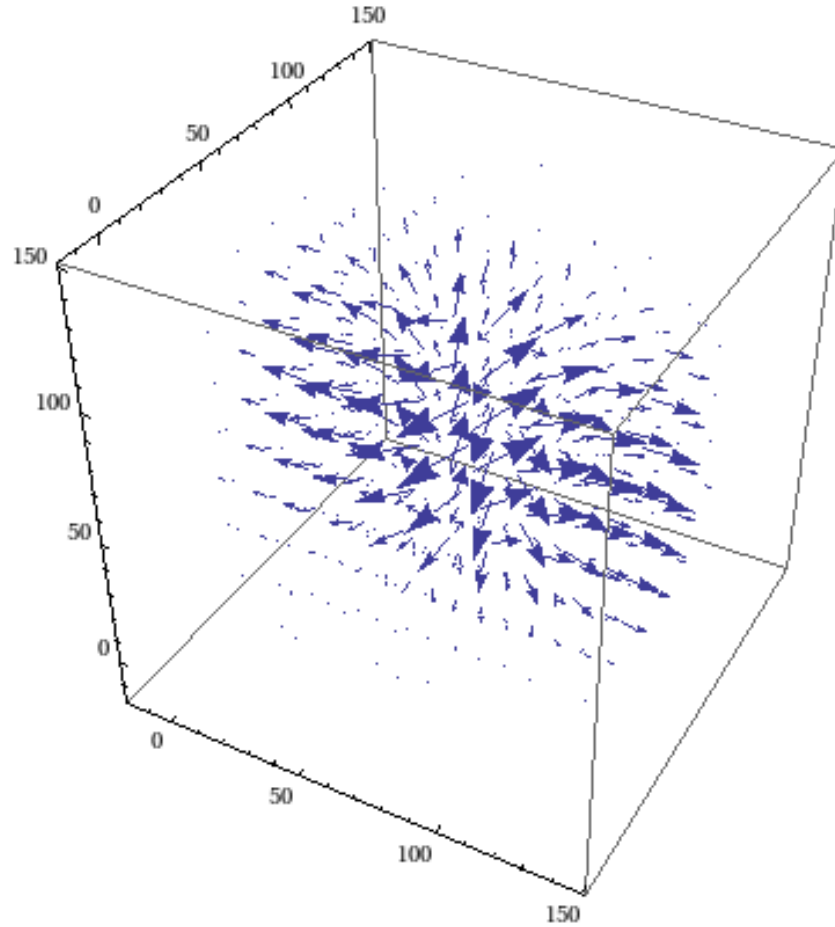


Figure 6 – 3D Electric Field Lines for the 133x133x133 array

These are the field lines produced from the 133x133x133 array. As in the first comparison test, the voltage potentials from the 67 array were compared, as a ratio to the 133 array. The following is a graphical representation of that comparison. Note that no single ratio from any of the 300,763 data points ever exceeded that of 1.1. The slight difference in values of 10 percent told us that the 67x67x67 bounded space would be sufficient, since our goal in this work is to gain intuition through a visual representation.

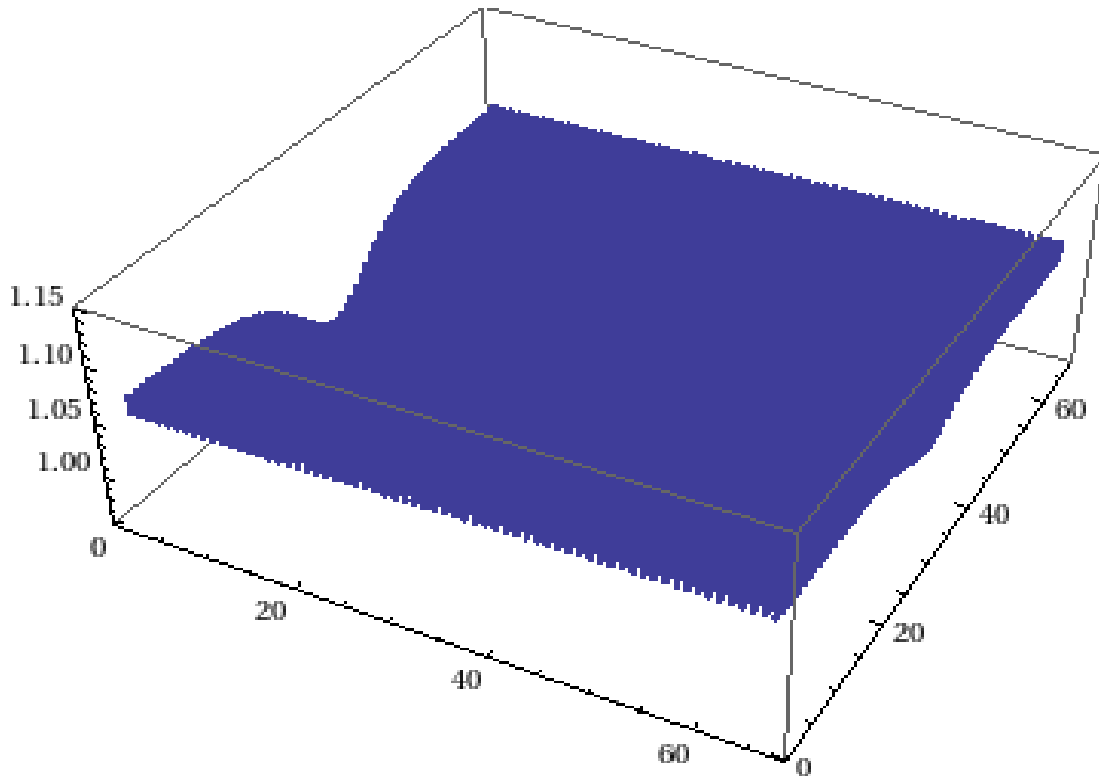


Figure 7 - Comparison of the 133 array to the 67 array. This picture shows a point by point comparison of the two arrays to see how much the data was changing between the two. A very small difference existed between the two runs. So the 67 array problem space was used as a result.

This picture represents the data from the 133x133x133 array compared to the data from the 67x67x67 array. Between the visual inspection of the field line vectors and the ratio comparison of the voltage potentials, it was determined that an array of 67x67x67 was large enough to satisfy the result of this simulation. In doing so, it was decided to increase the 67x67x67 space, convergence threshold to 1×10^{-7} and compare that 1×10^{-6} for good measure. The field lines were an exact match to the naked eye, as expected. When the dataset was compared as a ratio to the other, the results were quite close. In

fact, the data was an exact match along the middle of the dataset, and when it did vary it only differed by 0.05%, or 0.0005 in the worst case.

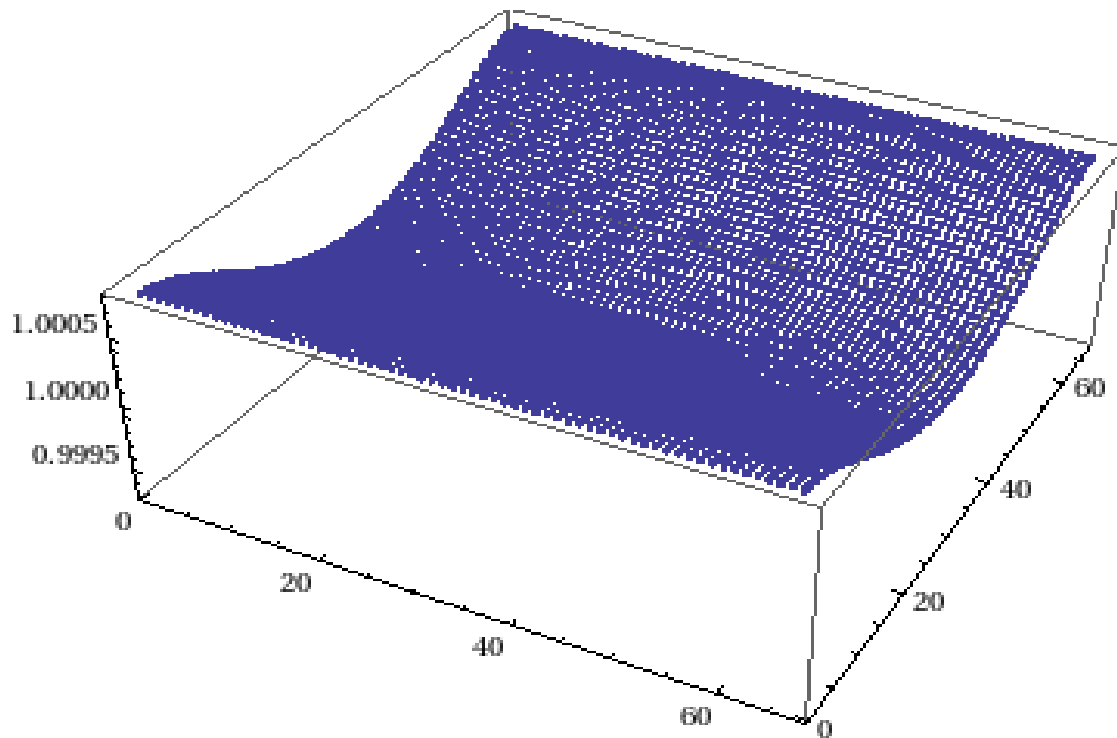


Figure 8 - Comparison between 1×10^{-6} and 1×10^{-7} arrays. This figure shows the amount of change between the resulting potential values when run at 1×10^{-6} and 1×10^{-7} convergence thresholds. The values were only different by .0005 or .05%.

This plot shows the comparison between the $67 \times 67 \times 67$ at 1×10^{-6} dataset and the $67 \times 67 \times 67$ at 1×10^{-7} dataset. Because of this, the algorithms were run against $67 \times 67 \times 67$ arrays set at 1×10^{-7} convergence thresholds

CHAPTER 4

COMPUTING THE DATA

The algebraic and geometric make-up of the Poisson Solver, field gradient solver and the acGNR8 were discussed in the previous chapters. This chapter will explain the computer algorithms behind the data. Remember, the end goal was to calculate and plot the electric field and potential associated with the given set of electron approximations. In order to do so, the electron probabilities were converted into the charge densities, which in turn were converted into voltage potentials using the derived 3-dimensional Poisson solver, (reference Chapter 3 for the derivation of that equation). Finally, taking the gradient of those potentials yields the electric field vectors. Referencing the Δx , Δy , Δz values from Chapter 3, it was determined that an array of 67 x 67 x 67 would mathematically suffice for the field lines. The table below shows the constant values used in the Poisson Solver.

Δx	0.409918691 Å
Δy	1 Å
Δz	1.42 Å
ϵ_0	$8.85418782 \times 10^{-12} \frac{s^4 A^2}{m^3 kg}$

Table 3 - Delta Coefficients – These are the spacing coefficients used in the computer algorithm to calculate the potentials

In what follows we describe the computer algorithms created to facilitate the research. The Mathematica algorithms and editors are listed in the appendices and will be referenced here. Standard notation for reference will look like X11, where X = appendix and 11 = line reference. Therefore B25 references line 25 of Appendix B.

First we describe the editor computation used to convert the given electron approximations into charge densities. The set of data points provided is a mathematical approximation of the location of the electron with respect to the arm chair lattice unit cell. Because the total probability equals 1, the sum of the sixteen points equals 1. Due to the propagation profile of the potential being sinusoidal, the approximations were scaled accordingly to match that profile across the nanoribbon in the Z direction. The scalar modifier applied to the charge densities was: $\sin\left[\frac{\pi}{2} * \frac{k}{34}\right]$ for a problem set equal in resolution to k ranging from 0 \rightarrow 67. Notice that for the middle of the nanoribbon at k = 34, the density values are at a maximum with $\sin\left[\frac{\pi}{2} * \frac{34}{34}\right]$. Holding true to the boundary conditions that $\varphi = 0$, notice that at k=0 and k=68, that the densities are equal to zero due to the scaling modifier being equal to zero. Using $\sin\left[\frac{\pi}{2} * \frac{0}{34}\right]$ and $\sin\left[\frac{\pi}{2} * \frac{68}{34}\right]$ respectively.

In order to calculate ρ , it is necessary to calculate ψ . A ψ editor was written in Mathematica to facilitate this. The editor can be found in Appendix A. Notice A27 demonstrates the summation of the single line approximation. The result after multiplying by its conjugate (A20) and summing with its nearest neighbor, is the charge density profile needed for Poisson's equation.

Next, the ρ values are placed at precise locations within the nanoribbon. The ρ editor can be found in Appendix B. The front and rear third of the ribbon in the X direction can be observed in B2 - 9. Notice the values are defined for X23, 26, 29, 32, 35, 38, 41, 44 and putting zeros in place for the others. B10 – 25 demonstrate scaling the remainder of the approximations sinusoidally. The editor ends with a PUT statement that writes the 67x67x67 Rho array to a file.

The Poisson Solver algorithm is the primary calculation engine and is documented in Appendix C. The iterative convergence looping is handled in this solver, along with the conversion to the electric field gradient. C16 starts the beginning of the 3 dimensional Poisson solver derived in Chapter 3. C24 documents the threshold convergence test and the parameter set to 1×10^{-7} . C34-79 are diagnostic, and required since these jobs take ~12 hours to compute depending on how different the initial charge densities are for the nearest neighbor contributions. Statements were added to show the progress of the loop and the amount of memory used. This was important to note, to stay within the processor and RAM constraints on the machine when running multiple jobs. As a lesson learned during research, statements were added to periodically print the voltage potentials prior to full convergence, in the event of an unexpected disruption to the calculations. This way the job could be continued where it left off instead of starting over from scratch. The end result is a 67x67x67 array of voltage potentials. C86 demonstrates calculation that converts the voltage potentials in electric field vector values. This data is then written to a file for manipulation in the rendering editors. This concludes the walk through of the conjugate and rho editors, along with the Poisson Solver and Gradient Field Lines algorithms.

Note that for the 67x67x67 array, the total run time varies based on the convergence threshold, and the differences between the ρ values. For N=8 each job took approximately 8.7 hours to run and approximately 9600 loop iterations were required to reach the convergence threshold. In addition each job took approximately 34,540,016 Bytes of memory. For N=5 each job took approximately 27.4 hours to run and 9605 loop iterations to reach the convergence threshold. In addition each job took approximately 34,540,032 Bytes of memory. Once the solver was finished, the data was ready to be rendered. The periodicity profile of the potential behaves like $\text{Sin}\left(\frac{\pi Z}{2L_z}\right)$ in the direction of propagation, z. Given the symmetry of the plasmon, in order to graphically render 2 full periods, the data was negated and shifted 67 points in the Z direction. This process was repeated twice to complete two full periods.

The given dataset of electron approximations consisted of 400 sets of 16 points for a total of 6400 point probabilities. Computational were performed on the first half of those 400 datasets to cover the unit cell.

The output voltage potential file created from the Poisson Solver explained in Chapter 4 required a little manipulation before it was ready to be rendered using Mathematica. The renderings consist of both 2-dimensional and 3-dimensional graphics. Editors were created to modify the potentials into their desired formats. The 3-dimensional data lists were reduced to 2-dimensions, by holding one of the axes constant while varying the other two. This proved quite useful in creating multiple renderings from various perspectives within the nanoribbon. Chapters 5 and 6 will step through the visualizations created from the algorithms.

CHAPTER 5

N=8 VISUALIZATIONS

The previous chapter explained how the renderings were created. This chapter will display the graphics themselves. Starting first with the 3-dimensional renderings and continuing with the 2-dimensional slices.

The potentials and field lines represent massless Dirac fermions with zero band gap. In order to cover the Brillouin Zone, due to symmetry, it is only necessary to analyze the first half or the first 400 electron probabilities provided for the N=8 graphene unit cell. This was accomplished by calculating the 1st, 41st, 81st, 121st, 161st, 201st Datasets of the approximations. Due to the N=8 band structure and the zero band gap. There is zero observable difference in the renderings for the entire dataset. Dataset 1 will be shown in detail. The calculated ρ values for Dataset 1 are listed in the following table.

Position in acGNR {X,Y,Z}	Calculated ρ Values for $k = 6.70352$
{23,34,34}	0.02599506187566887
{26,34,34}	0.09181686914811862
{29,34,34}	0.166666666666666635
{32,34,34}	0.2155214023095454
{35,34,34}	0.2155214023095458
{38,34,34}	0.166666666666666696
{41,34,34}	0.09181686914811915
{44,34,34}	0.025995061875669113

Table 4 – acGNR positions of the ρ values and their associated calculated values for N=8 Dataset 1

Notice the symmetry between values in the table above. The approximations are smallest on the outside edges of the ribbon, and increase to their maximums at the center of the ribbon. This holds true for all k points investigated. For comparison, the same table representing Dataset 41 will be given below. Notice here that the value for the point {23, 34, 34} does not differ from point {44, 34, 34} until the 15th decimal place, and even then it only changes by 1. As you move towards the center of the ribbon, each symmetrical pair displays this same resolution of likeness.

Position in acGNR {X,Y,Z}	Calculated ρ Values For k = 6.87977
{23,34,34}	0.025995061875669304
{26,34,34}	0.09181686914811957
{29,34,34}	0.16666666666666671
{32,34,34}	0.21552140230954528
{35,34,34}	0.21552140230954547
{38,34,34}	0.166666666666666596
{41,34,34}	0.09181686914811867
{44,34,34}	0.02599506187566893

Table 5 – acGNR positions of the ρ values and their associated calculated values for N=8 Dataset 41

The exact same symmetry calculated for Dataset 1 is observed in Dataset 41. Notice that the symmetrical pairs match down to the 15th decimal place. The following table will display the values from Dataset 1 side by side with the values from Dataset 41 for comparison.

Calculated ρ from Dataset 1	Calculated ρ from Dataset 41
0.02599506187566887	0.025995061875669304
0.09181686914811862	0.09181686914811957
0.16666666666666635	0.16666666666666671
0.2155214023095454	0.21552140230954528
0.2155214023095458	0.21552140230954547
0.16666666666666696	0.166666666666666596
0.09181686914811915	0.09181686914811867
0.025995061875669113	0.02599506187566893

Table 6 – Side by side comparison of the ρ values for N=8 Dataset 1 and N=8 Dataset 41.

Looking at the values side by side, it is quite easy to see why the visual representations of the potentials and field lines do not change drastically enough to be noticed. The following figure is a plot of the Dataset 1 potentials by the Dataset 41 potentials.

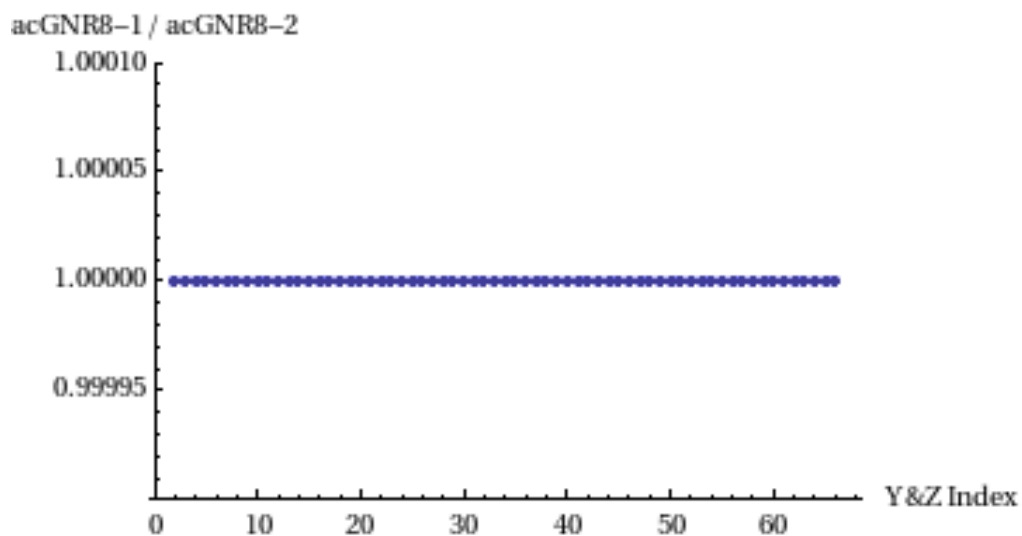


Figure 9 - Plot of the Dataset 1 potentials divided by the Dataset 2 potentials for comparison holding the X axis constant at 50.

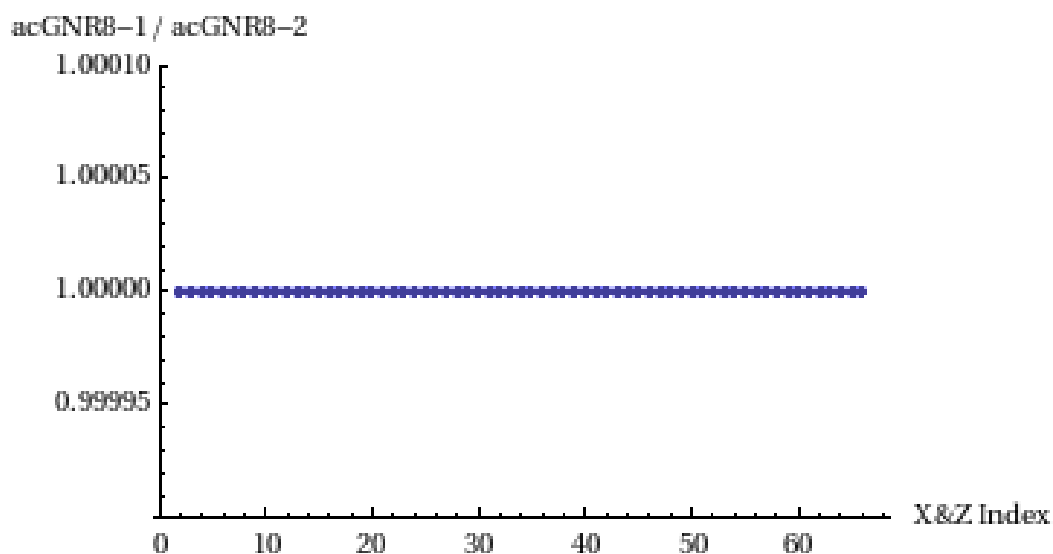


Figure 10 - Plot of the Dataset 1 potentials divided by the Dataset 2 potentials for comparison holding the Y axis constant at 20.

Although not very exciting, the figures above back up the claim that the values are not changing between datasets in the acGNR8 case. These plots illustrate that even though the probabilities in the acGNR8 structure are calculated with different k wave numbers, there is zero change in the potentials as a result. Thus in the acGNR8 case, there is no dependence on the wave number in terms of the potentials and the field lines. Therefore only Dataset 1 will be displayed below due to repetition.

Dataset 1

Using the ρ values from the Dataset 1 table above, the Poisson algorithm returned a set of potential values that illustrate the symmetrical properties identified in the tables above. The figure below is the 3 Dimensional representation of the potential.

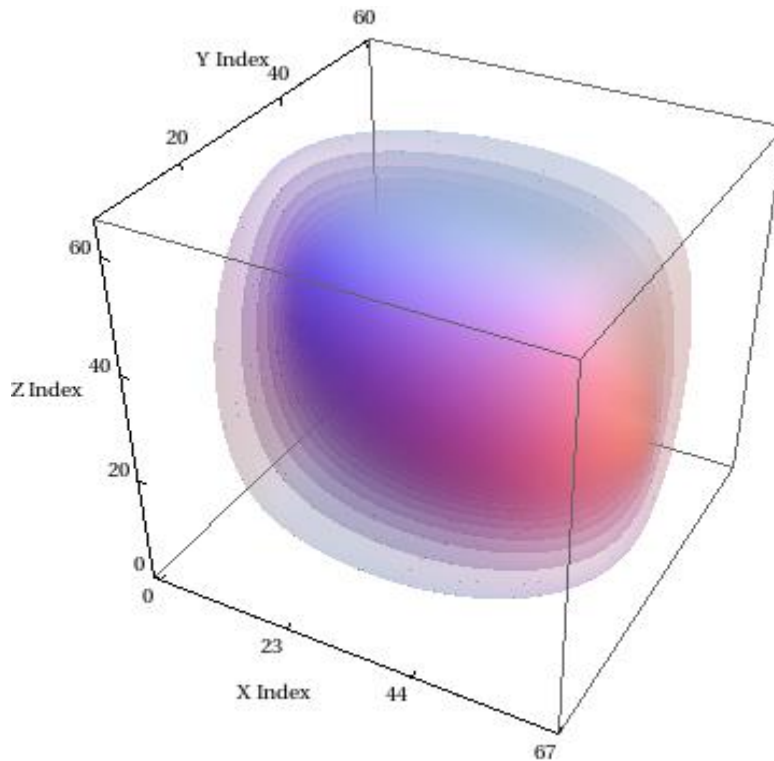


Figure 11 - 3D representation of the potential calculated for Dataset 1.

The tick marks along the X axis are set up to show where the edges of the nanoribbon would lie. The plane of the ribbon lies in the X axis and runs along the Z axis. The next representation is the field lines calculated from the previous potentials.

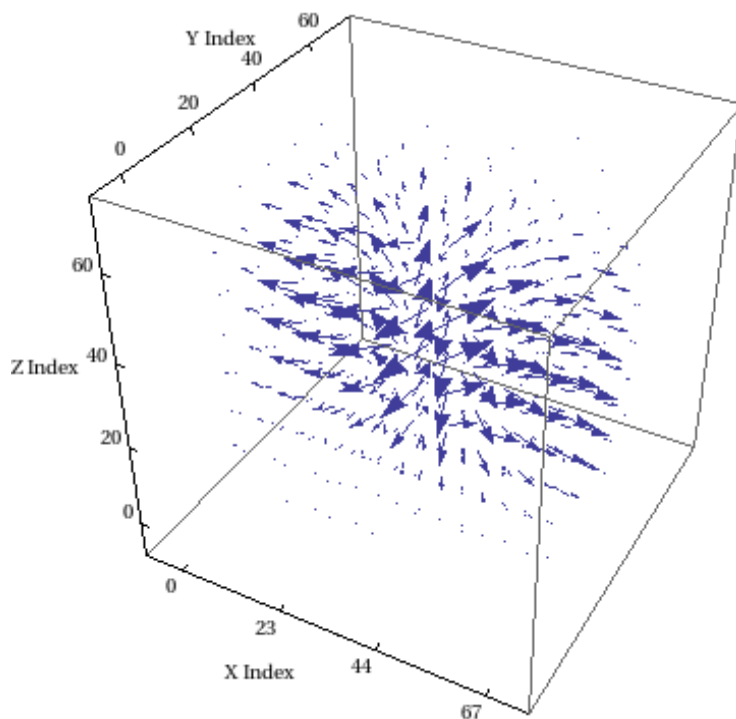


Figure 12 - 3D representation of the field lines calculated from acGNR8 Dataset 1.

Notice the direction of the field lines. It is clear that the potentials that produced these field lines are positive. The following graphic shows the potentials and the field lines together.

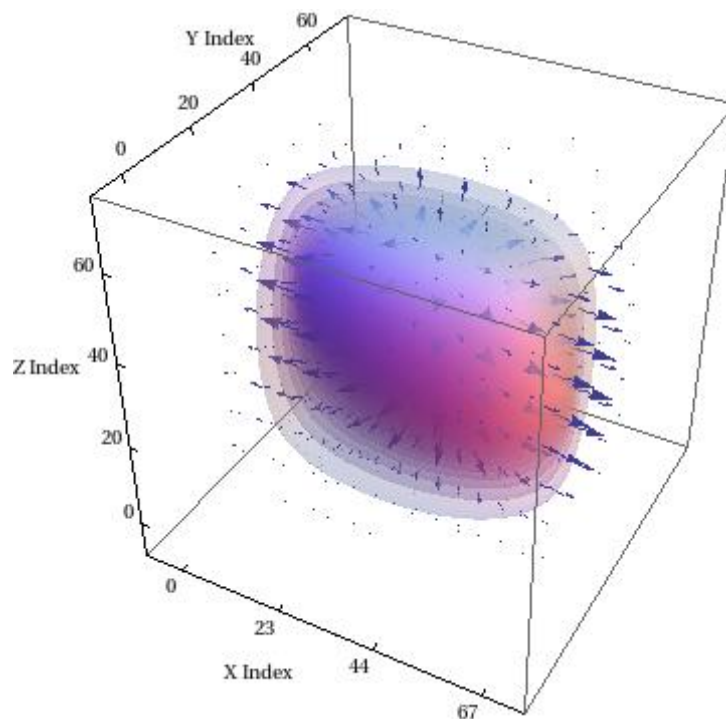


Figure 13 - 3D representation of the Field Lines and the Potentials associated acGNR8

The above figure shows both the field lines and the potentials that were calculated for the first dataset on the acGNR8 ribbon. It should be noted here that these graphics represent $\frac{1}{2}$ period of the profile. The following graphics will follow this convention but represent 2 full periods of propagation. The nanoribbon will be placed in to give perspective.

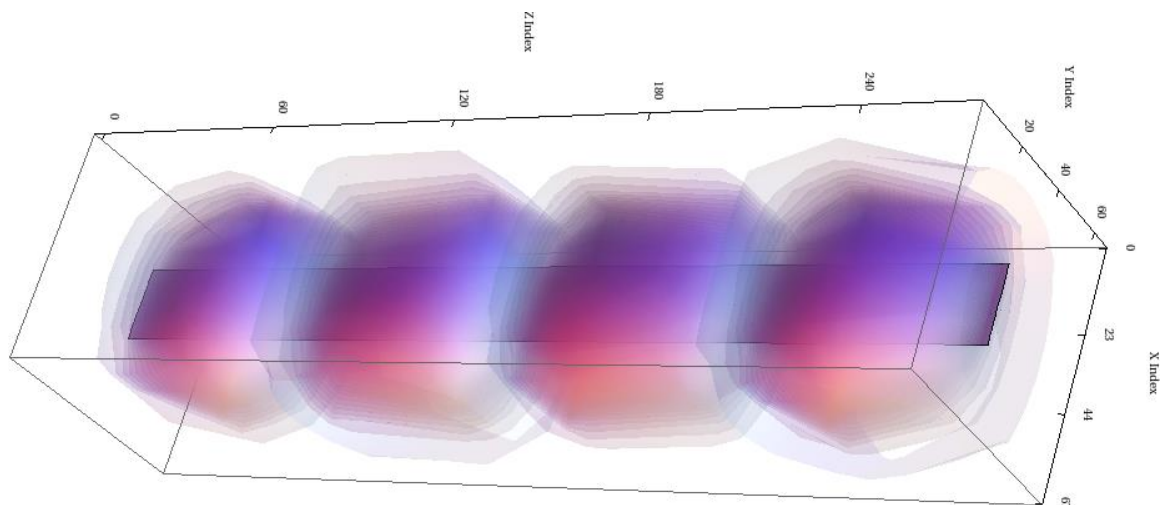


Figure 14 - 3D representation of 2 full periods of the potentials calculated from Dataset 1

Notice in the above picture, that a representation of the acGNR8 has been added.

The following represents the field lines.

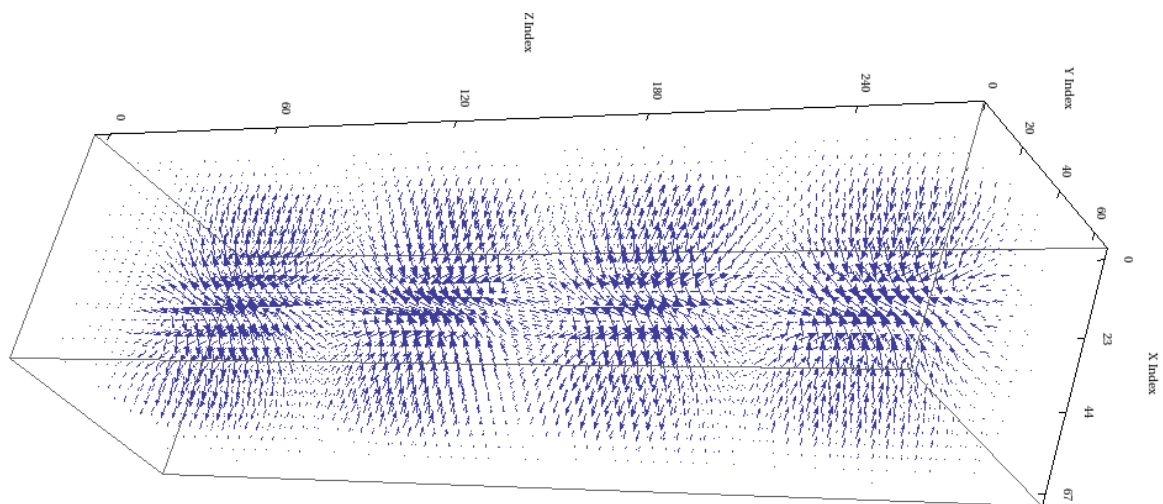


Figure 15 - 3D representation of the field lines calculated from the potentials for 2 full periods.

Looking closely at the figure above, you can see the changes in direction in the field lines. Not only can you notice the field lines moving from one unit cell to another, you can also see the change in sign of the potentials between one field line cluster to another. As done with the $\frac{1}{2}$ period. The next figure represent the total picture of field lines and potentials, along with the nanoribbon for 2 periods of propagation.

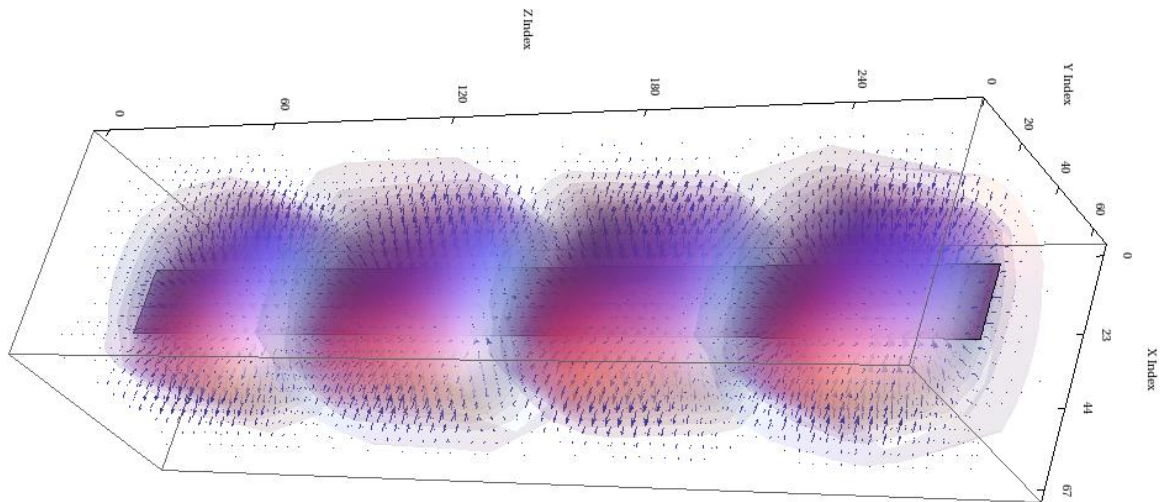


Figure 16 - 3D representation of the calculated field lines and potentials from the first dataset.

Now that the data has been rendered in 3D, the next set of illustrations will focus on 2 dimensional slices taken from the potentials and field lines.

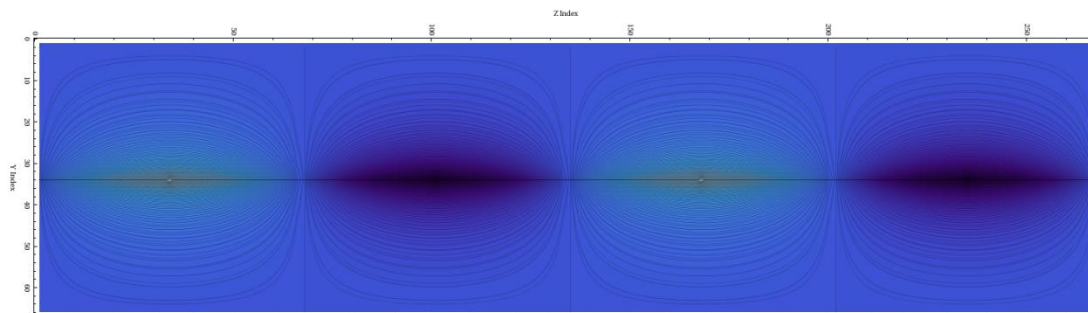


Figure 17 - 2D representation of the potential of the first dataset, holding the X axis constant at 34.

The above figure represents 2 full periods of the potentials calculated for the first dataset. This figure shows the profile of the Y and Z axes while holding X constant at 34. This represents a section through the problem space in the direction normal to the nanoribbon plane. As mentioned in the opening of this chapter, there is zero observable differences in any of the visualizations for $N=8$ between Dataset sets. Even though the acGNR8 is practically 2D due to its atomically small thickness, a black line has been inserted in the figure above for perspective of the placement of the ribbon.

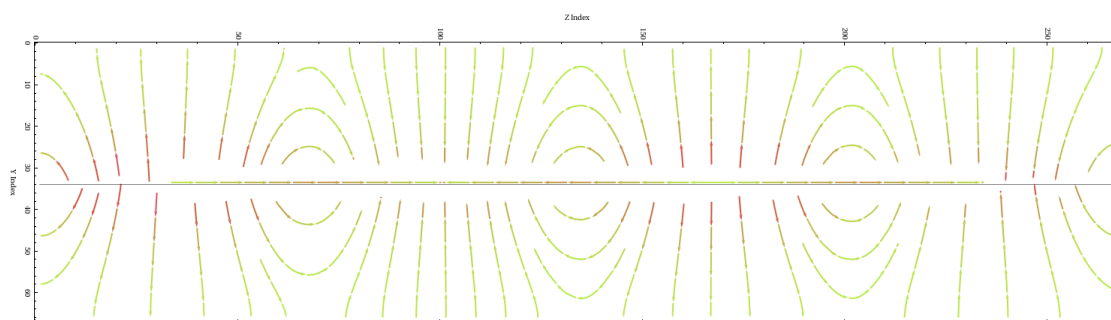


Figure 18 - 2D representation of the field lines of the first dataset, holding the X axis constant at 34.

The figure above represents the field lines calculated from the potentials associated with the Y and Z axes. Again this slice was taken holding the X axis constant at 34. This figure shows really clear direction lines in the field profile, along with the changes in magnitude. The following figure shows the field lines and the potentials for the Y and Z axes combined.

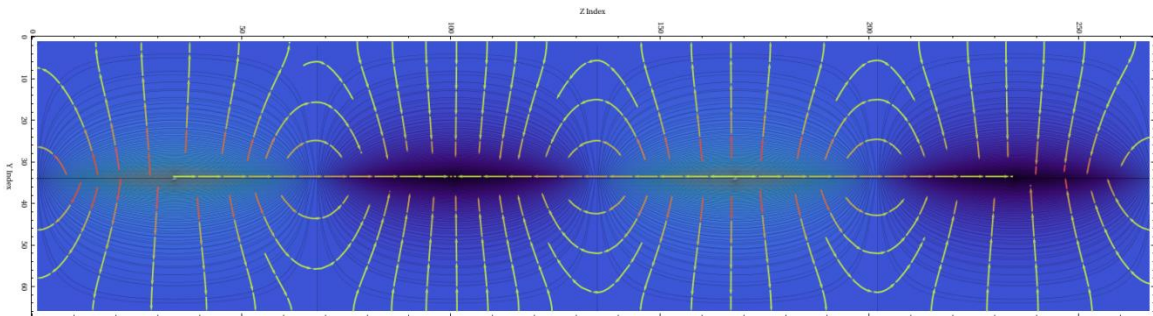


Figure 19 - 2D representation of the field lines and potentials calculated for the scGNR8 Dataset 1.

Looking closely at the above figure, you can see in the center of the positive potential cluster, the maximum value for ϕ that correlates to the maximum value of ρ listed in the tables in the chapter opening. The next set of slices will focus on the X and Z axes while holding the Y axis constant at 34.

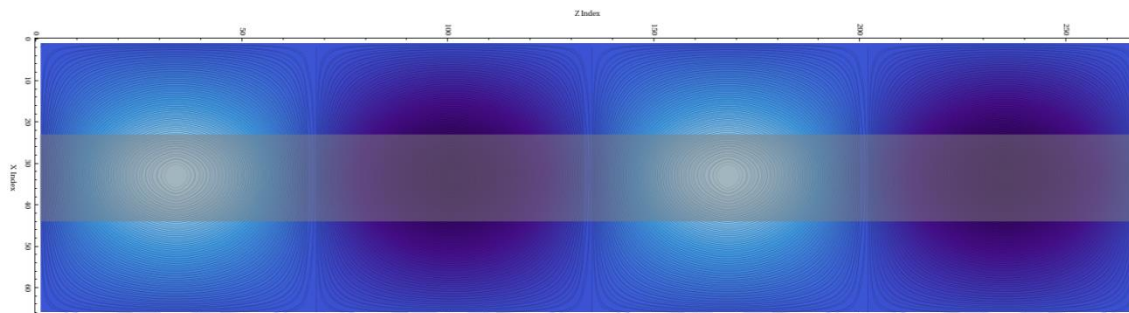


Figure 20 - 2D representation of the potentials calculated along the X and Z axes. This figure also shows the acGNR8 nanoribbon.

The graphic above is oriented with respect to the direction of propagation Z and represents a section through the problem space in the plane of the nanoribbon. This is consistent with the layout of the nanoribbon.

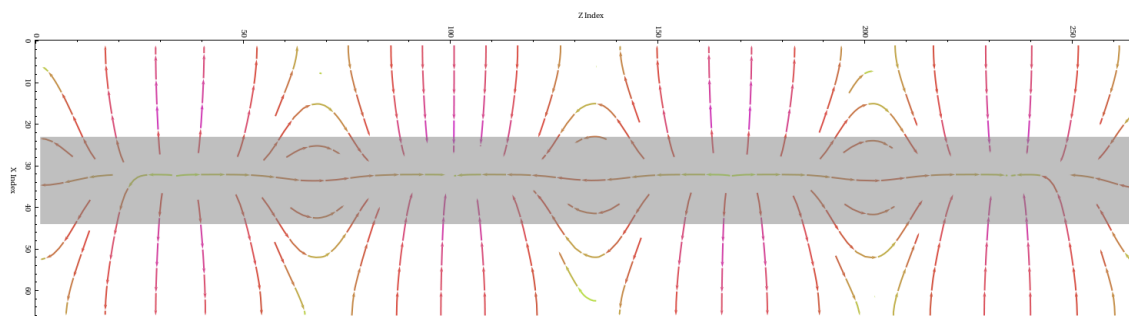


Figure 21 - 2D representation of the field lines for Dataset 1 holding the Y axis constant. Also shown here is the location of the nanoribbon.

Shown here are the electric field lines. These field lines follow the same orientation as the potentials above. Notice the arrow heads are oriented with respect to the electric field lines. Also, shown here, are changes in color in the field lines, representing a change in magnitude.

Overlaying to the two images to render the potentials and the field lines together results in:

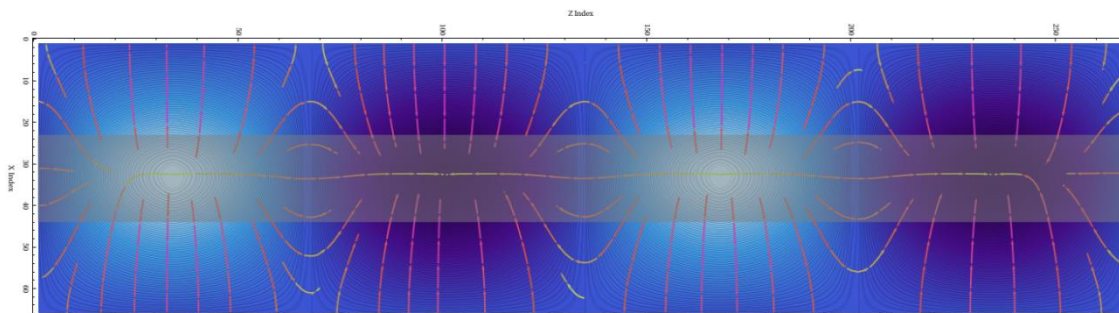


Figure 22 - 2D representation of the potentials and the field lines for Dataset 1 holding the Y axis constant.

The next set will focus on the X-Y plane. Taking a 2D slice out of Z_{34} results in the following potential profile:

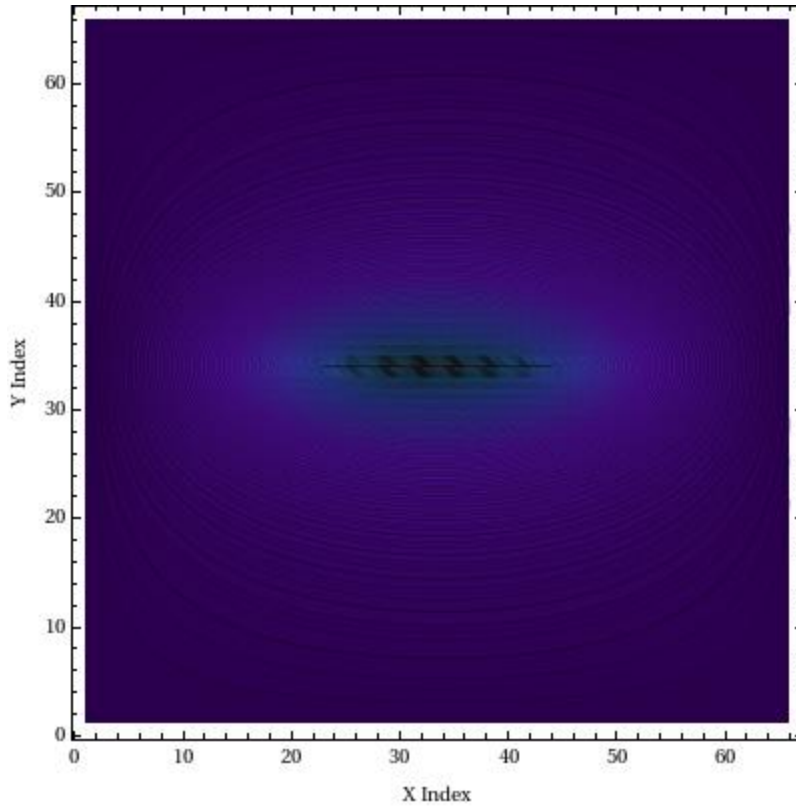


Figure 23 - 2D representation of the potentials for Dataset 1 while holding the Z axis constant. The black line running in the Y axis at position 34 is the acGNR8.

As expected, the potential profile follows the width of the acGNR8. The same slice with respect to the field lines look like:

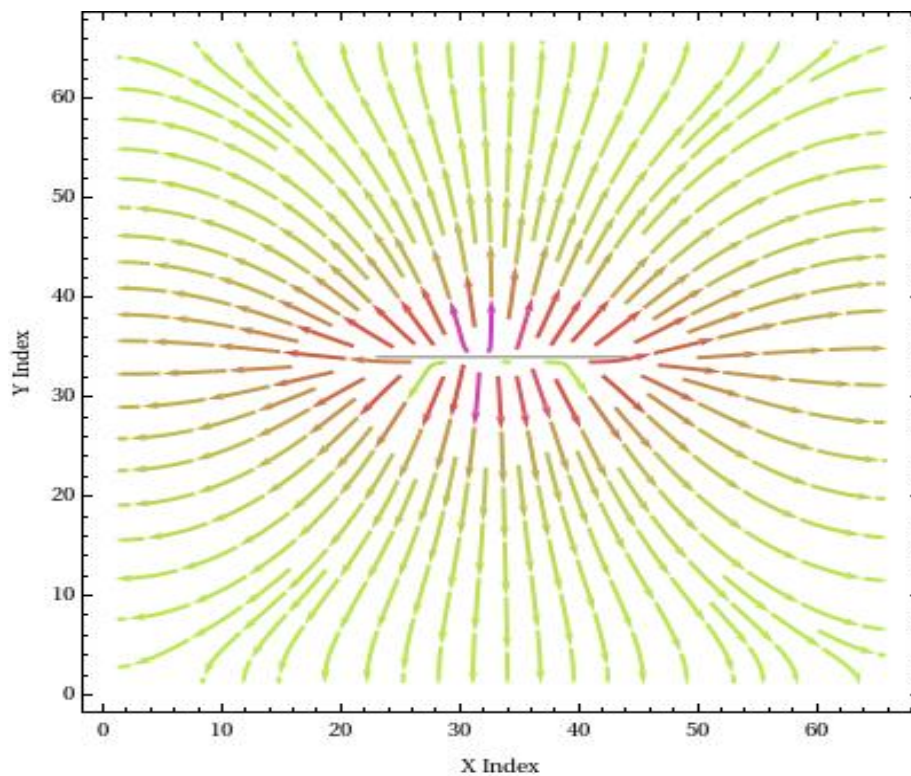


Figure 24 - 2D representation of the field lines for Dataset 1 while holding the Z axis constant.

Again, it is very clear as to the direction of the field lines, indicating that the associated potentials are positive. Rendering the potentials and the field lines for the Z axis results in the following figure:

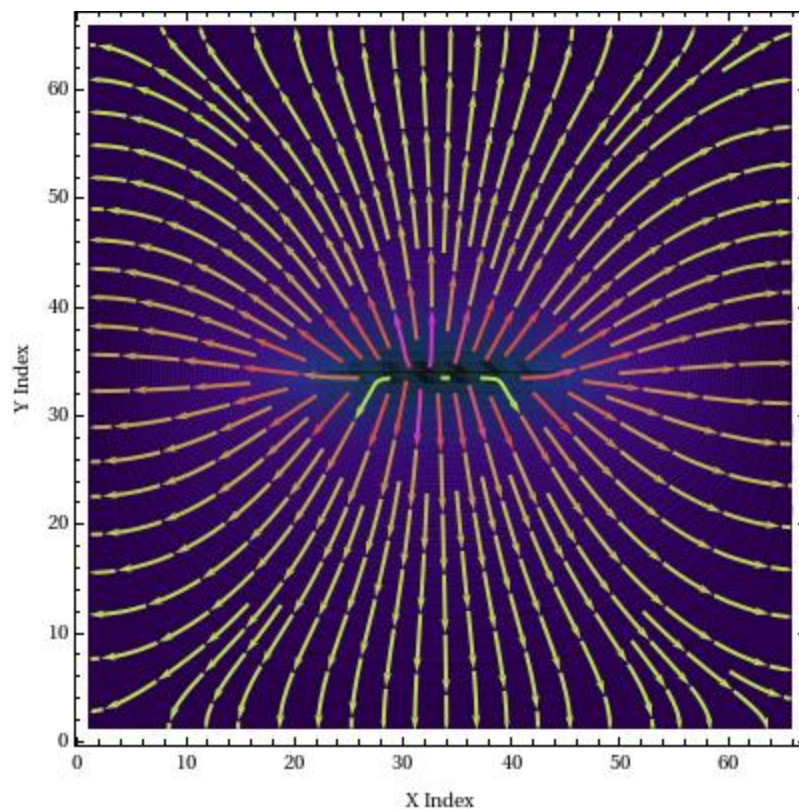


Figure 25 - 2D representation of the potentials and the field lines for Dataset 1 while holding the Z axis constant at position 34.

Graphical representation has covered the $\frac{1}{2}$ period and the 2 period case of the 3D representation. The potentials and the field lines profiles have been rendered for the X, Y and Z axes, respectively. This completes the rendering of the N=8 dataset. The following chapter will show the acGNR5 case.

CHAPTER 6

N=5 VISUALIZATIONS

The previous chapter showed the voltage potentials and field lines specific to the N=8 armchair nanoribbon. Seven sets of electron approximations were provided for N=5 armchair nanoribbon. In addition to slightly smaller width, the electron approximations provided for the N=5 graphene are for massive Dirac fermions, with a band gap of ~64 meV. This chapter will cover those graphics. For consistency, the order and format will follow that of Chapter 5.

Unlike the N=8 band structure, there is observable difference in the renderings for the N=5 dataset. This is directly attributed to the band gap. The acGNR5 case has a distinct dependence on the wave number unlike the acGNR8 case. The Datasets will be shown in detail. The calculated ρ values for Dataset 1 are listed in the following table.

Position in acGNR {X,Y,Z}	Calculated ρ Values For k= 0.05315402341494809
{27,34,34}	0.2440934700590991
{30,34,34}	0.2538018427644523
{33,34,34}	$1.239657653857084 \times 10^{-8}$
{36,34,34}	0.25595087934816363
{39,34,34}	0.24615379543170846

Table 7 – acGNR positions of the ρ values and their associated calculated values for N=5 Dataset 1

Notice there is still symmetry between values in the table above. Like the N=8 case, the approximations are smallest on the outside edges of the ribbon, and increase slightly towards the center. However, the one key difference for the acGNR5 case is that due to the band gap, the charge density for the Dirac fermion lying in the center is essentially zero. This has some effect on the profile properties of the acGNR5. For comparison, the same table representing Dataset 2 will be given below. Notice here that the value for the point {23, 34, 34} does differ from point {44, 34, 34} at the 3rd decimal place.

Position in acGNR {X,Y,Z}	Calculated ρ Values For $k= 0.226502274177099$
{27,34,34}	0.24661223178846572
{30,34,34}	0.2533575229139936
{33,34,34}	$1.071988224937808 \times 10^{-7}$
{36,34,34}	0.25324070572563334
{39,34,34}	0.24678943237308476

Table 8 – acGNR positions of the ρ values and their associated calculated values for N=5 Dataset 2

The following table will display the values from Dataset 1 side by side with the values from Dataset 2 for comparison.

Calculated ρ from Dataset 1	Calculated ρ from Dataset 2
0.2440934700590991	0.24661223178846572
0.2538018427644523	0.2533575229139936
$1.239657653857084 \times 10^{-8}$	$1.071988224937808 \times 10^{-7}$
0.25595087934816363	0.25324070572563334
0.24615379543170846	0.24678943237308476

Table 9 – Side by side comparison of the ρ values for N=5 Dataset 1 and N=5 Dataset 2.

Looking at the values side by side, there is a noticeable difference between the two datasets. The following figure represents a comparison of the Dataset 1 potentials by the Dataset 2 potentials. As shown in the acGNR8 case. The following figures will represent of the potentials between the first acGNR5 dataset and the second acGNR5 dataset.

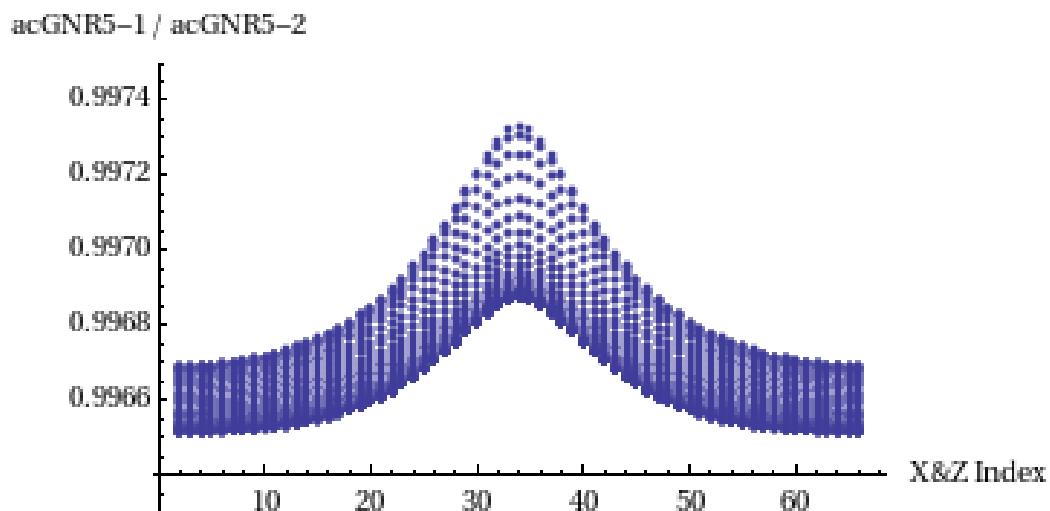


Figure 26 - Comparison of acGNR5 Dataset 1 potentials divided by Dataset 2 potentials while holding the X axis constant at 50.

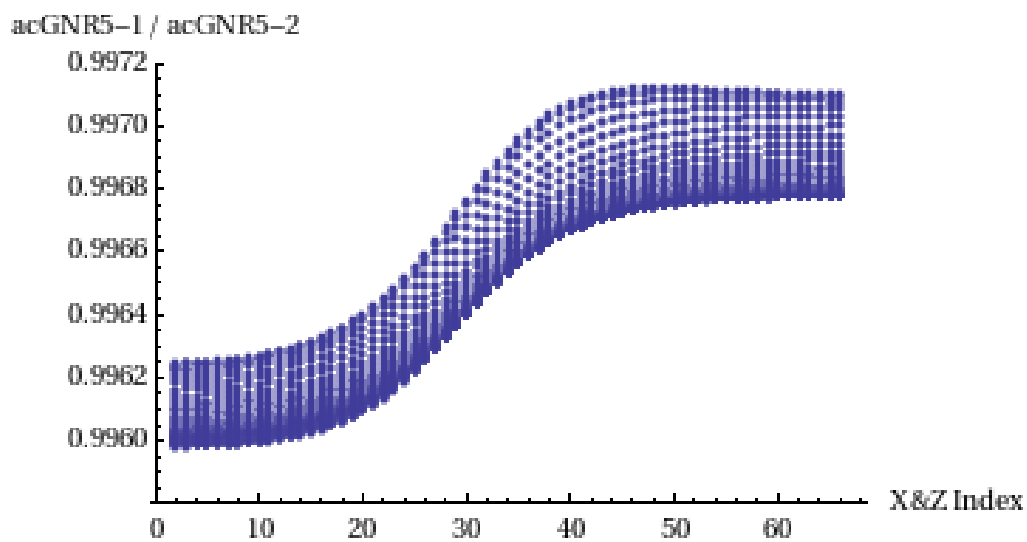


Figure 27 - Comparison of acGNR5 Dataset 1 potentials divided by Dataset 2 potentials while holding the Y axis constant at 40.

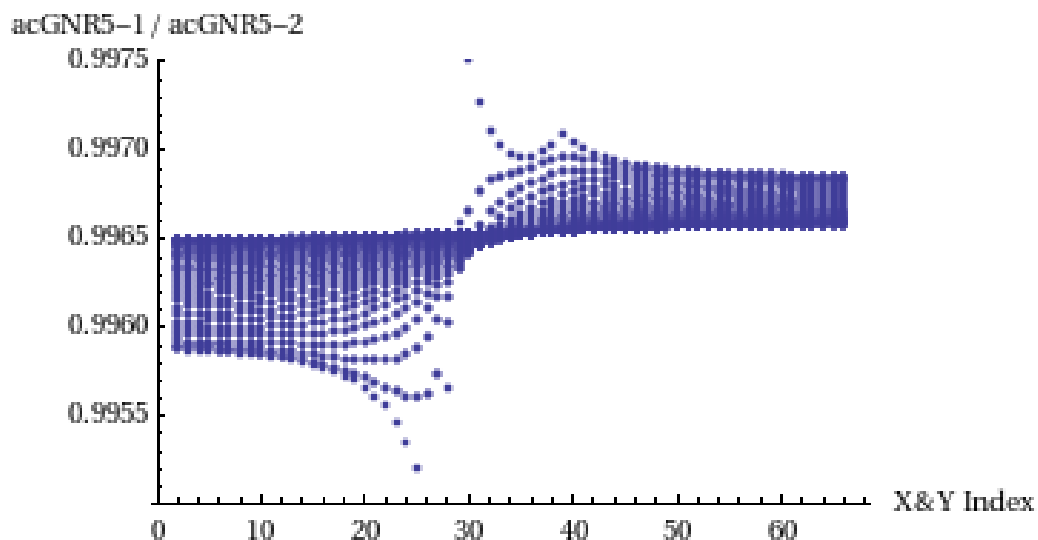


Figure 28 - Comparison of acGNR5 Dataset 1 potentials divided by Dataset 2 while holding the Z axis constant at 50.

The figures above are comparisons of the first acGNR5 calculated potential compared to the second acGNR5 calculated potential. Unlike the acGNR8 potentials, differences do exist between the potentials of the acGNR5 datasets, although the rate of change is not drastic, change still exist. And noticeable along all 3 axes is change for every point in the dataset Therefore, all 7 Datasets of acGNR5 will be documented below.

Dataset 1

Using the ρ values from the Dataset 1 table above, the Poisson algorithm returned a set of potential values that illustrate the double hump properties identified in the tables above. The figure below is the 3 Dimensional representation of the potential.

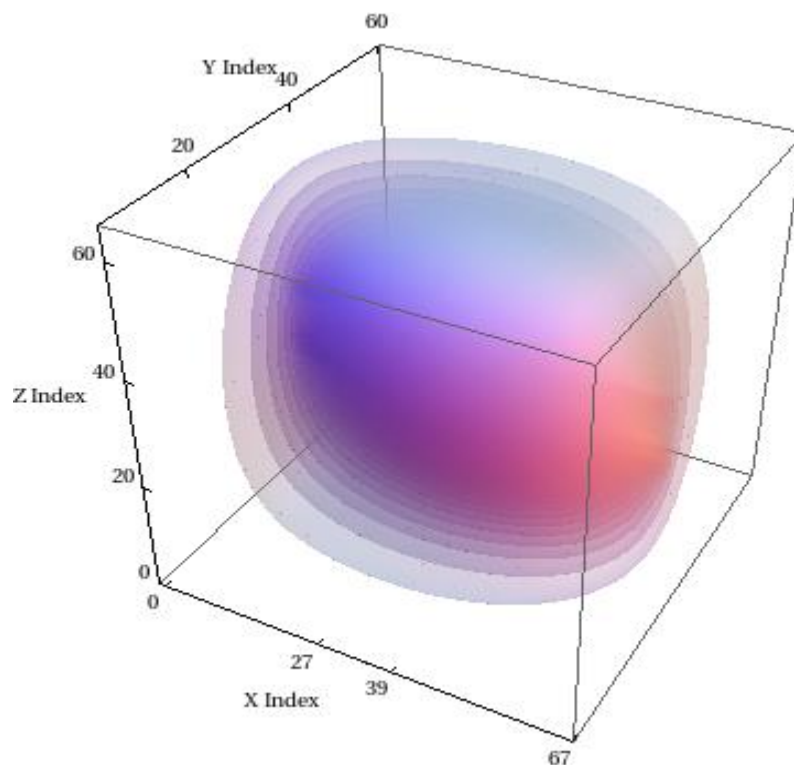


Figure 29 - 3D representation of the potential calculated for Dataset 1.

The tick marks along the X axis are set up to show where the edges of the nanoribbon would lie as they did in the acGNR8 case. The width of the ribbon lies in the X axis and runs along the Z axis. The next representation is the field lines calculated from the previous potentials.

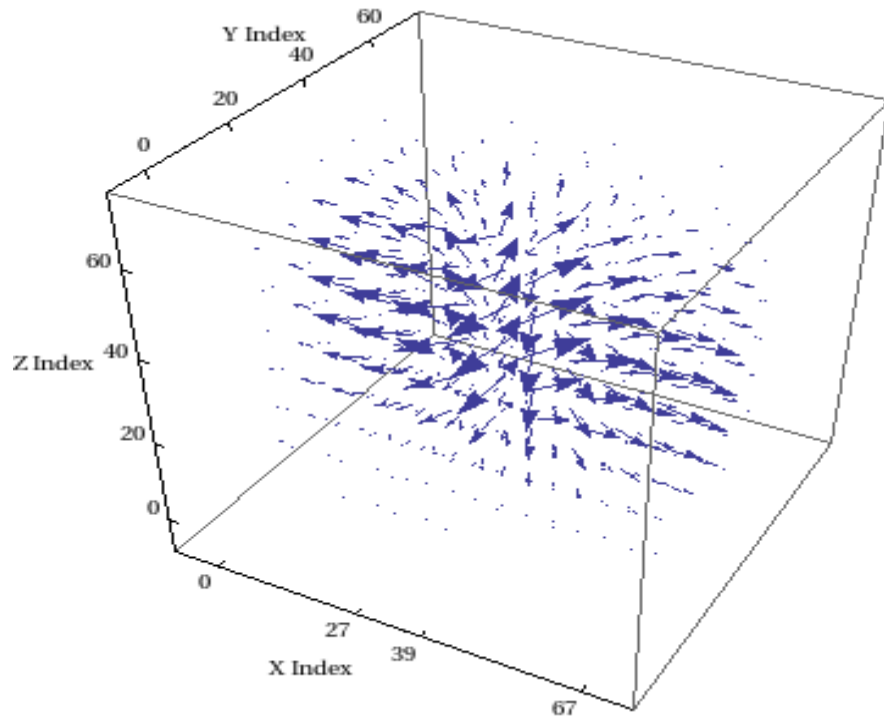


Figure 30 - 3D representation of the field lines calculated from the acGNR5 Dataset 1.

Notice the direction of the field lines. It is clear that the potentials that produced these field lines are positive. The following graphic shows the potentials and the field lines together.

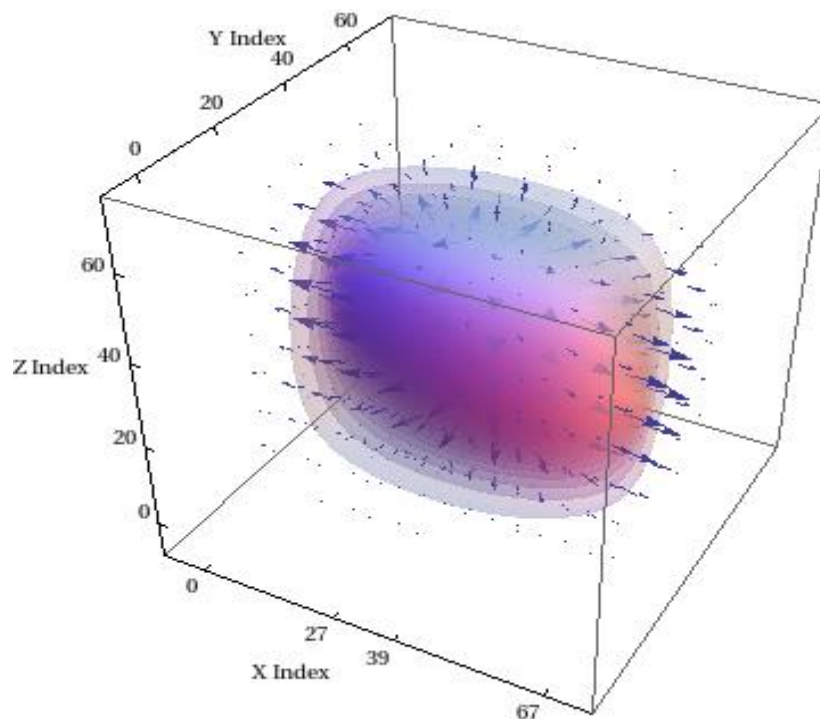


Figure 31 - 3D representation of the Field Lines and the Potentials associated with the acGNR5 Dataset 1.

The above figure shows both the field lines and the potentials that were calculated for the first dataset on the acGNR5 ribbon. It should be noted here that these graphics represent $\frac{1}{2}$ period of the profile. The following graphics will follow this convention but represent 2 full periods of propagation. The nanoribbon will be placed in to give perspective.

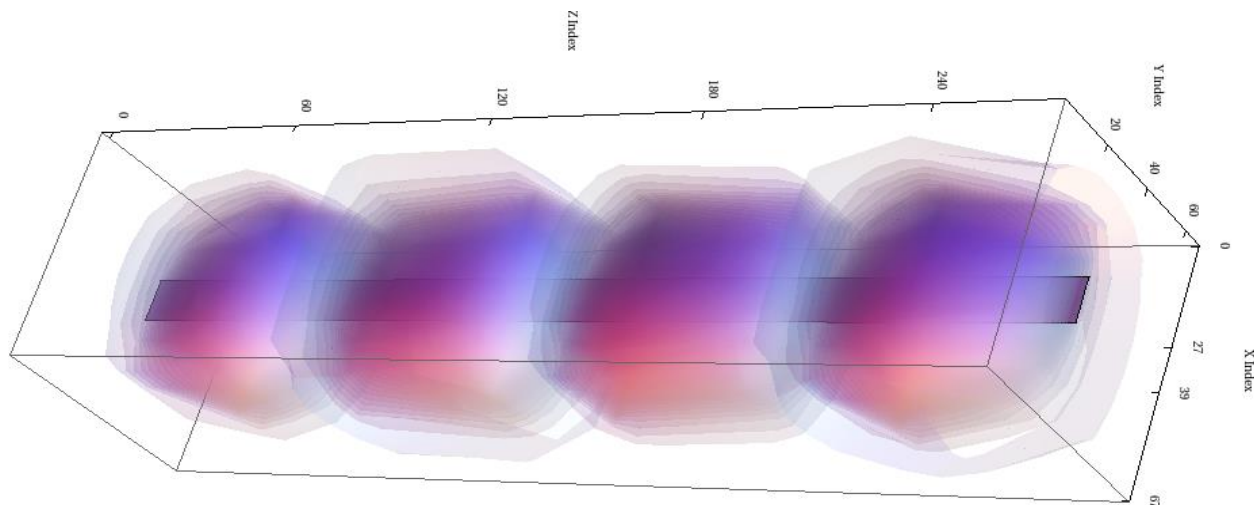


Figure 32 - 3D representation of 2 full periods of the potentials calculated from Dataset 1

Notice in the above picture, that the acGNR5 has been added and that it lines up nicely with the tick marks on the X axis. This ribbon is not quite as wide as the acGNR8. The following will represent the field lines.

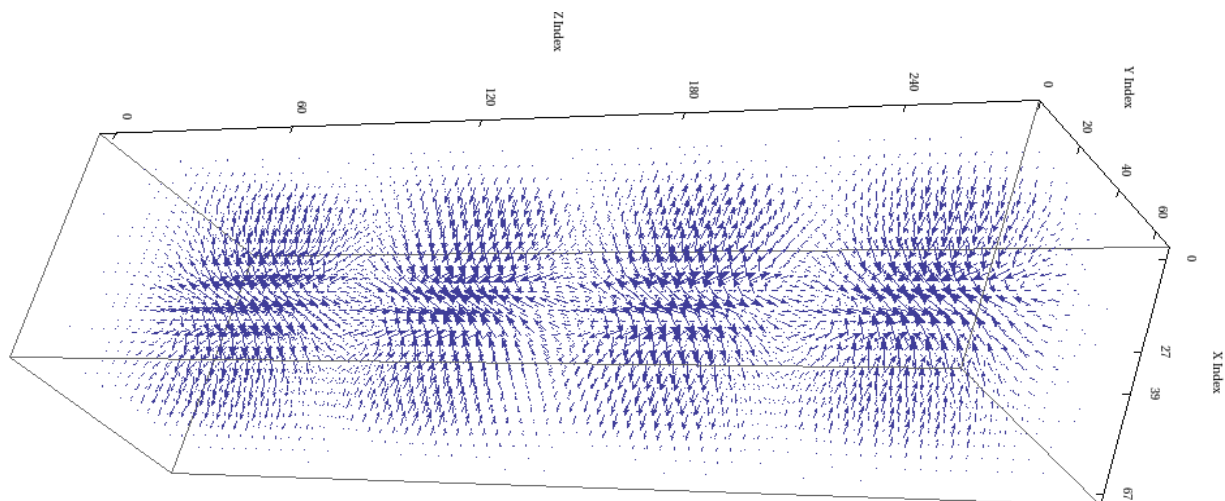


Figure 33 - 3D representation of the field lines calculated from the potentials for 2 full periods.

Looking closely at the figure above, you can see the changes in direction in the field lines. Not only can you notice the field lines moving from one unit cell to another, you can also see the change in sign of the potentials between field line clusters, as done with the $\frac{1}{2}$ period. The next figure represents the total picture of field lines and potentials, along with the nanoribbon for 2 periods of propagation.

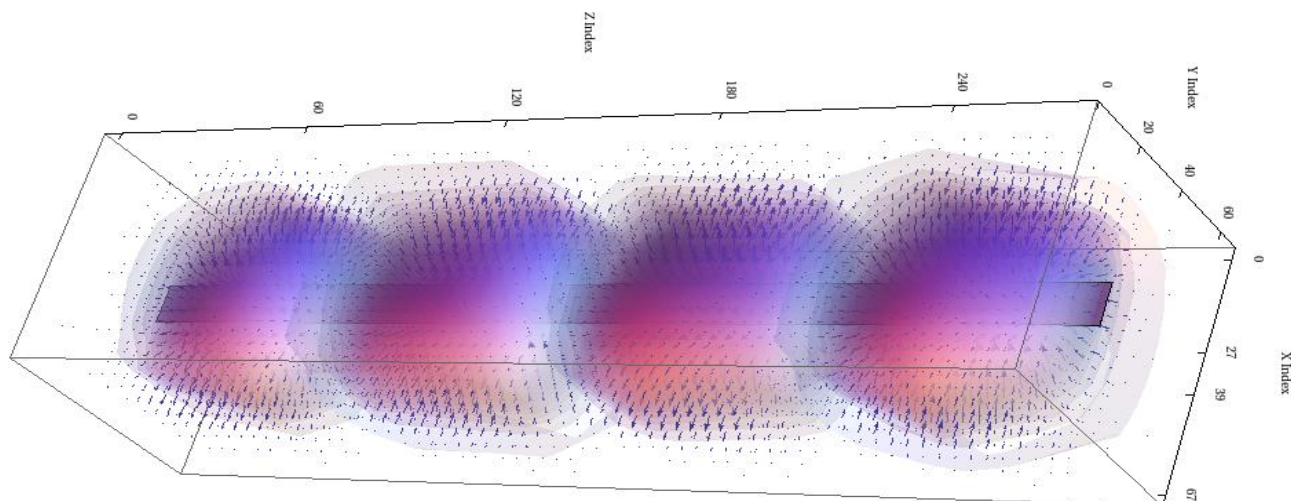


Figure 34 - 3D representation of the calculated field lines and potentials from the first dataset.

Now that the data has been rendered in 3D, the next set of illustrations will focus on 2 dimensional slices taken from the potentials and field lines.

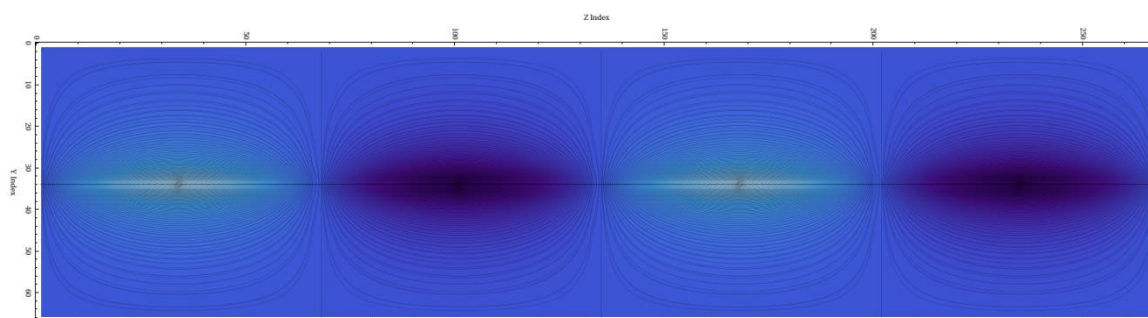


Figure 35 - 2D representation of the potential of the first dataset, holding the X axis constant at 34.

The above figure represents 2 full periods of the potentials calculated for the first dataset. This figure shows the profile of the Y and Z axes while holding X constant at 34. Even though the acGNR5 is practically 2D due to its atomically small thickness, a black line has been inserted in the figure above for perspective of the placement of the ribbon.

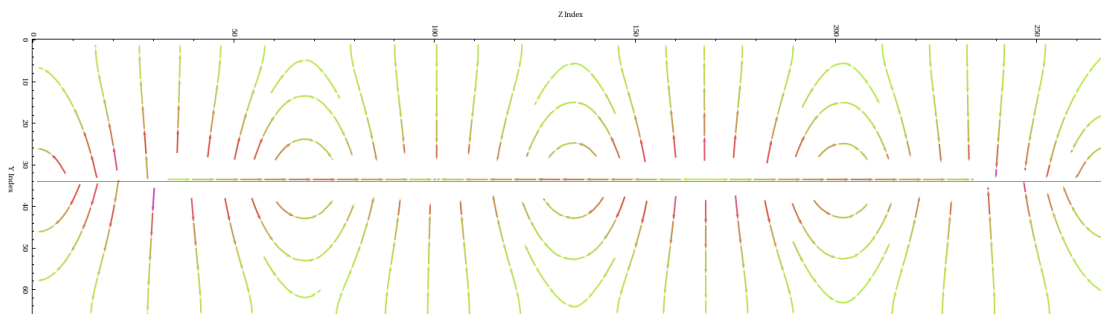


Figure 36 - 2D representation of the field lines of the first dataset, holding the X axis constant at 34.

The figure above represents the field lines calculated from the potentials associated with the Y and Z axes. Again this slice was taken holding the X axis constant at 34. This figure shows really clear direction lines in the field profile, along with the changes in magnitude. The following figure shows the field lines and the potentials for the Y and Z axes combined.

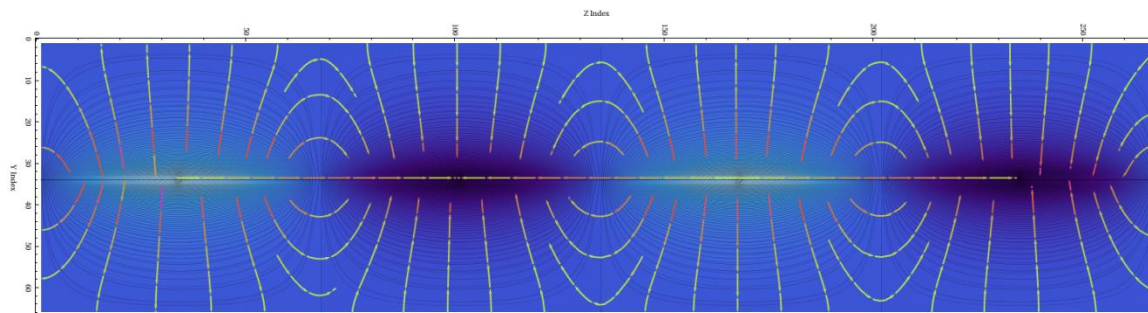


Figure 37 - 2D representation of the field lines and potentials calculated for the scGNR5 dataset 1.

Looking closely at the above figure, you can see in the center of the positive potential cluster, the maximum value for ϕ that correlates to the maximum value of ρ listed in the tables in the chapter opening. The next set of slices will focus on the X and Z axes while holding the Y axis constant at 34.

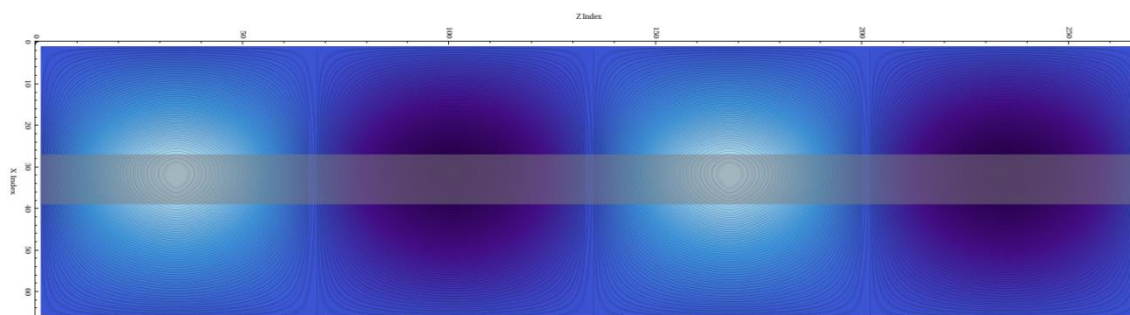


Figure 38 - 2D representation of the potentials calculated along the X and Z axes. This figure also shows the acGNR5 nanoribbon.

The graphic above is oriented with respect to the direction of propagation Z. This is consistent with the layout of the nanoribbon.

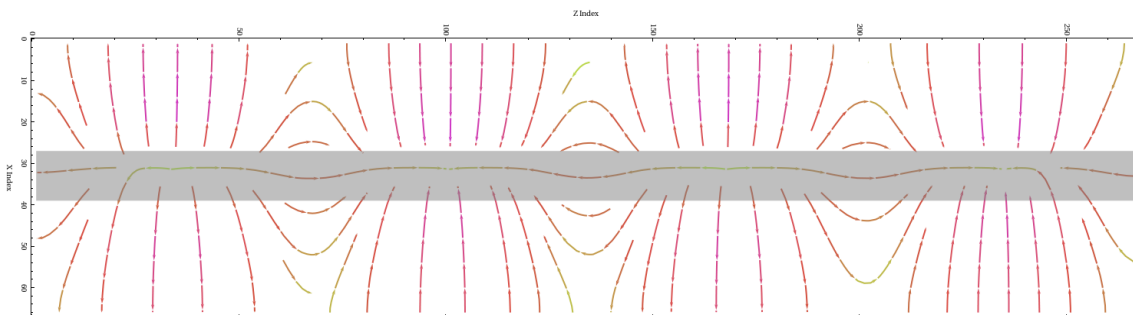


Figure 39 - 2D representation of the field lines for Dataset 1 holding the Y axis constant. Also shown here is the location of the nanoribbon

Shown here are the electric field lines. These field lines follow the same orientation as the potentials above. Notice the arrow heads are oriented with respect to the electric field lines. Also, shown here, are changes in color in the field lines, representing a change in magnitude.

Overlaying to the two images to render the potentials and the field lines together results in:

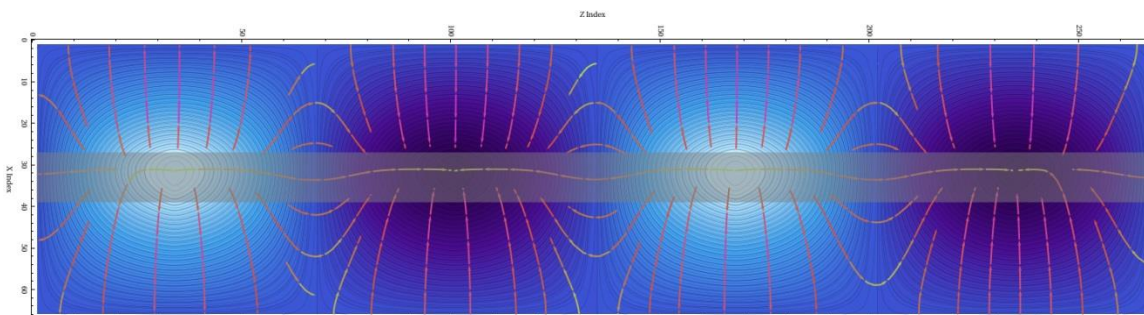


Figure 40 - 2D representation of the potentials and the field lines for Dataset 1 holding the Y axis constant.

The next set will focus on the X-Y plane. Taking a 2D slice out of Z_{34} results in the following potential profile:

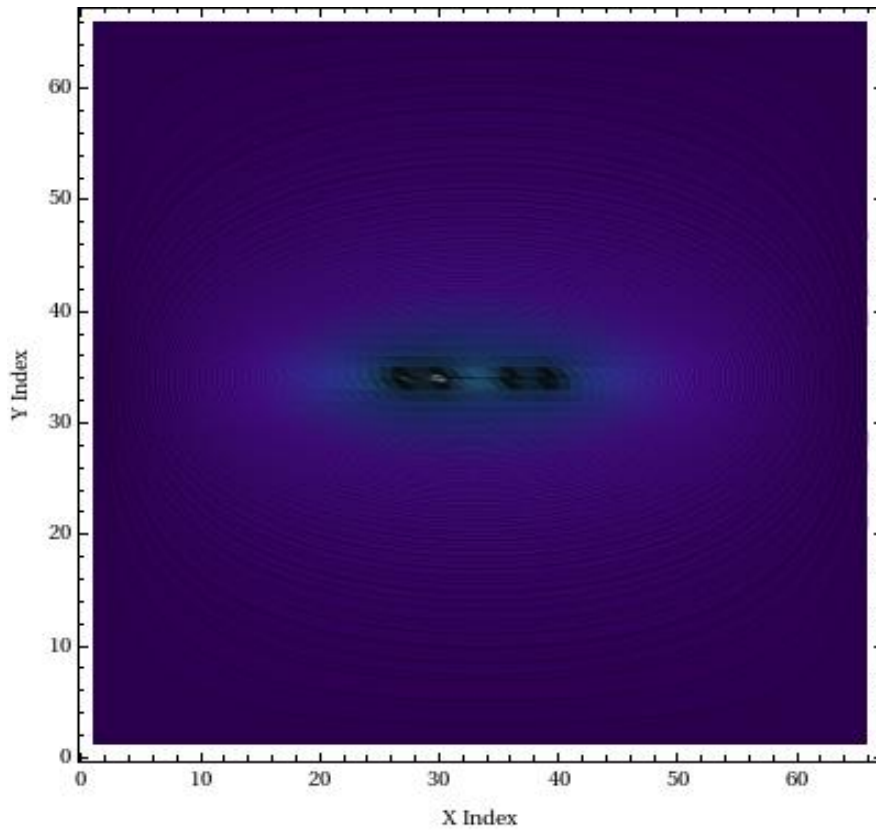


Figure 41 - 2D representation of the potentials for Dataset 1 while holding the Z axis constant. The black line running in the Y axis at position 34 is the acGNR5.

As expected, the potential profile follows the width of the acGNR5. The same slice with respect to the field lines look like:

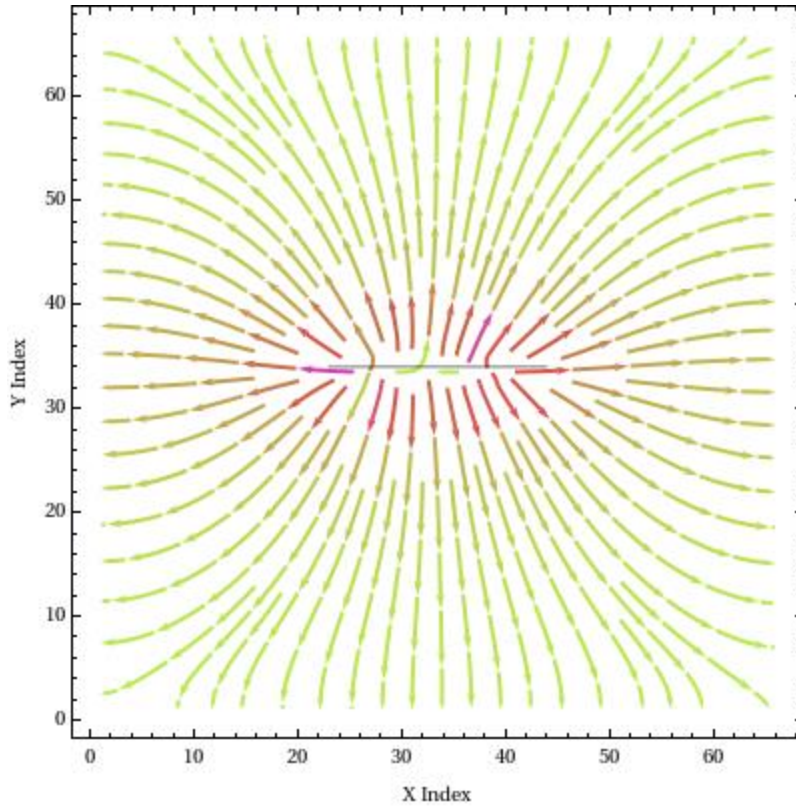


Figure 42 - 2D representation of the field lines for Dataset 1 while holding the Z axis constant.

Again, it is very clear as to the direction of the field lines, indicating that the associated potentials are positive. Rendering the potentials and the field lines for the Z axis results in the following figure:

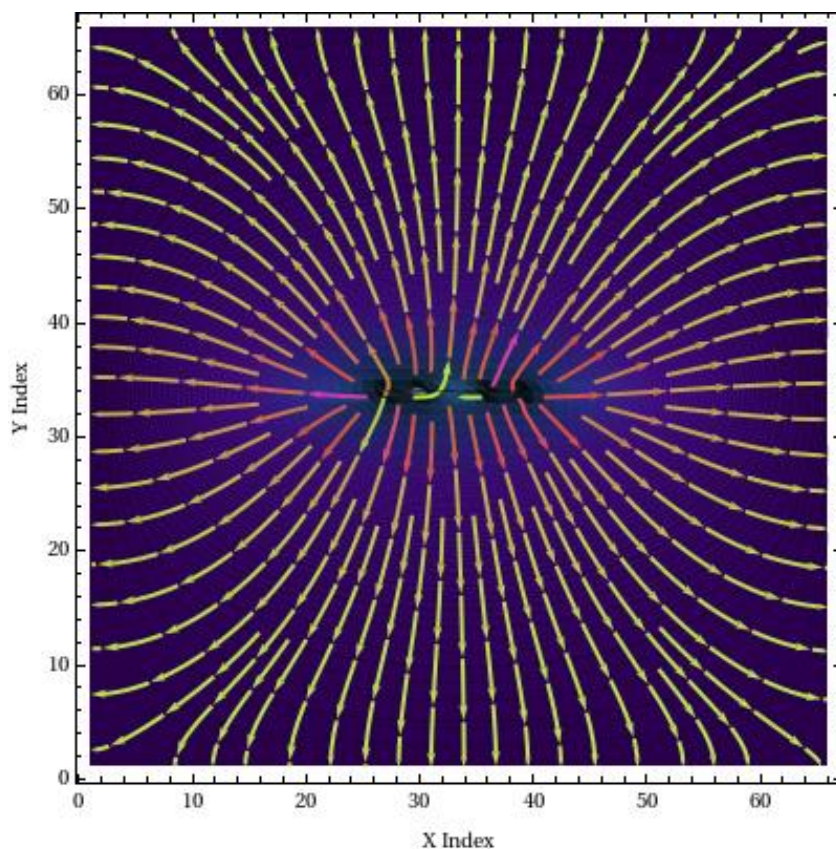


Figure 43 - 2D representation of the potentials and the field lines for Dataset 1 while holding the Z axis constant at position 34.

Graphical representation has covered the $\frac{1}{2}$ period and the 2 period case of the 3D representation of Dataset 1. The potentials and the field lines profiles have been rendered for the X, Y and Z axes, respectively. This completes the rendering of the N=5 Dataset 1 dataset. The following Dataset will show the acGNR5 Dataset 2 case.

The previous chapter showed the voltage potentials and field lines specific to the N=8 armchair nanoribbon. Seven sets of electron approximations were provided for N=5 armchair nanoribbon. In addition to slightly smaller graphene ribbon, the electron approximations provided for the N=5 graphene are for massive Dirac fermions, with a

band gap of ~64 meV. This chapter will cover those graphics. The order and format will follow that of Chapter 5.

Dataset 2

Dataset 2 will follow the same layout as Dataset 1. The following ρ values were used to create the second set of N=5 renderings. There is no observable difference in the 3D representations. Therefore, they will be omitted and the remaining Datasets will consist of the 2D representations.

Position in acGNR {X,Y,Z}	Calculated ρ Values For $k= 0.226502274177099$
{27,34,34}	0.24661223178846572
{30,34,34}	0.2533575229139936
{33,34,34}	$1.071988224937808 \times 10^{-7}$
{36,34,34}	0.25324070572563334
{39,34,34}	0.24678943237308476

Table 10 – acGNR positions of the ρ values and their associated calculated values for N=5 Dataset 2

As shown in Dataset 2, this Dataset will begin with the Y-Z plane, continue with the X-Z plan and wrap up with the X-Y plane.

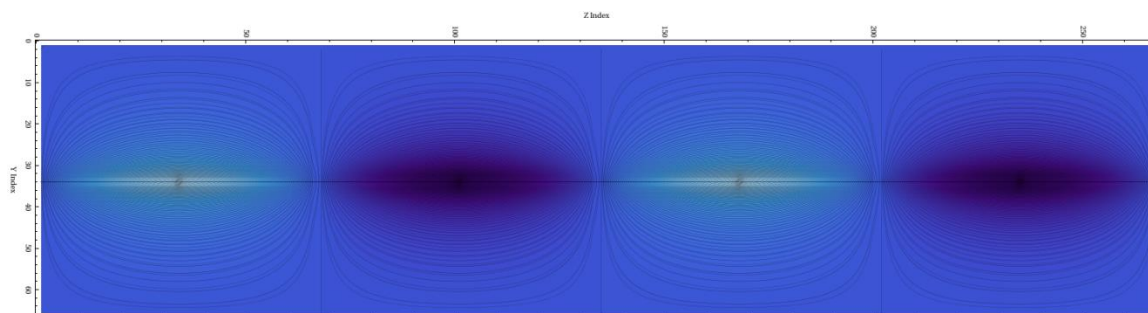


Figure 44 - 2D representation of the potential of the 2 dataset, holding the X axis constant at 34.

The above figure represents 2 full periods of the potentials calculated for the second dataset. This figure shows the profile of the Y and Z axes while holding X constant at 34. Even though the acGNR5 is practically 2D due to its atomically small thickness, a black line has been inserted in the figure above for perspective of the placement of the ribbon.

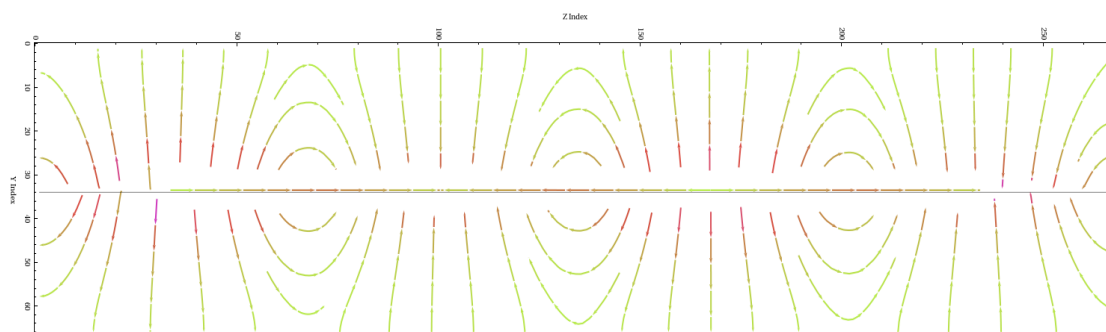


Figure 45 - 2D representation of the field lines of the 2 dataset, holding the X axis constant at 34.

The figure above represents the field lines calculated from the potentials associated with the Y and Z axes. Again this slice was taken holding the X axis constant at 34. This figure shows really clear direction lines in the field profile, along with the changes in magnitude. The following figure shows the field lines and the potentials for the Y and Z axes combined.

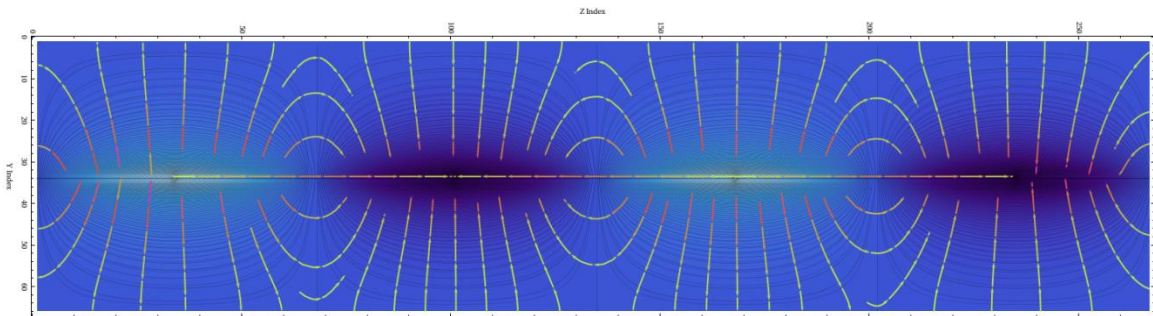


Figure 46 - 2D representation of the field lines and potentials calculated for the scGNR5 Dataset 2.

Looking closely at the above figure, you can see in the center of the positive potential cluster, the maximum value for ϕ that correlates to the maximum value of ρ listed in the tables in the chapter opening. The next set of slices will focus on the X and Z axes while holding the Y axis constant at 34.

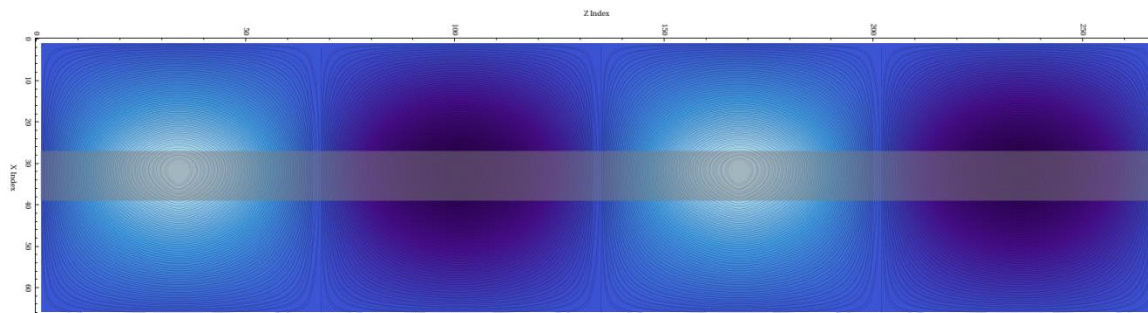


Figure 47 - 2D representation of the potentials calculated along the X and Z axes. This figure also shows the acGNR5 nanoribbon.

The graphic above is oriented with respect to the direction of propagation Z. This is consistent with the layout of the nanoribbon.

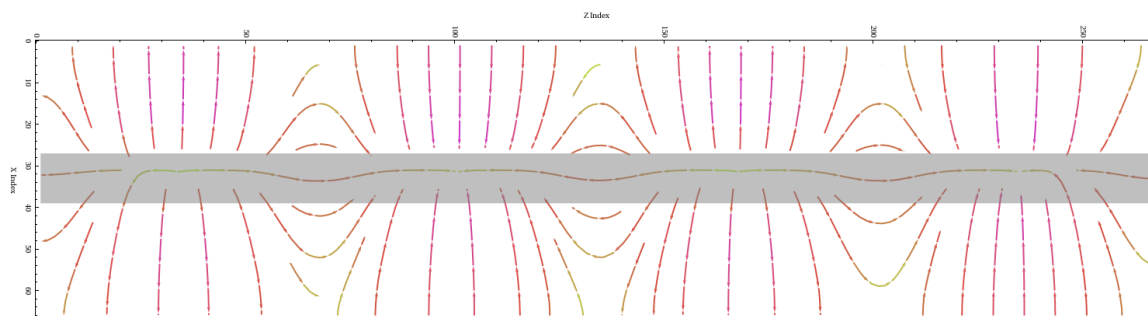


Figure 48 - 2D representation of the field lines for Dataset 2 holding the Y axis constant. Also shown here is the location of the nanoribbon

Shown here are the electric field lines. These field lines follow the same orientation as the potentials above. Notice the arrow heads are oriented with respect to

the electric field lines. Also, shown here, are changes in color in the field lines, representing a change in magnitude.

Overlaying to the two images to render the potentials and the field lines together results in:

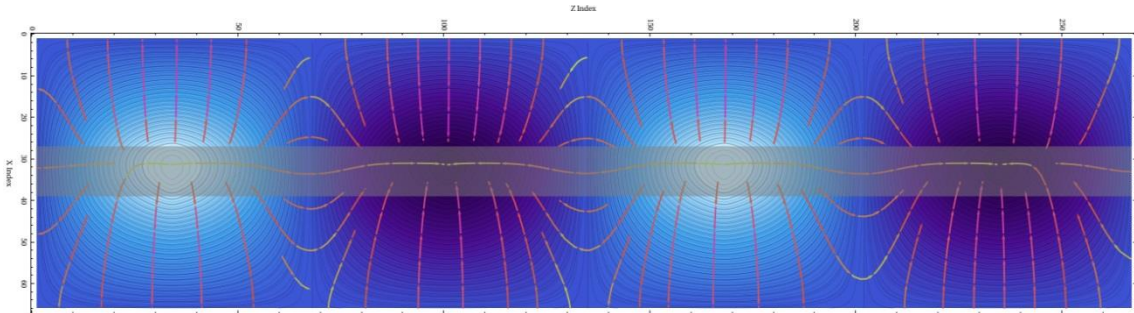


Figure 49 - 2D representation of the potentials and the field lines for Dataset 2 holding the Y axis constant.

The next set will focus on the X-Y plane. Taking a 2D slice out of Z_{34} results in the following potential profile:

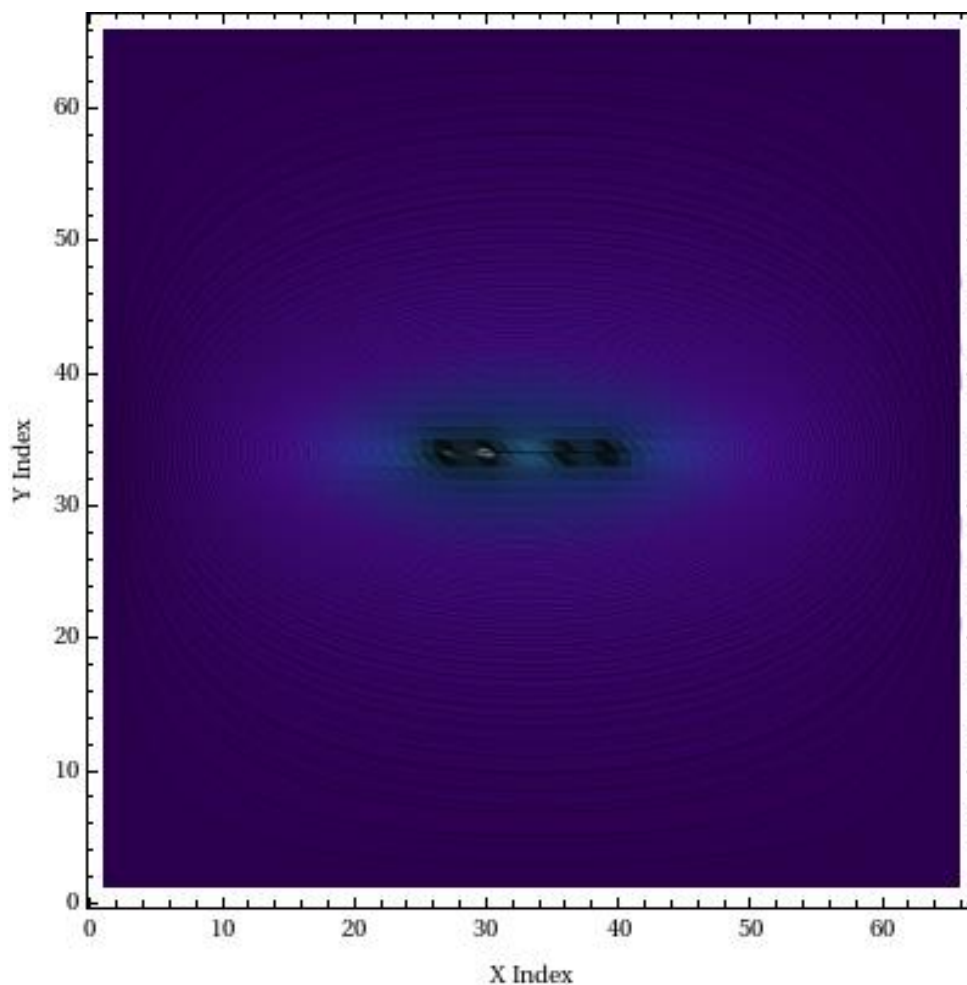


Figure 50 - 2D representation of the potentials for Dataset 2 while holding the Z axis constant. The black line running in the Y axis at position 34 is the acGNR5.

As expected, the potential profile follows the width of the acGNR5. Notice here the gap in the center of the ribbon at $X=32$. This is consistent with the initial ρ values.

The same slice with respect to the field lines look like:

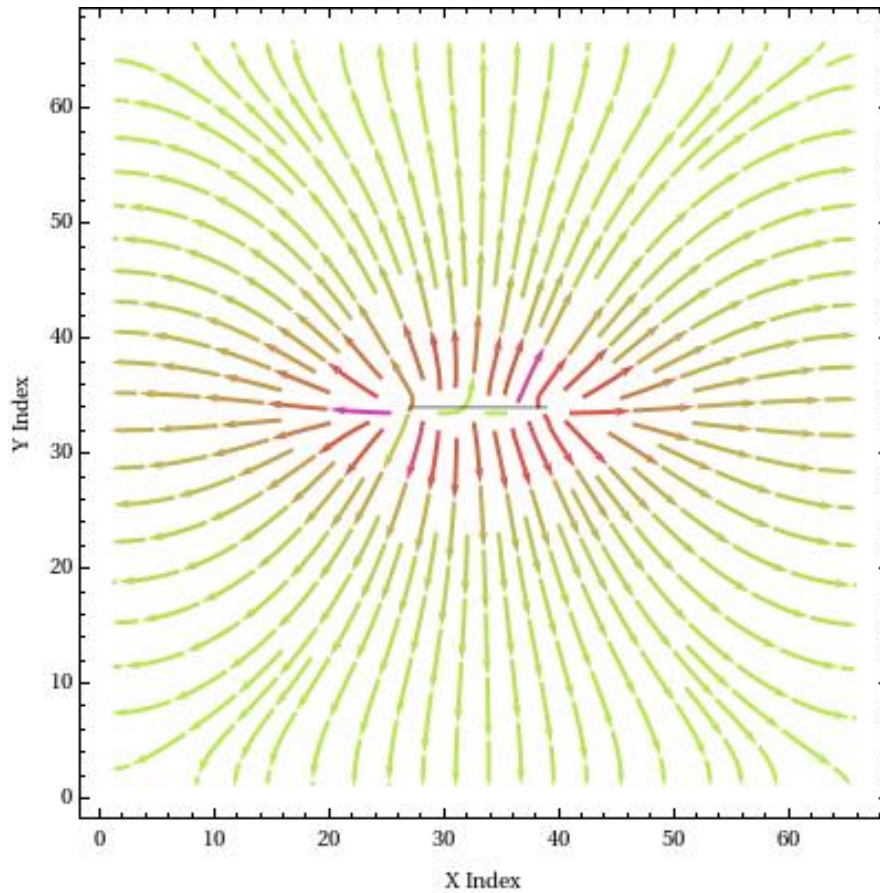


Figure 51 - 2D representation of the field lines for Dataset 2 while holding the Z axis constant.

Again, it is very clear as to the direction of the field lines, indicating that the associated potentials are positive. Rendering the potentials and the field lines for the Z axis results in the following figure:

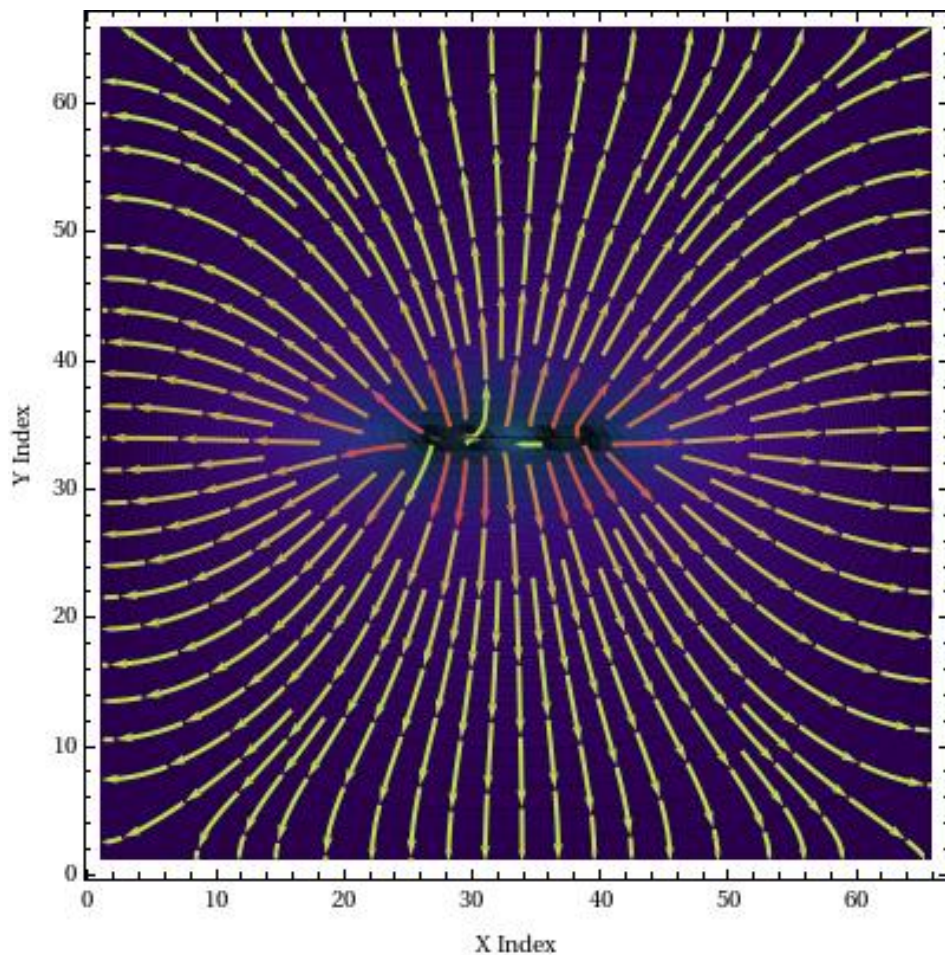


Figure 52 - 2D representation of the potentials and the field lines for Dataset 2 while holding the Z axis constant at position 34.

The potentials and the field lines profiles have been rendered for the X, Y and Z axes, respectively. This completes the rendering of the N=5 Dataset 2 dataset. The following Dataset will show the acGNR5 Dataset 3 case.

Dataset 3

Dataset 3 will follow the same layout as Dataset 2. The following ρ values were used to create the 3rd set of N=5 renderings. There is no observable difference in the 3D representations; therefore they will be omitted here. The remaining Datasets will consist of the 2D representations.

Position in acGNR {X,Y,Z}	Calculated ρ Values For k= 0.4283939625140709
{27,34,34}	0.246805772087055
{30,34,34}	0.2535912571939378
{33,34,34}	$4.143083154085276 \times 10^{-7}$
{36,34,34}	0.25287642583515113
{39,34,34}	0.24672613057554033

Table 11 – acGNR positions of the ρ values and their associated calculated values for N=5 Dataset 3

As shown in Dataset 2, this Dataset will begin with the Y-Z plane, continue with the X-Z plan and wrap up with the X-Y plane.

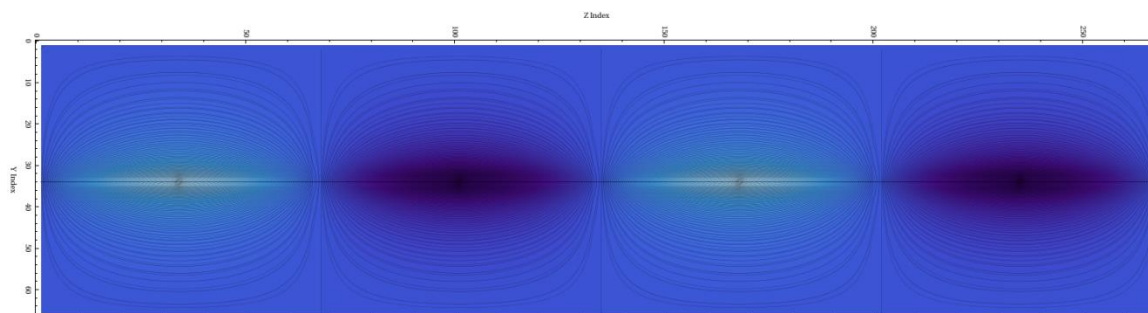


Figure 53 - 2D representation of the potential of the 3rd dataset, holding the X axis constant at 34.

The above figure represents 2 full periods of the potentials calculated for the second dataset. This figure shows the profile of the Y and Z axes while holding X constant at 34. Even though the acGNR5 is practically 2D due to its atomically small thickness, a black line has been inserted in the figure above for perspective of the placement of the ribbon.

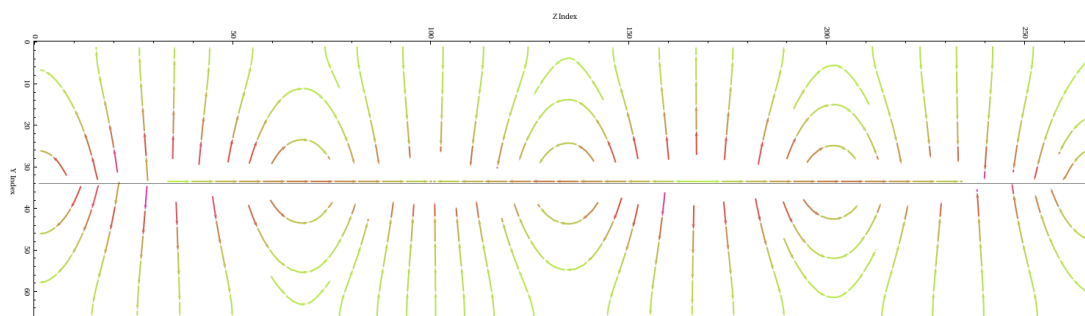


Figure 54 - 2D representation of the field lines of the 3rd dataset, holding the X axis constant at 34.

The figure above represents the field lines calculated from the potentials associated with the Y and Z axes. Again this slice was taken holding the X axis constant at 34. This figure shows really clear direction lines in the field profile, along with the changes in magnitude. The following figure shows the field lines and the potentials for the Y and Z axes combined.

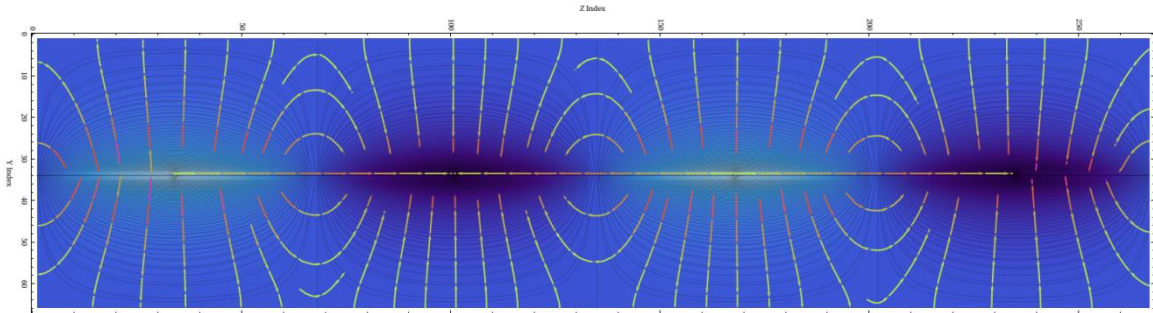


Figure 55 - 2D representation of the field lines and potentials calculated for the scGNR5 Dataset 3.

Looking closely at the above figure, you can see in the center of the positive potential cluster, the maximum value for ϕ that correlates to the maximum value of ρ listed in the tables in the Dataset opening. The next set of slices will focus on the X and Z axes while holding the Y axis constant at 34.

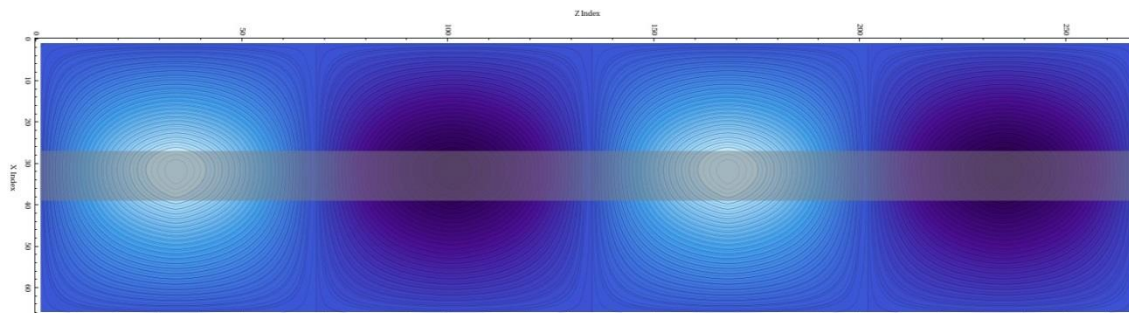


Figure 56 - 2D representation of the potentials calculated along the X and Z axes. This figure also shows the acGNR5 nanoribbon.

The graphic above is oriented with respect to the direction of propagation Z.

This is consistent with the layout of the nanoribbon.

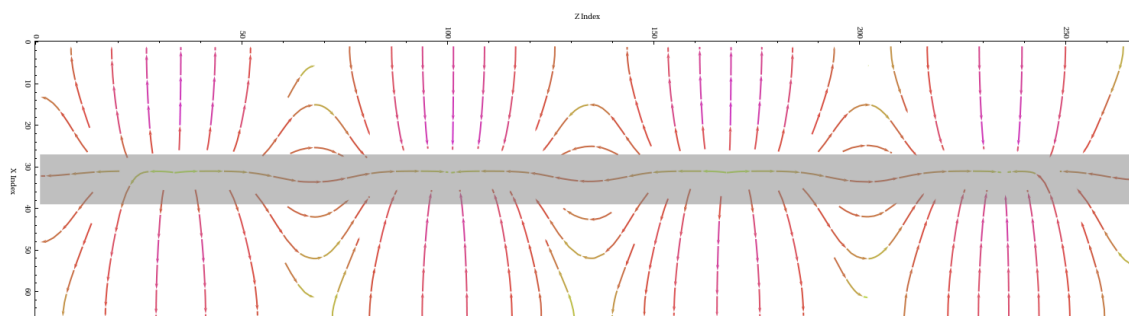


Figure 57 - 2D representation of the field lines for Dataset 3 holding the Y axis constant. Also shown here is the location of the nanoribbon

Shown here are the electric field lines. These field lines follow the same orientation as the potentials above. Notice the arrow heads are oriented with respect to the electric field lines. Also, shown here, are changes in color in the field lines, representing a change in magnitude.

Overlaying to the two images to render the potentials and the field lines together results in:

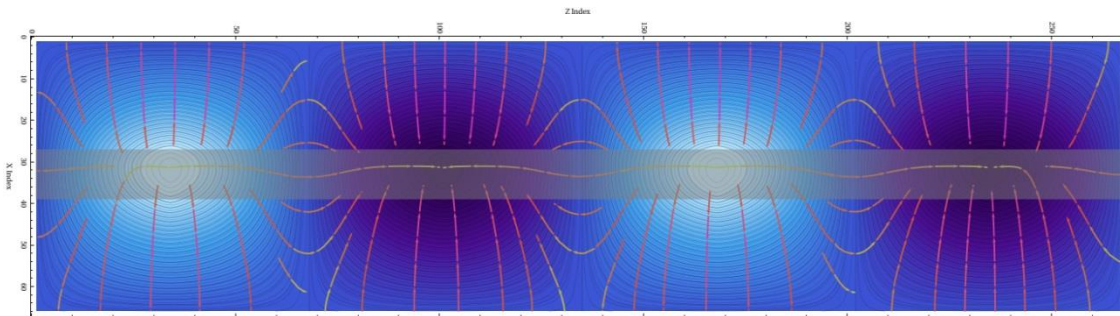


Figure 58 - 2D representation of the potentials and the field lines for Dataset 3 holding the Y axis constant.

The next set will focus on the X-Y plane. Taking a 2D slice out of Z_{34} results in the following potential profile:

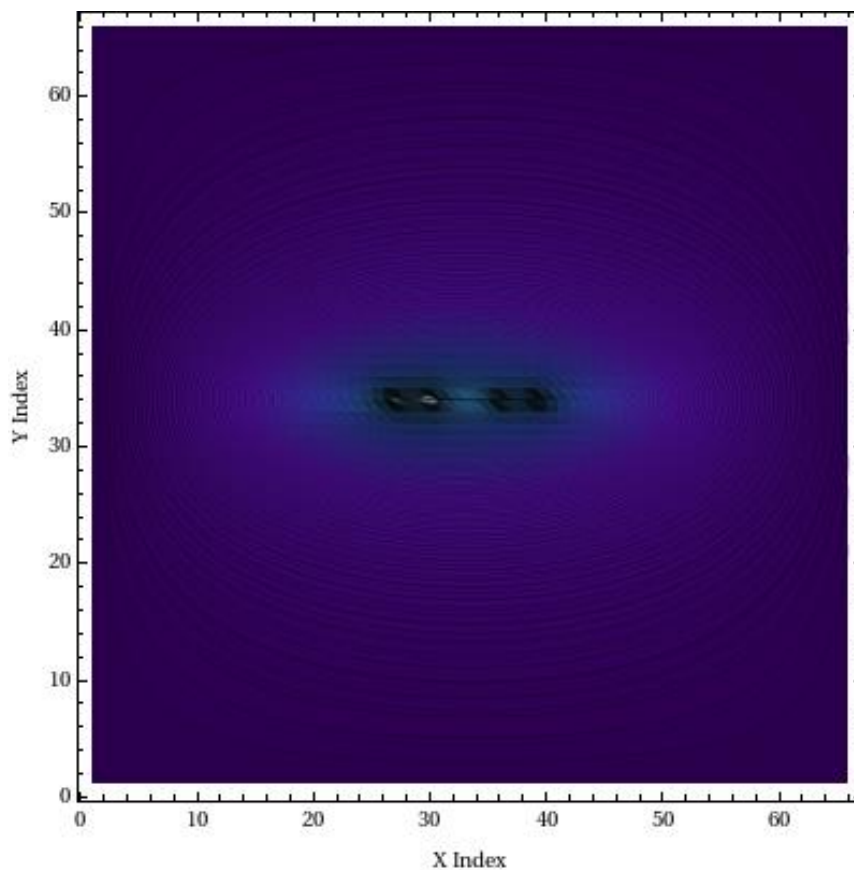


Figure 59 - 2D representation of the potentials for Dataset 3 while holding the Z axis constant. The black line running in the Y axis at position 34 is the acGNR5.

As expected, the potential profile follows the width of the acGNR5. Notice here the gap in the center of the ribbon at X=32. This is consistent with the initial ρ values.

The same slice with respect to the field lines look like:

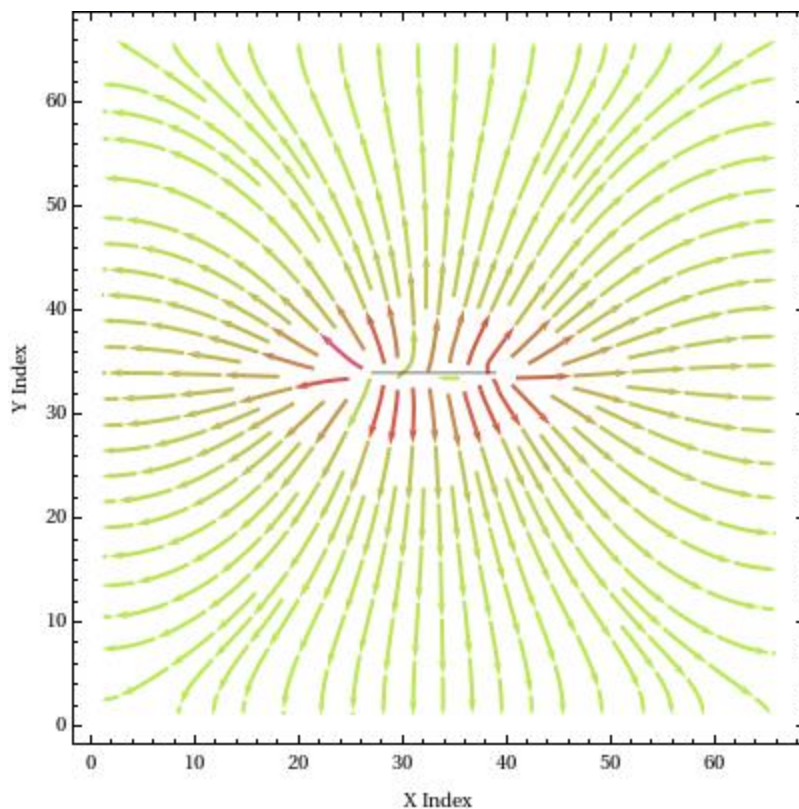


Figure 60 - 2D representation of the field lines for Dataset 3 while holding the Z axis constant.

Again, it is very clear as to the direction of the field lines, indicating that the associated potentials are positive. Rendering the potentials and the field lines for the Z axis results in the following figure:

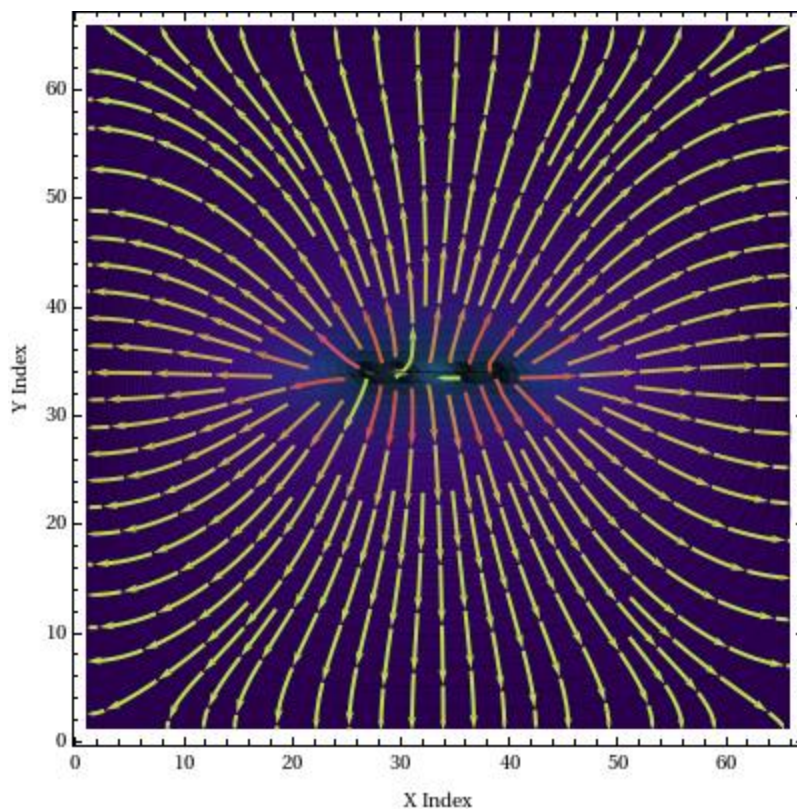


Figure 61 - 2D representation of the potentials and the field lines for Dataset 3 while holding the Z axis constant at position 34.

The potentials and the field lines profiles have been rendered for the X, Y and Z axes, respectively. This completes the rendering of the N=5 Dataset 3 dataset. The following Dataset will show the acGNR5 Dataset 4 case.

Dataset 4

The following ρ values were used to create the 4th set of N=5 renderings. There is no observable difference in the 3D representations; therefore they will be omitted here.

The remaining Datasets will consist of the 2D representations.

Position in acGNR {X,Y,Z}	Calculated ρ Values For $k= 0.12745922776435492$
{27,34,34}	0.24618485838218201
{30,34,34}	0.2533317467170475
{33,34,34}	$3.284342581334505 \times 10^{-8}$
{36,34,34}	0.25375918559809657
{39,34,34}	0.2467241764592481

Table 12 – acGNR positions of the ρ values and their associated calculated values for N=5 Dataset 4

As shown previous, this Dataset will begin with the Y-Z plane, continue with the X-Z plan and wrap up with the X-Y plane.

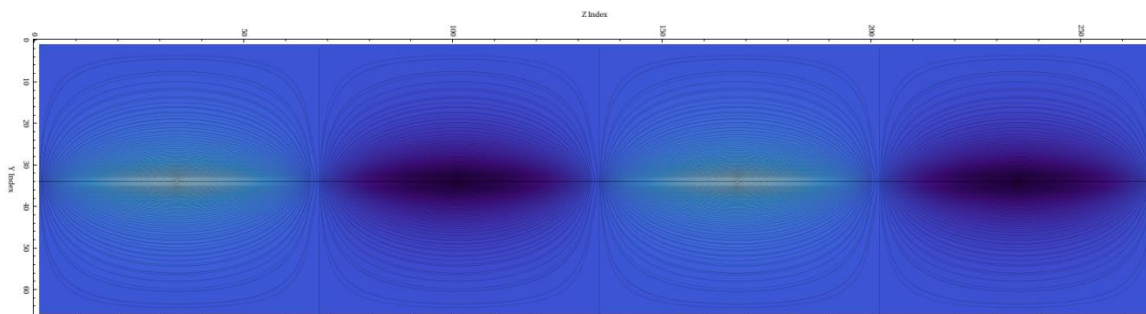


Figure 62 - 2D representation of the potential of the 4th dataset, holding the X axis constant at 34.

The above figure represents 2 full periods of the potentials calculated for the second dataset. This figure shows the profile of the Y and Z axes while holding X

constant at 34. Even though the acGNR5 is practically 2D due to its atomically small thickness, a black line has been inserted in the figure above for perspective of the placement of the ribbon.

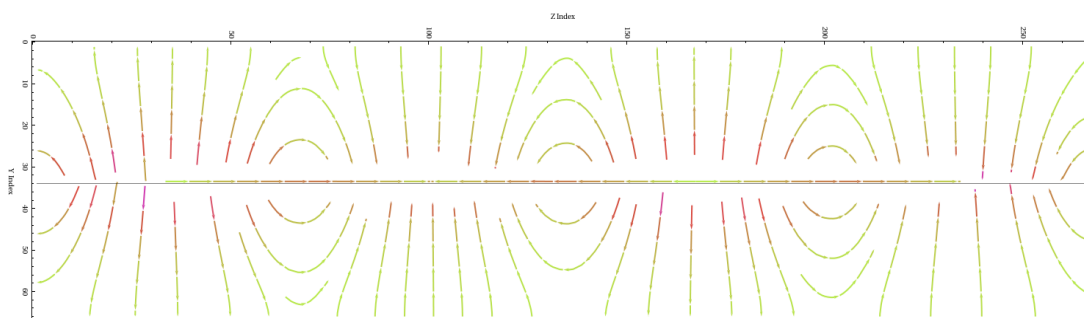


Figure 63 - 2D representation of the field lines of the 4th dataset, holding the X axis constant at 34.

The figure above represents the field lines calculated from the potentials associated with the Y and Z axes. Again this slice was taken holding the X axis constant at 34. This figure shows really clear direction lines in the field profile, along with the changes in magnitude. The following figure shows the field lines and the potentials for the Y and Z axes combined.

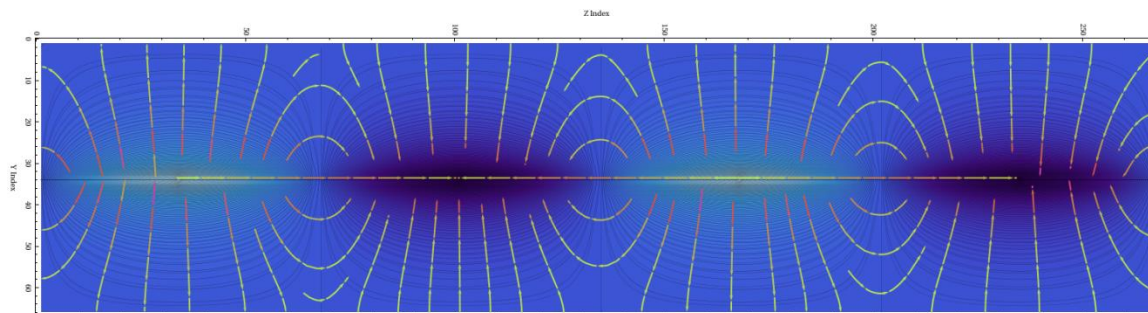


Figure 64 - 2D representation of the field lines and potentials calculated for the scGNR5 Dataset 4.

Looking closely at the above figure, you can see in the center of the positive potential cluster, the maximum value for ϕ that correlates to the maximum value of ρ listed in the tables in the Dataset opening. The next set of slices will focus on the X and Z axes while holding the Y axis constant at 34.

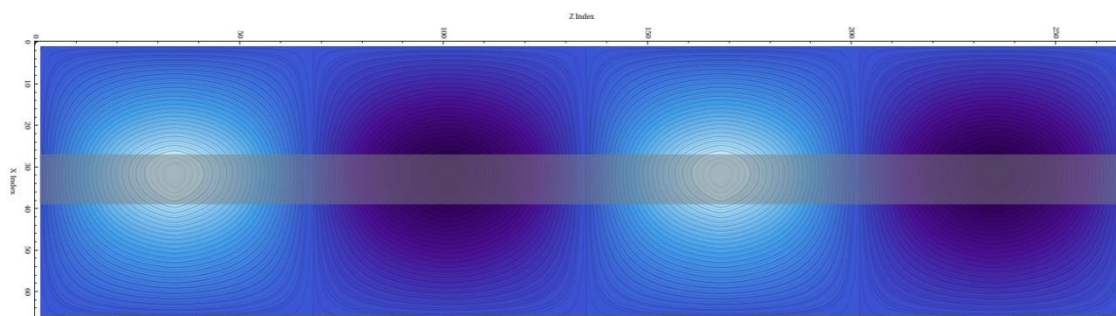


Figure 65 - 2D representation of the potentials calculated along the X and Z axes. This figure also shows the acGNR5 nanoribbon.

The graphic above is oriented with respect to the direction of propagation Z. This is consistent with the layout of the nanoribbon.

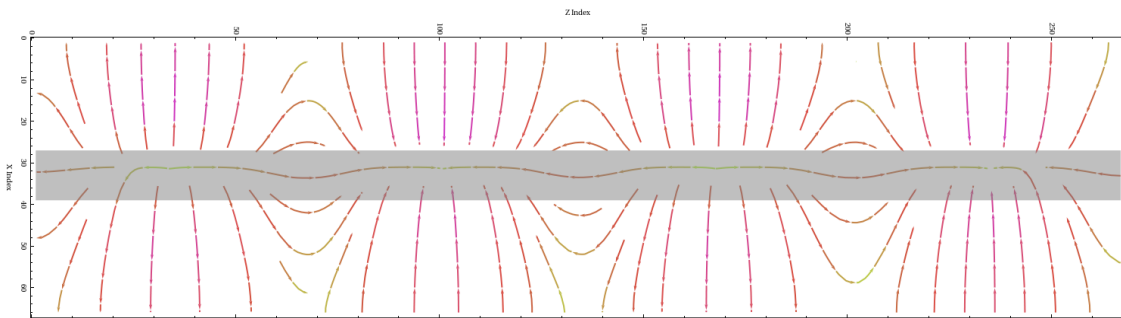


Figure 66 - 2D representation of the field lines for Dataset 4 holding the Y axis constant. Also shown here is the location of the nanoribbon

Shown here are the electric field lines. These field lines follow the same orientation as the potentials above. Notice the arrow heads are oriented with respect to the electric field lines. Also, shown here, are changes in color in the field lines, representing a change in magnitude.

Overlaying to the two images to render the potentials and the field lines together results in:

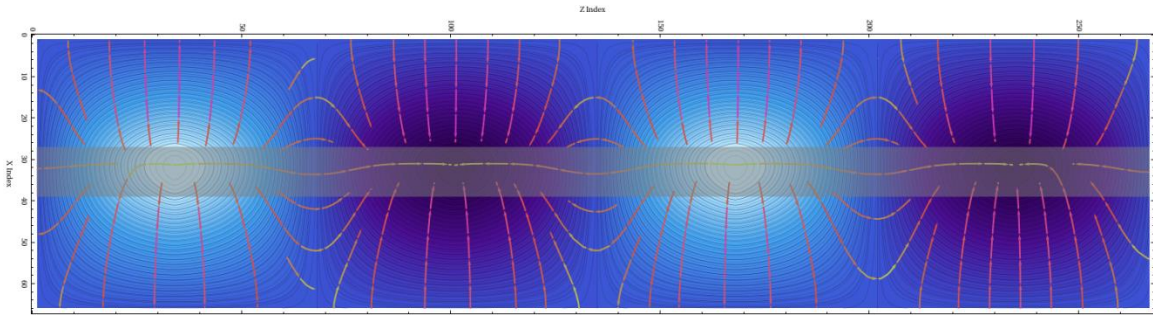


Figure 67 - 2D representation of the potentials and the field lines for Dataset 4 holding the Y axis constant.

The next set will focus on the X-Y plane. Taking a 2D slice out of Z_{34} results in the following potential profile:

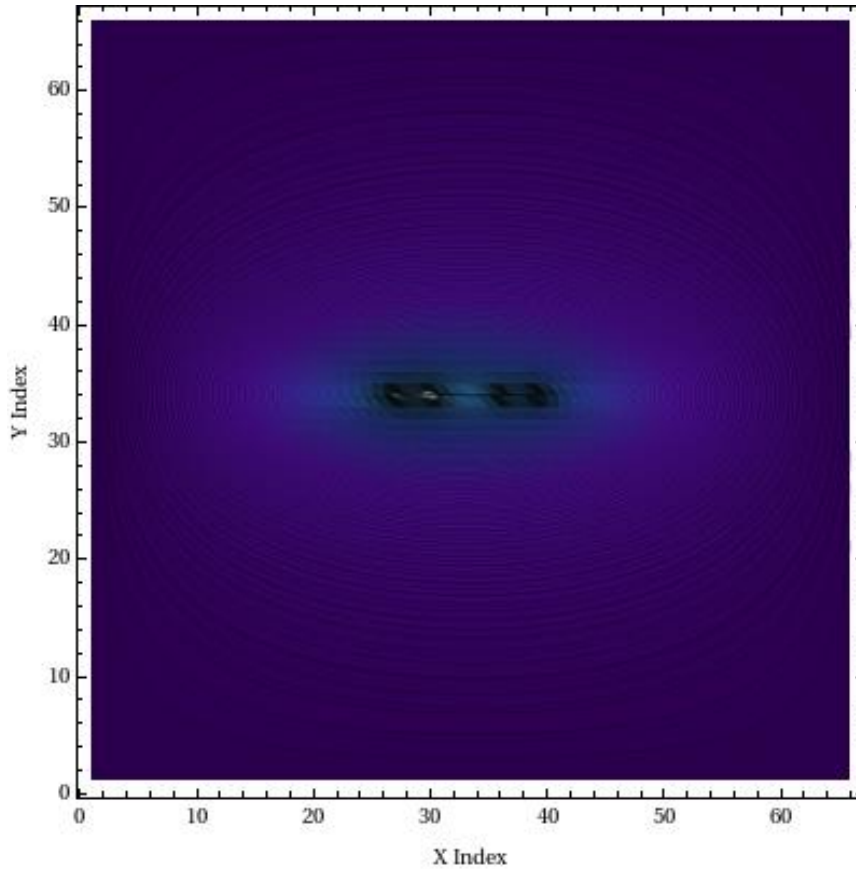


Figure 68 - 2D representation of the potentials for Dataset 4 while holding the Z axis constant. The black line running in the Y axis at position 34 is the acGNR5.

As expected, the potential profile follows the width of the acGNR5. Notice here the gap in the center of the ribbon at $X=32$. This is consistent with the initial ρ values.

The same slice with respect to the field lines look like:

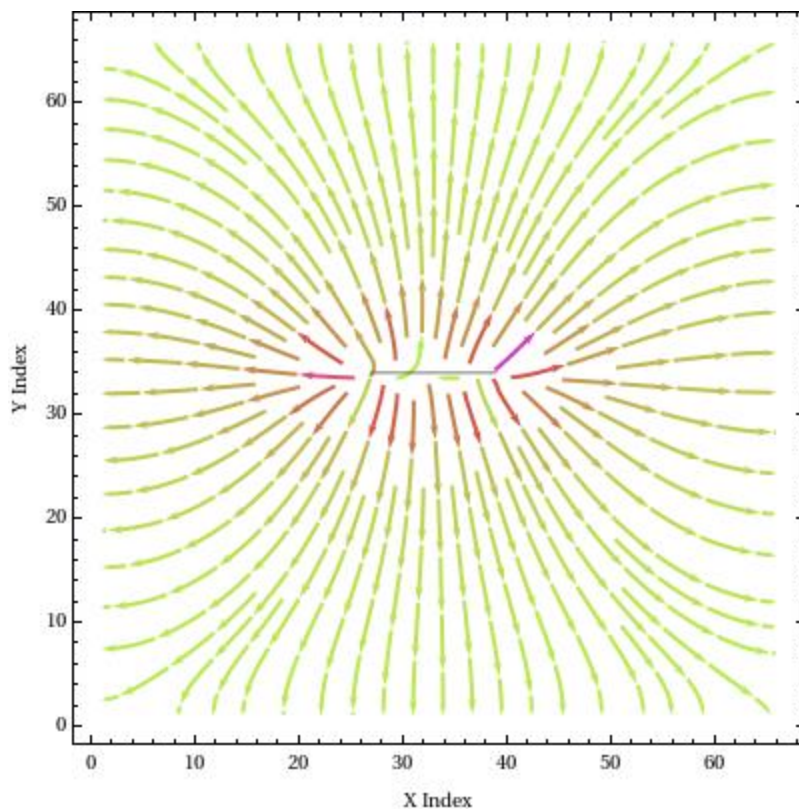


Figure 69 - 2D representation of the field lines for Dataset 4 while holding the Z axis constant.

Again, it is very clear as to the direction of the field lines, indicating that the associated potentials are positive. Rendering the potentials and the field lines for the Z axis results in the following figure:

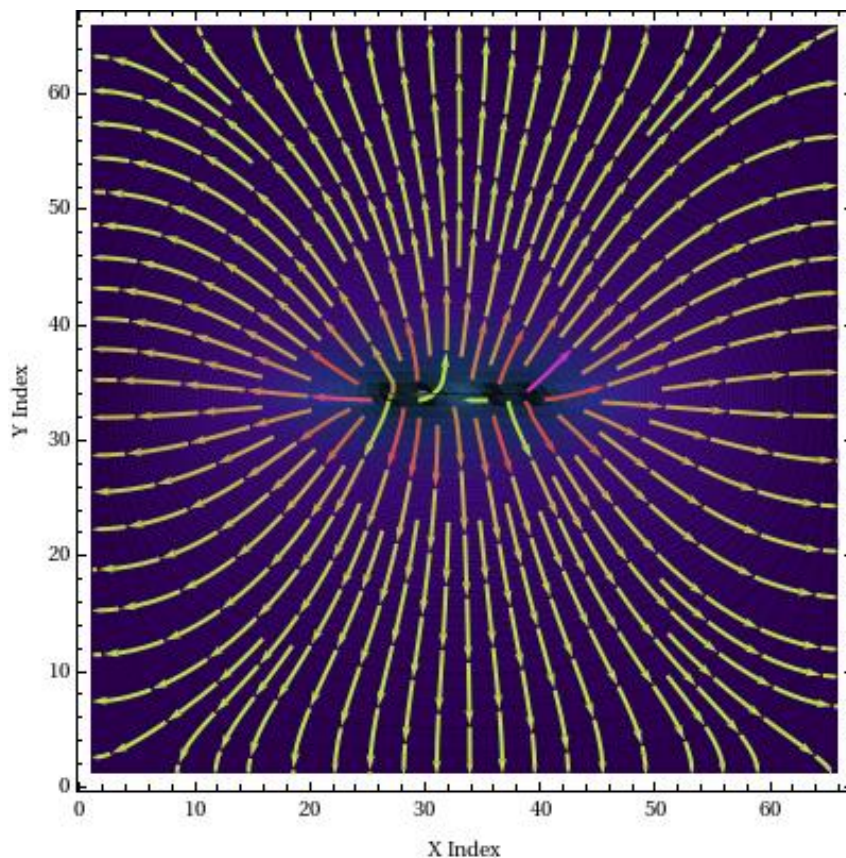


Figure 70 - 2D representation of the potentials and the field lines for Dataset 4 while holding the Z axis constant at position 34.

The potentials and the field lines profiles have been rendered for the X, Y and Z axes, respectively. This completes the rendering of the N=5 Dataset 4 dataset. The following Dataset will show the acGNR5 Dataset 5 case.

Dataset 5

The following ρ values were used to create the 5th set of N=5 renderings. There is no observable difference in the 3D representations; therefore they will be omitted here.

The remaining Datasets will consist of the 2D representations.

Position in acGNR {X,Y,Z}	Calculated ρ Values For k= 0.6312158039812097
{27,34,34}	0.2468055480210266
{30,34,34}	0.253861957845413
{33,34,34}	$9.046884173404786 \times 10^{-7}$
{36,34,34}	0.2527136070496206
{39,34,34}	0.24661798239552246

Table 13 – acGNR positions of the ρ values and their associated calculated values for N=5 Dataset 5

As shown previous, this Dataset will begin with the Y-Z plane, continue with the X-Z plan and wrap up with the X-Y plane.

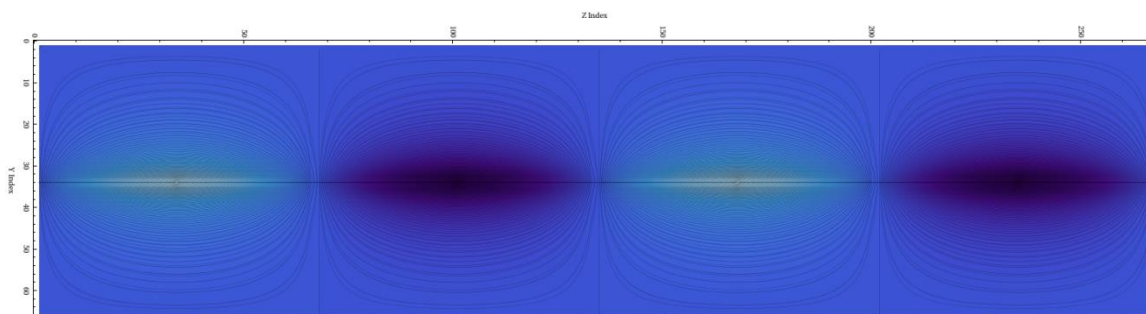


Figure 71 - 2D representation of the potential of the 5th dataset, holding the X axis constant at 34.

The above figure represents 2 full periods of the potentials calculated for the second dataset. This figure shows the profile of the Y and Z axes while holding X constant at 34. Even though the acGNR5 is practically 2D due to its atomically small thickness, a black line has been inserted in the figure above for perspective of the placement of the ribbon.

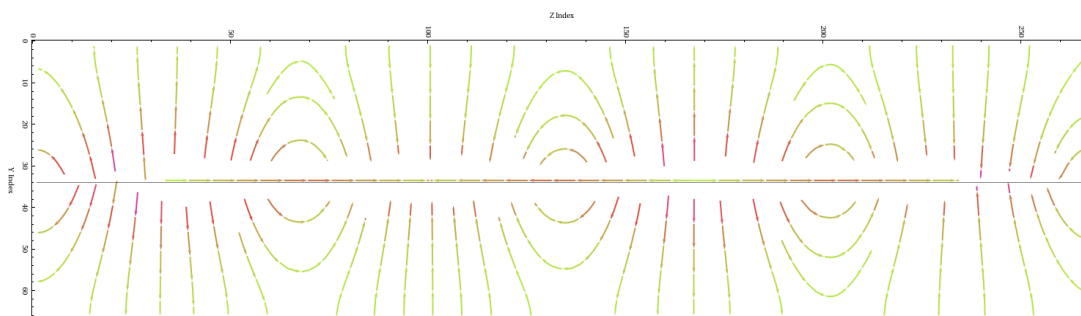


Figure 72 - 2D representation of the field lines of the 5th dataset, holding the X axis constant at 34.

The figure above represents the field lines calculated from the potentials associated with the Y and Z axes. Again this slice was taken holding the X axis constant at 34. This figure shows really clear direction lines in the field profile, along with the changes in magnitude. The following figure shows the field lines and the potentials for the Y and Z axes combined.

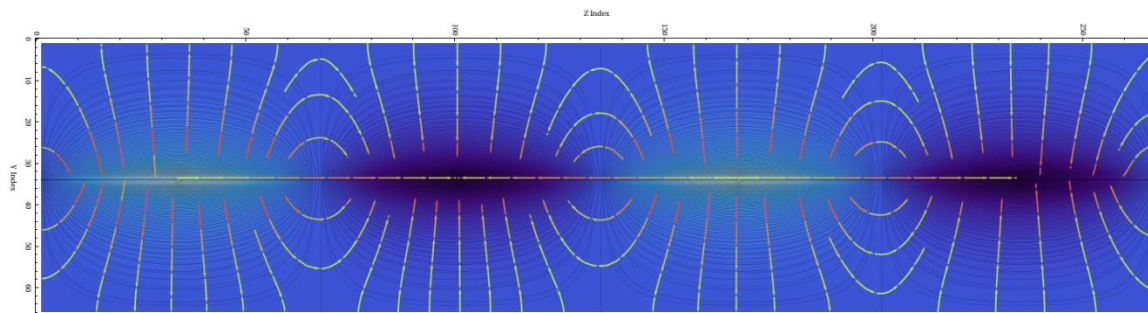


Figure 73 - 2D representation of the field lines and potentials calculated for the scGNR5 Dataset 5.

Looking closely at the above figure, you can see in the center of the positive potential cluster, the maximum value for ϕ that correlates to the maximum value of ρ listed in the table in the Dataset opening. The next set of slices will focus on the X and Z axes while holding the Y axis constant at 34.

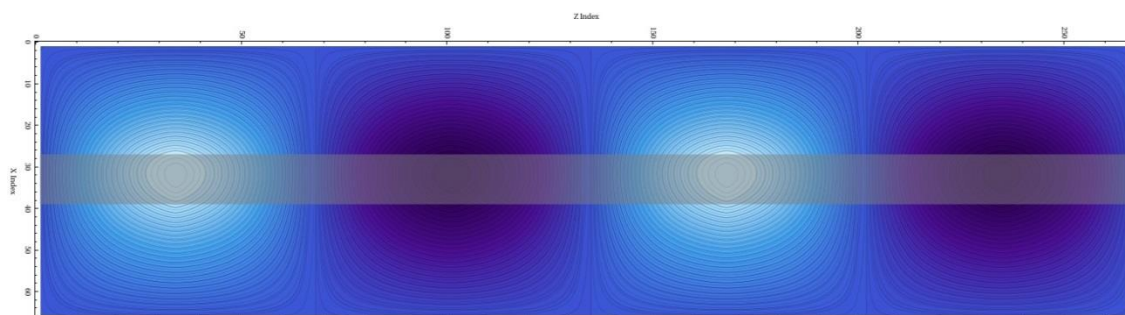


Figure 74 - 2D representation of the potentials calculated along the X and Z axes. This figure also shows the acGNR5 nanoribbon.

The graphic above is oriented with respect to the direction of propagation Z.

This is consistent with the layout of the nanoribbon.

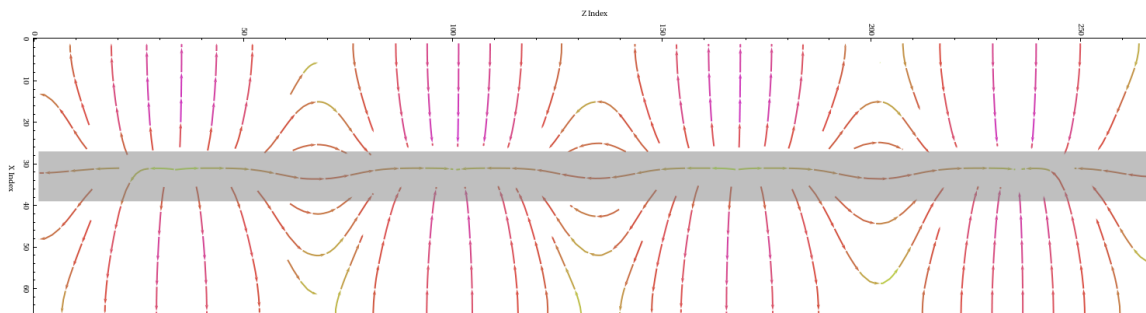


Figure 75 - 2D representation of the field lines for Dataset 5 holding the Y axis constant. Also shown here is the location of the nanoribbon

Shown here are the electric field lines. These field lines follow the same orientation as the potentials above. Notice the arrow heads are oriented with respect to the electric field lines. Also, shown here, are changes in color in the field lines, representing a change in magnitude. Overlaying to the two images to render the potentials and the field lines together results in:

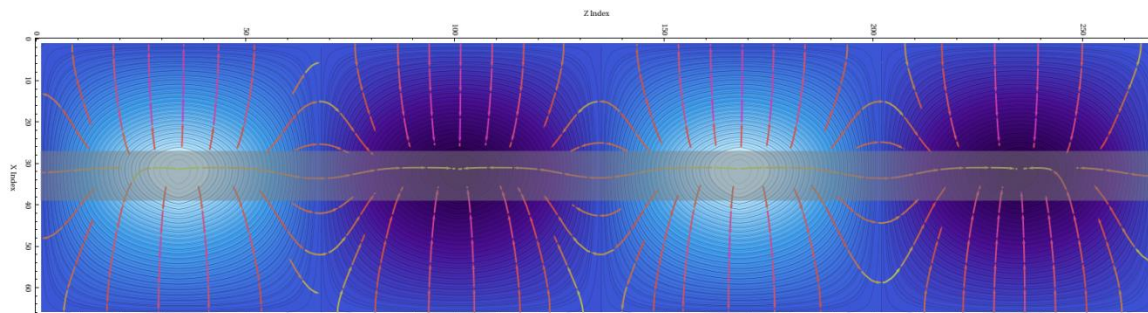


Figure 76 - 2D representation of the potentials and the field lines for Dataset 5 holding the Y axis constant.

The next set will focus on the X-Y plane. Taking a 2D slice out of Z_{34} results in the following potential profile:

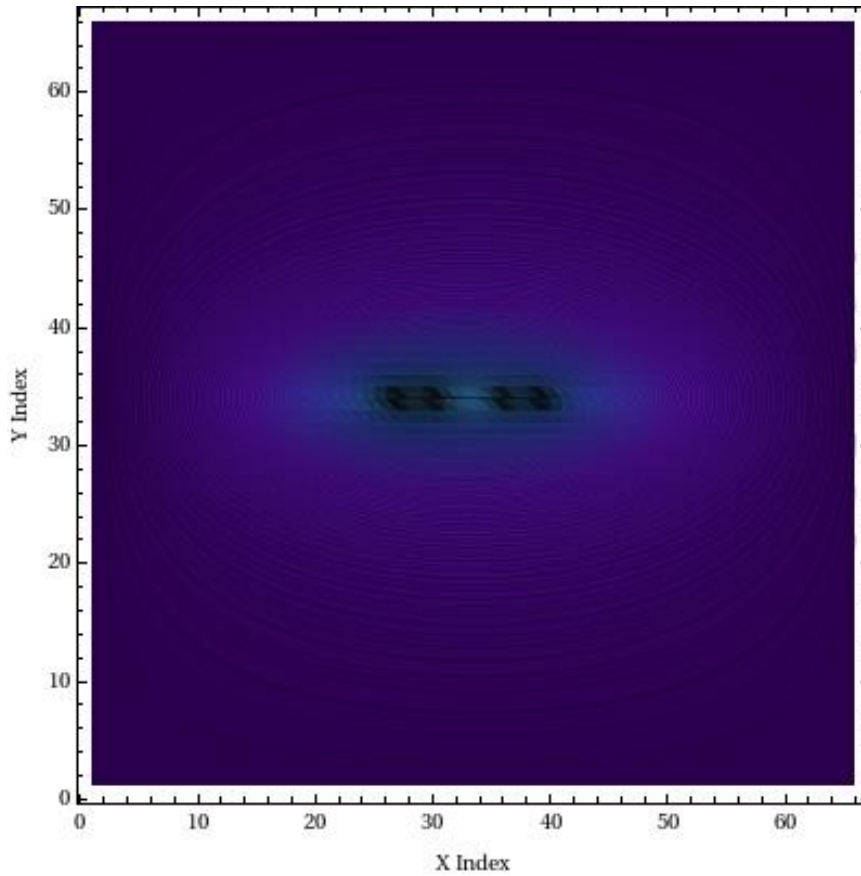


Figure 77 - 2D representation of the potentials for Dataset 5 while holding the Z axis constant. The black line running in the Y axis at position 34 is the acGNR5.

As expected, the potential profile follows the width of the acGNR5. Notice here the gap in the center of the ribbon at $X=32$. This is consistent with the initial ρ values.

The same slice with respect to the field lines look like:

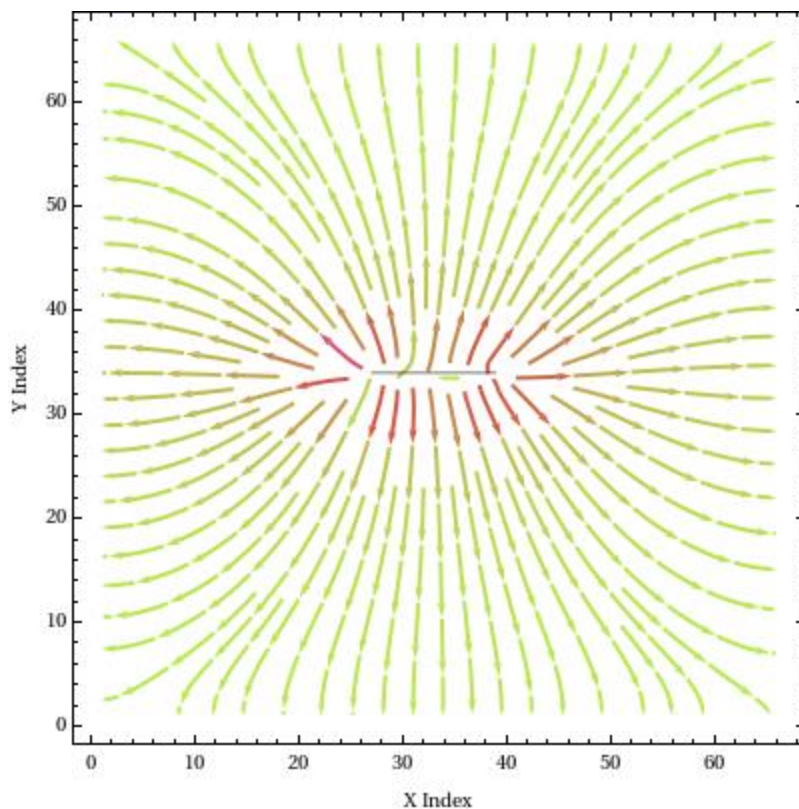


Figure 78 - 2D representation of the field lines for Dataset 5 while holding the Z axis constant.

Again, it is very clear as to the direction of the field lines, indicating that the associated potentials are positive. Rendering the potentials and the field lines for the Z axis results in the following figure:

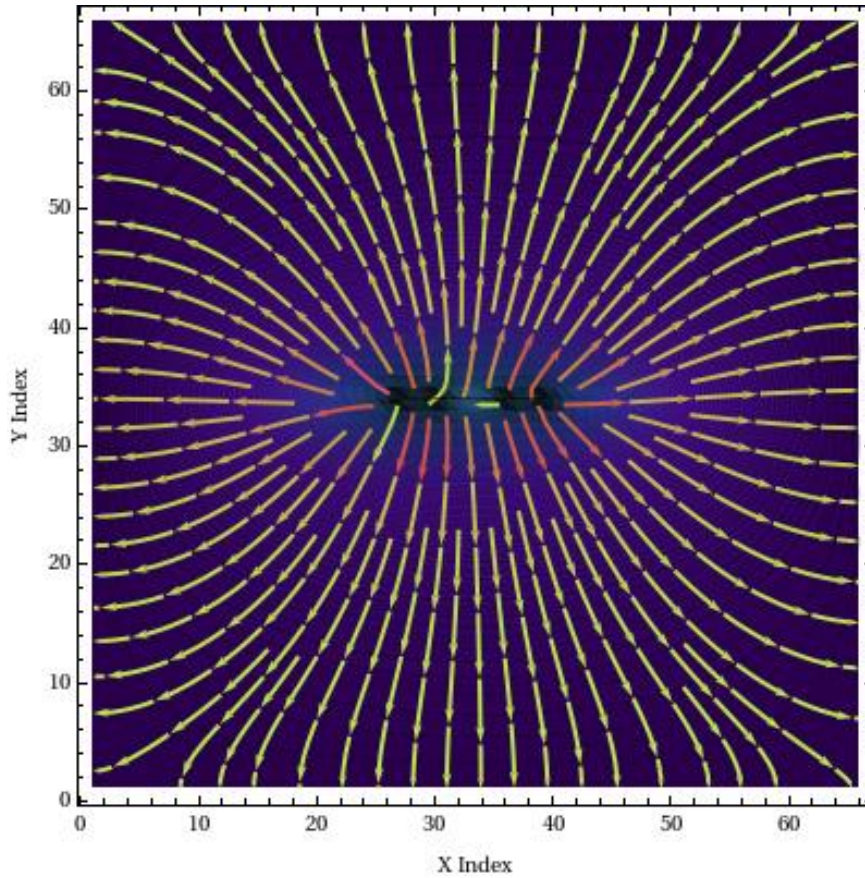


Figure 79 - 2D representation of the potentials and the field lines for Dataset 5 while holding the Z axis constant at position 34.

The potentials and the field lines profiles have been rendered for the X, Y and Z axes, respectively. This completes the rendering of the N=5 Dataset 5 dataset. The following Dataset will show the acGNR5 Dataset 6 case.

Dataset 6

The following ρ values were used to create the 6th set of N=5 renderings. There is no observable difference in the 3D representations; therefore they will be omitted here.

The remaining Datasets will consist of the 2D representations.

Position in acGNR {X,Y,Z}	Calculated ρ Values For k= -0.01079837154688825
{27,34,34}	0.250082229246683
{30,34,34}	0.25205536323516947
{33,34,34}	$1.990616704563155 \times 10^{-8}$
{36,34,34}	0.249909489167656
{39,34,34}	0.24795289844432453

Table 14 – acGNR positions of the ρ values and their associated calculated values for N=5 Dataset 6

As shown previous, this Dataset will begin with the Y-Z plane, continue with the X-Z plan and wrap up with the X-Y plane.

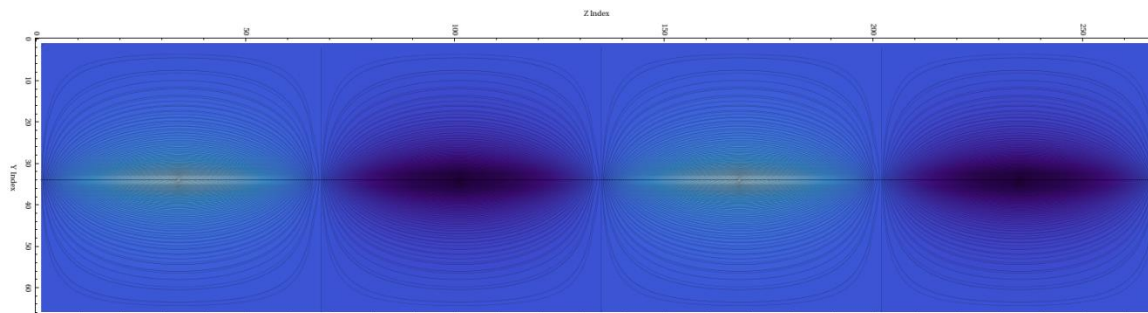


Figure 80 - 2D representation of the potential of the 6th dataset, holding the X axis constant at 34.

The above figure represents 2 full periods of the potentials calculated for the second dataset. This figure shows the profile of the Y and Z axes while holding X constant at 34. Even though the acGNR5 is practically 2D due to its atomically small thickness, a black line has been inserted in the figure above for perspective of the placement of the ribbon.

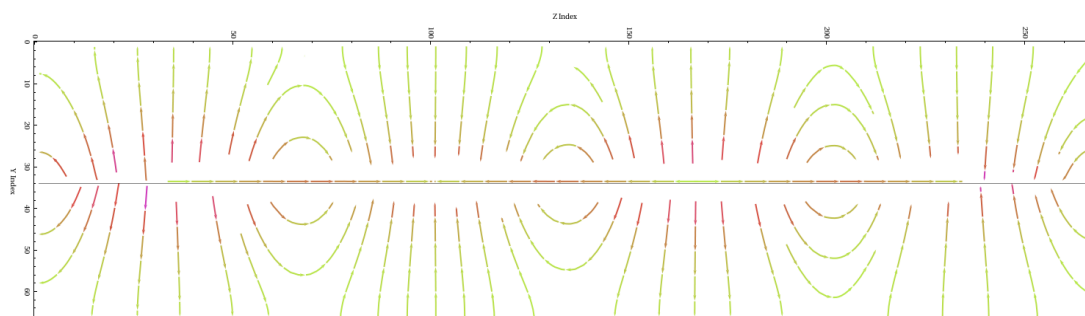


Figure 81 - 2D representation of the field lines of the 6th dataset, holding the X axis constant at 34.

The figure above represents the field lines calculated from the potentials associated with the Y and Z axes. Again this slice was taken holding the X axis constant at 34. This figure shows really clear direction lines in the field profile, along with the changes in magnitude. The following figure shows the field lines and the potentials for the Y and Z axes combined.

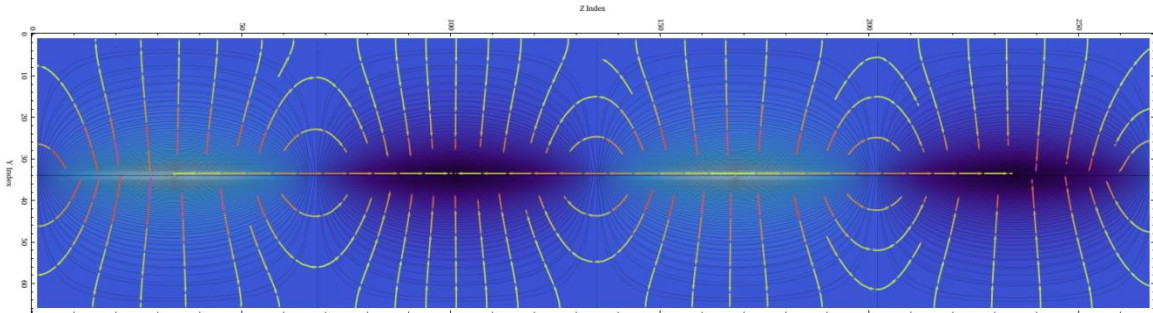


Figure 82 - 2D representation of the field lines and potentials calculated for the scGNR5 Dataset 6.

Looking closely at the above figure, you can see in the center of the positive potential cluster, the maximum value for ϕ that correlates to the maximum value of ρ listed in the table in the Dataset opening. The next set of slices will focus on the X and Z axes while holding the Y axis constant at 34.

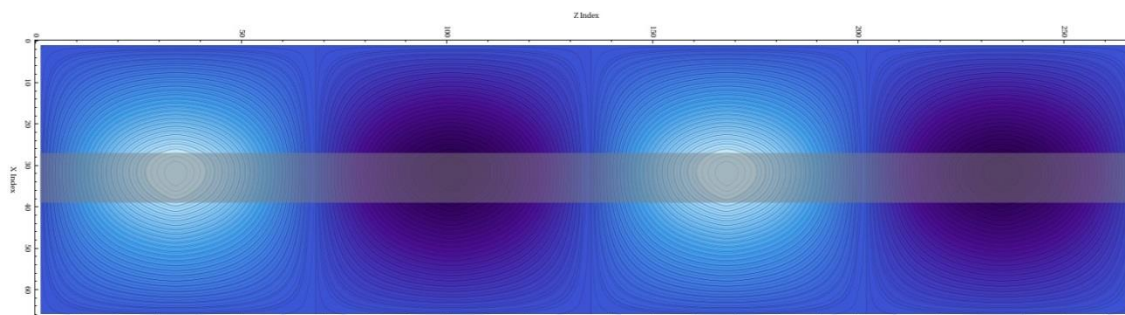


Figure 83 - 2D representation of the potentials calculated along the X and Z axes. This figure also shows the acGNR5 nanoribbon.

The graphic above is oriented with respect to the direction of propagation Z.

This is consistent with the layout of the nanoribbon.

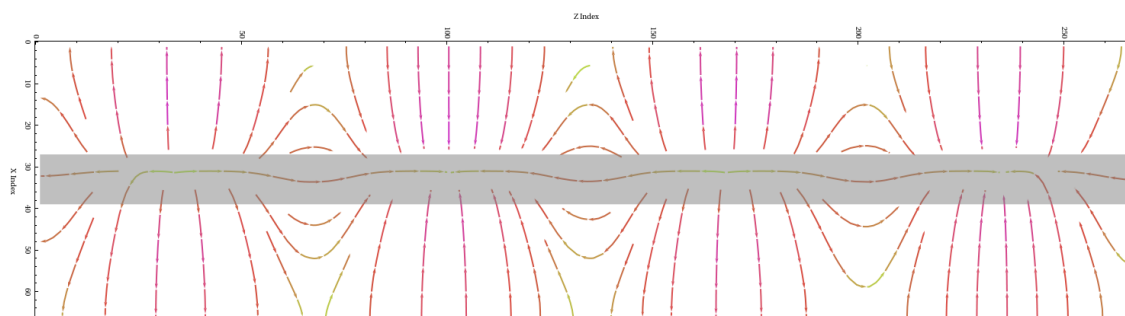


Figure 84 - 2D representation of the field lines for Dataset 6 holding the Y axis constant. Also shown here is the location of the nanoribbon

Shown here are the electric field lines. These field lines follow the same orientation as the potentials above. Notice the arrow heads are oriented with respect to the electric field lines. Also, shown here, are changes in color in the field lines,

representing a change in magnitude. Overlaying to the two images to render the potentials and the field lines together results in:

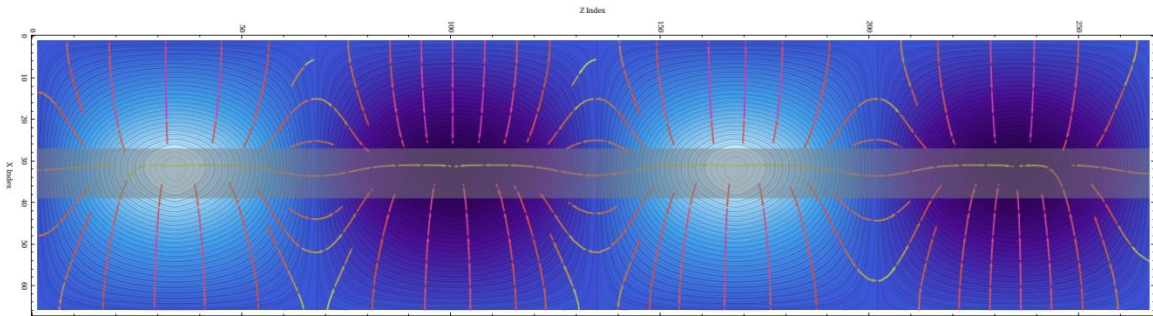


Figure 85 - 2D representation of the potentials and the field lines for Dataset 6 holding the Y axis constant.

The next set will focus on the X-Y plane. Taking a 2D slice out of Z_{34} results in the following potential profile:

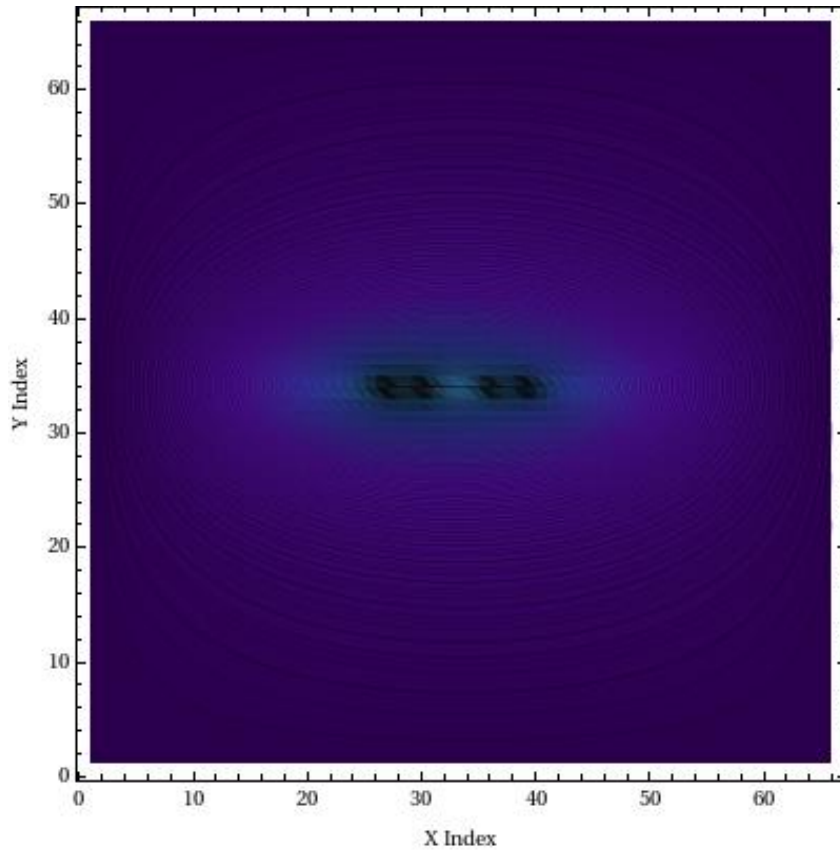


Figure 86 - 2D representation of the potentials for Dataset 6 while holding the Z axis constant. The black line running in the Y axis at position 34 is the acGNR5.

As expected, the potential profile follows the width of the acGNR5. Notice here the gap in the center of the ribbon at $X=32$. This is consistent with the initial ρ values. The same slice with respect to the field lines look like:

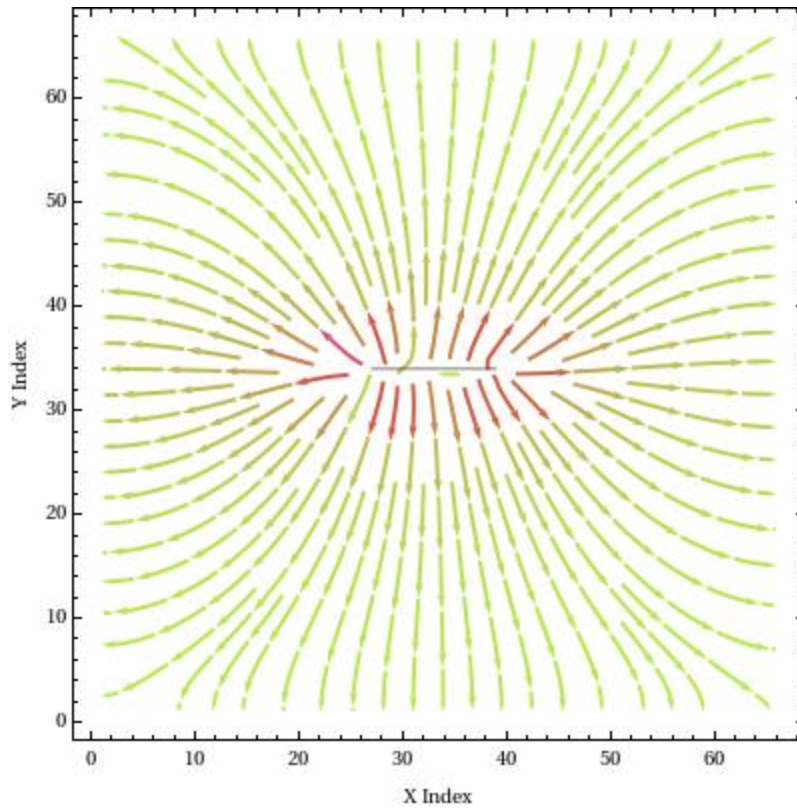


Figure 87 - 2D representation of the field lines for Dataset 6 while holding the Z axis constant.

Again, it is very clear as to the direction of the field lines, indicating that the associated potentials are positive. Rendering the potentials and the field lines for the Z axis results in the following figure:

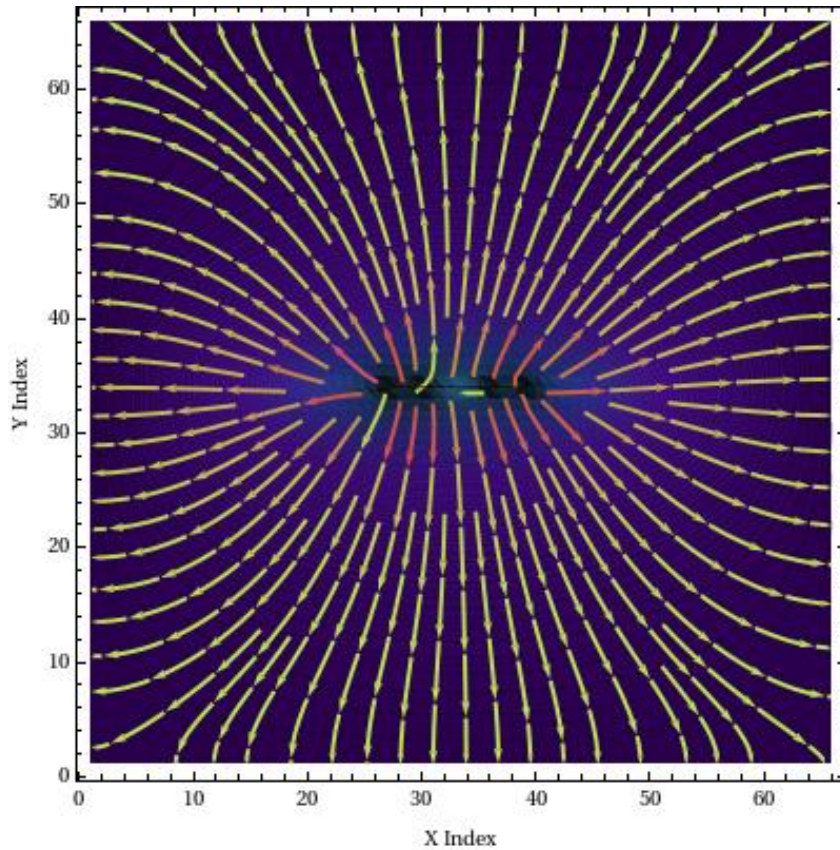


Figure 88 - 2D representation of the potentials and the field lines for Dataset 6 while holding the Z axis constant at position 34.

The potentials and the field lines profiles have been rendered for the X, Y and Z axes, respectively. This completes the rendering of the N=5 Dataset 5 dataset. The following Dataset will show the acGNR5 Dataset 7 case.

Dataset 7

The following ρ values were used to create the 7th set of N=5 renderings. There is no observable difference in the 3D representations; therefore they will be omitted here. The remaining Datasets will consist of the 2D representations.

Position in acGNR {X,Y,Z}	Calculated ρ Values For k= -0.08496814621621751
{27,34,34}	0.247986734498357
{30,34,34}	0.2525295211809991
{33,34,34}	$5.719688545090018 \times 10^{-8}$
{36,34,34}	0.25210531017401683
{39,34,34}	0.24737837694974155

Table 15 – acGNR positions of the ρ values and their associated calculated values for N=5 Dataset 7

As shown previous, this Dataset will begin with the Y-Z plane, continue with the X-Z plan and wrap up with the X-Y plane.

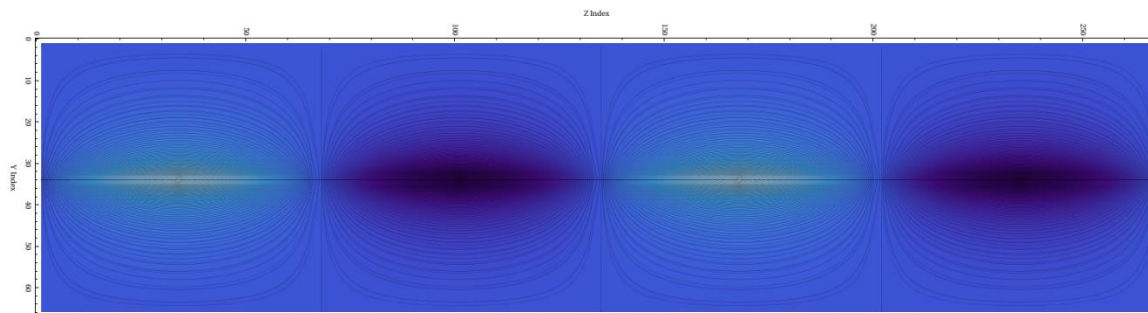


Figure 89 - 2D representation of the potential of the 7th dataset, holding the X axis constant at 34.

The above figure represents 2 full periods of the potentials calculated for the second dataset. This figure shows the profile of the Y and Z axes while holding X constant at 34. Even though the acGNR5 is practically 2D due to its atomically small thickness, a black line has been inserted in the figure above for perspective of the placement of the ribbon.

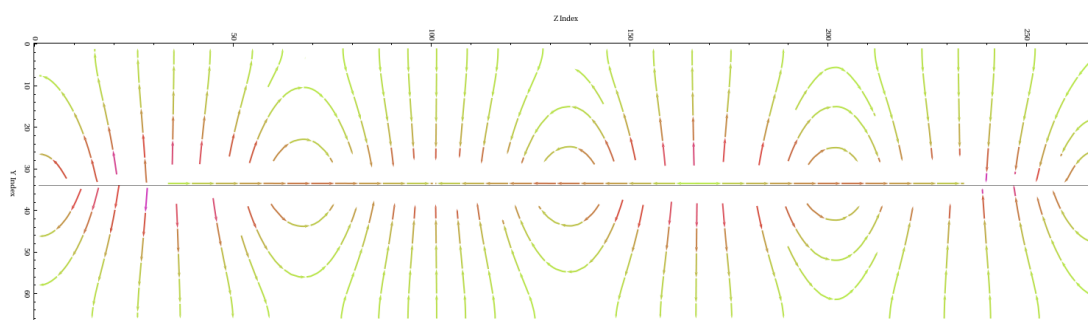


Figure 90 - 2D representation of the field lines of the 7th dataset, holding the X axis constant at 34.

The figure above represents the field lines calculated from the potentials associated with the Y and Z axes. Again this slice was taken holding the X axis constant at 34. This figure shows really clear direction lines in the field profile, along with the changes in magnitude. The following figure shows the field lines and the potentials for the Y and Z axes combined.

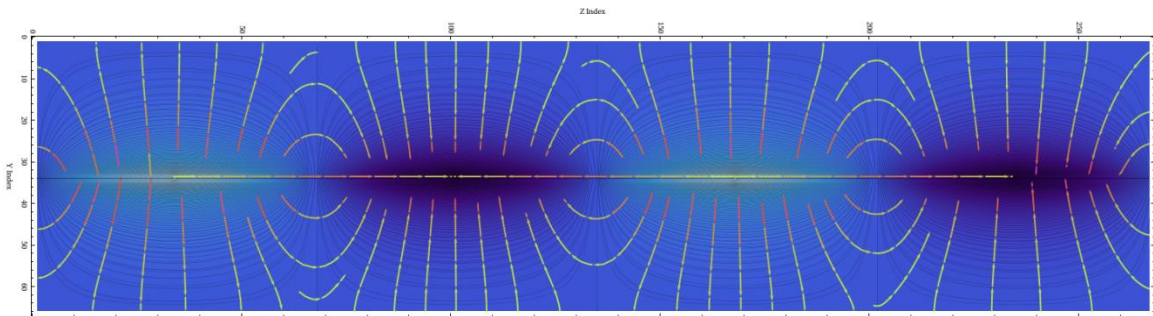


Figure 91 - 2D representation of the field lines and potentials calculated for the scGNR5 Dataset 7.

Looking closely at the above figure, you can see in the center of the positive potential cluster, the maximum value for ϕ that correlates to the maximum value of ρ listed in the table in the Dataset opening. The next set of slices will focus on the X and Z axes while holding the Y axis constant at 34.

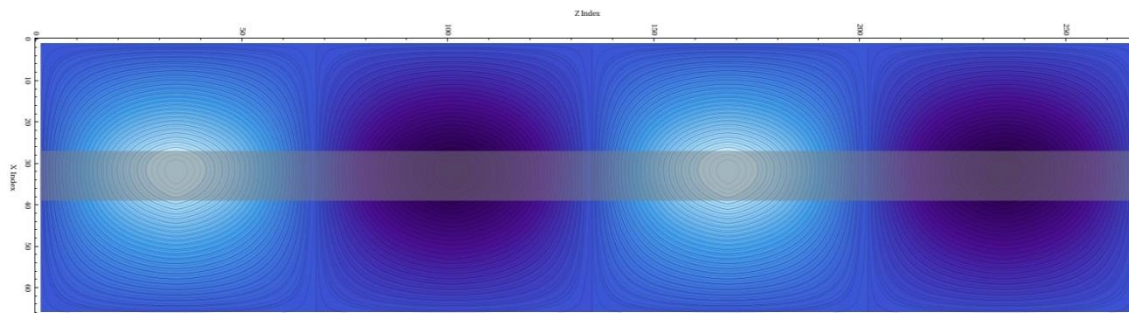


Figure 92 - 2D representation of the potentials calculated along the X and Z axes. This figure also shows the acGNR5 nanoribbon.

The graphic above is oriented with respect to the direction of propagation Z. This is consistent with the layout of the nanoribbon.

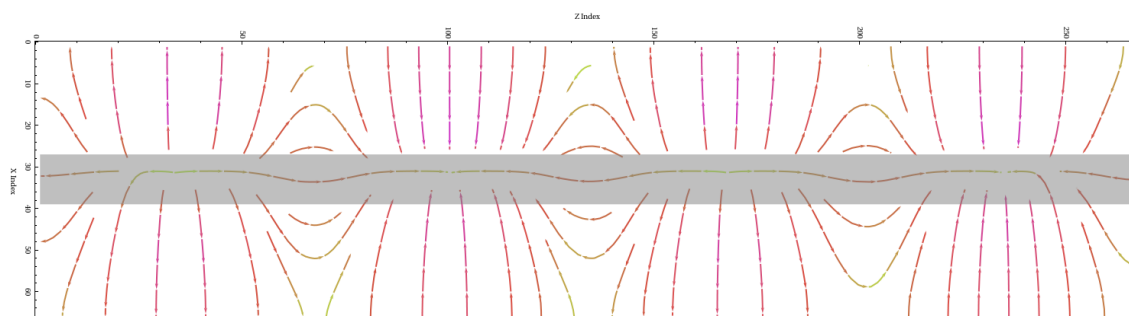


Figure 93 - 2D representation of the field lines for Dataset 7 holding the Y axis constant. Also shown here is the location of the nanoribbon

Shown here are the electric field lines. These field lines follow the same orientation as the potentials above. Notice the arrow heads are oriented with respect to the electric field lines. Also, shown here, are changes in color in the field lines, representing a change in

magnitude. Overlaying to the two images to render the potentials and the field lines together results in:

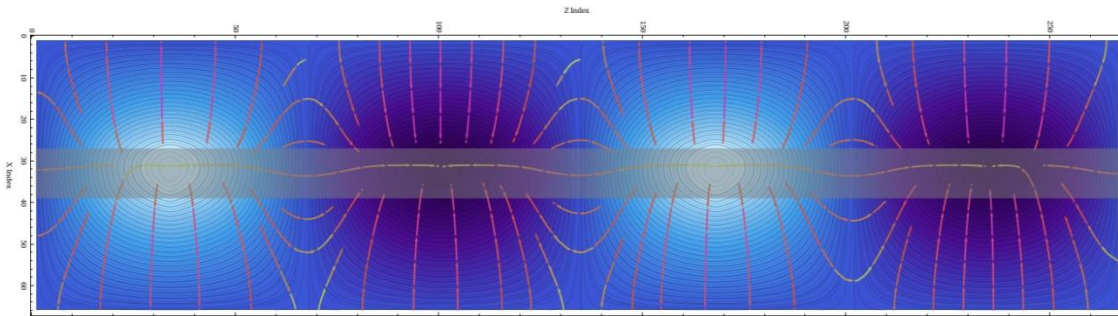


Figure 94 - 2D representation of the potentials and the field lines for Dataset 7 holding the Y axis constant.

The next set will focus on the X-Y plane. Taking a 2D slice out of Z_{34} results in the following potential profile:

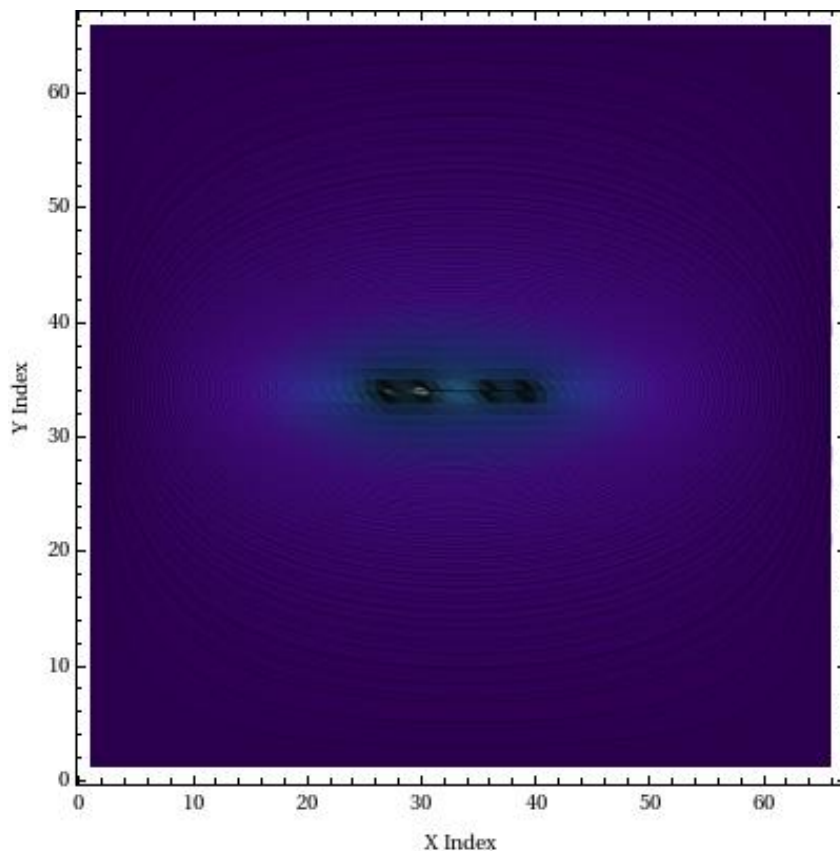


Figure 95 - 2D representation of the potentials for Dataset 7 while holding the Z axis constant. The black line running in the Y axis at position 34 is the acGNR5.

As expected, the potential profile follows the width of the acGNR5. Notice here the gap in the center of the ribbon at $X=32$. This is consistent with the initial ρ values.

The same slice with respect to the field lines look like:

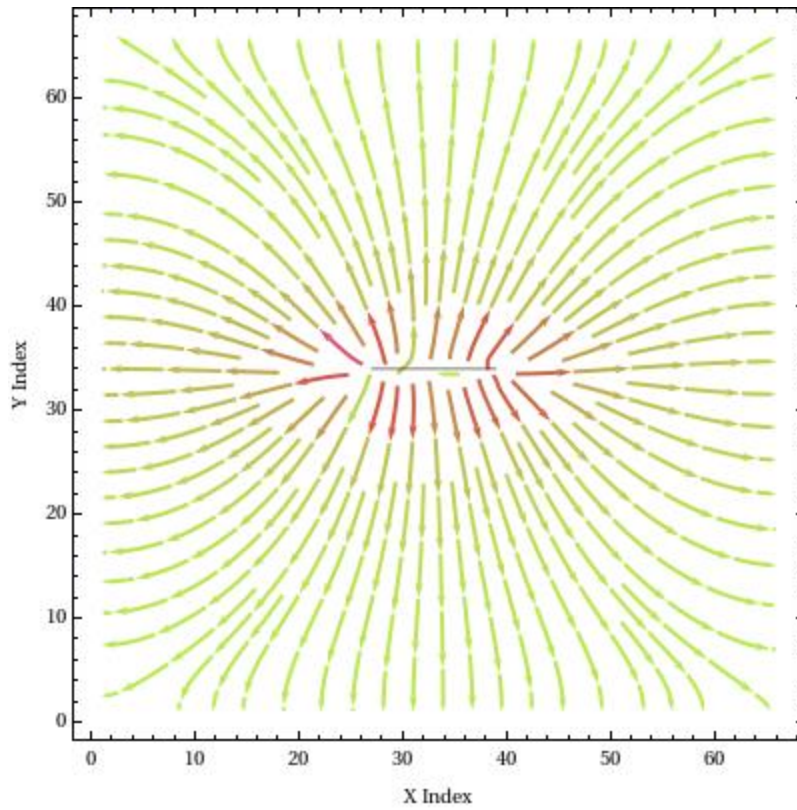


Figure 96 - 2D representation of the field lines for Dataset 7 while holding the Z axis constant.

Again, it is very clear as to the direction of the field lines, indicating that the associated potentials are positive. Rendering the potentials and the field lines for the Z axis results in the following figure:

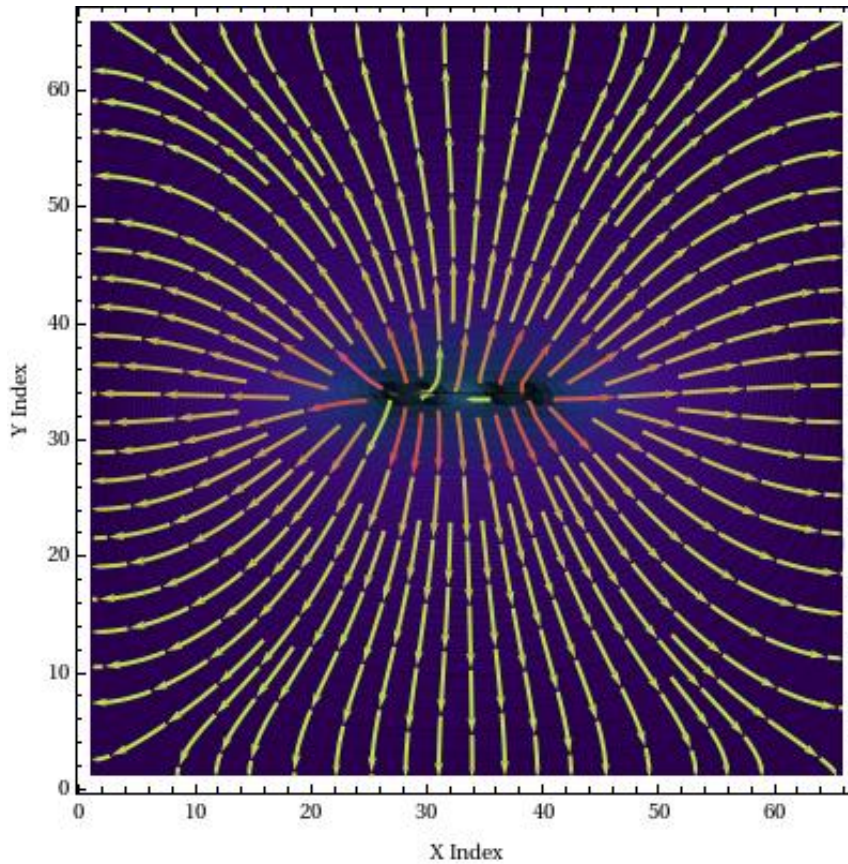


Figure 97 - 2D representation of the potentials and the field lines for Dataset 7 while holding the Z axis constant at position 34.

The potentials and the field lines profiles have been rendered for the X, Y and Z axes, respectively. This completes the rendering of the N=5 Dataset 5 dataset. This concludes the graphical representation for the acGNR5.

CHAPTER 7

DIFFERENCES BETWEEN GRAPHENE RIBBONS

There are a few key similarities and differences between the acGNR8 and acGNR5 structure worth noting. The first is the most apparent. There are eight carbon atoms contained in the acGNR8 unit cell. The acGNR5 unit cell only has five. With that said, each carbon atom has 4 electrons. Three of those electrons are used to form the tight bonding required of graphene. The fourth, electron is the one that contributes to the calculation of the potential and the field lines. This electron is found in the pz orbital, and is allowed to move among the graphene. The charge densities, ψ are calculated probabilities for where those free flowing electrons are expected to be located. In terms of similarity, both the acGNR8 and acGNR5 structures exhibit semi-metallic properties. Armchair graphene nanoribbons (acGNRs) 14–18 of atomic width N of $\text{mod}(N, 3) = -1$, where $N = 2, 5, 8, 11, 14, 17, \dots$ are also semi-metallic within the continuum and the pzTB approximation [5]. The $\text{mod}(N, 3) = -1$ acGNR's also display linear electric bands. These semi-metallic acGNRs display linear and symmetric dispersions for the low-lying conduction and valence bands within the pzTB theory [5]. This helps explain the ballistic electron transport properties appreciated in graphene. Both acGNR configurations promote nearest neighbor coupling, but there are slight differences between the two. The acGNR8 electron approximations can be solved using a 16×16 matrix pzTB Hamiltonian. The pzTB Hamiltonian of this structure is a $2N \times 2N$ matrix containing only nearest-neighbor couplings [5]. The acGNR5 structure, even though linear, requires a slightly more complex pzTB Hamiltonian to solve. AcGNRs with odd atomic widths $N = 5, 11, 17, \dots$ are not considered in the continuum theory, although they do exhibit the semi-metallic characteristics necessary to allow plasmon propagation [5]. The acGNR5 case relies on nearest neighbor contributions from three carbon atoms. Although, when using a theory that includes an extended basis set, the semi-metallic acGNRs also develop a

small bandgap on the order of a few meV and some nonlinearity around the band edge [5]. In this case the acGNR5 band gap is measured to be 64meV. Due to the linear band structure and zero band gap, the 1st NN acGNR8 cases have no dependence on the associated wave number. By comparison, the hyperbolic band structure and presence of a band gap in the 3rd NN acGNR5 case, results in a dependence on the associated wave number. These differences contribute directly to the deltas observed in the voltage potential and the electric field lines. The eigenvectors result from the pzTB Hamiltonian, and those are precisely what makes up the electron probabilities ψ . It should be noted that acGNRs of $\text{mod}(N, 3) = 0$ and 1, are not conducive to electron transport. For the cases where $\text{mod}(N, 3) = 0, 1$, intrinsic acGNRs are semiconducting with appreciable bandgap and do not support plasmon propagation [5].

N=8

Now that both acGNR structures have been calculated and rendered, this chapter will illustrate comparisons between the two sets of nanoribbon. The following will represent the comparison between the massless fermion potentials of the N=8 ribbon to show the lossless transport properties. See Appendix F for the complete list of ρ values that were used to calculate the potentials and the field lines. Taking the 4th ρ value from each Dataset shows how similar the values are, which is evidence of the lossless electron transport properties of the N=8 nanoribbon.

Dataset 1	0.2155214023095454
Dataset 41	0.21552140230954528
Dataset 81	0.21552140230954564
Dataset 121	0.21552140230954608
Dataset 161	0.21552140230954592
Dataset 201	0.21552140230954636

Table 16 - Calculated Rho values at position 4 in each respective Dataset of the Brillouin Zone for N=8

Notice that the values are the exact same until 15th decimal place, and even then the values are only different by 1 increment. Because of this, there is expected to be very little difference in the potentials and field lines between the datasets. Observe below, that when compared to one another, there is zero noticeable difference in the voltage potentials throughout the Brillouin zone. Shown again here, is a plot of the first dataset compared to the second dataset.

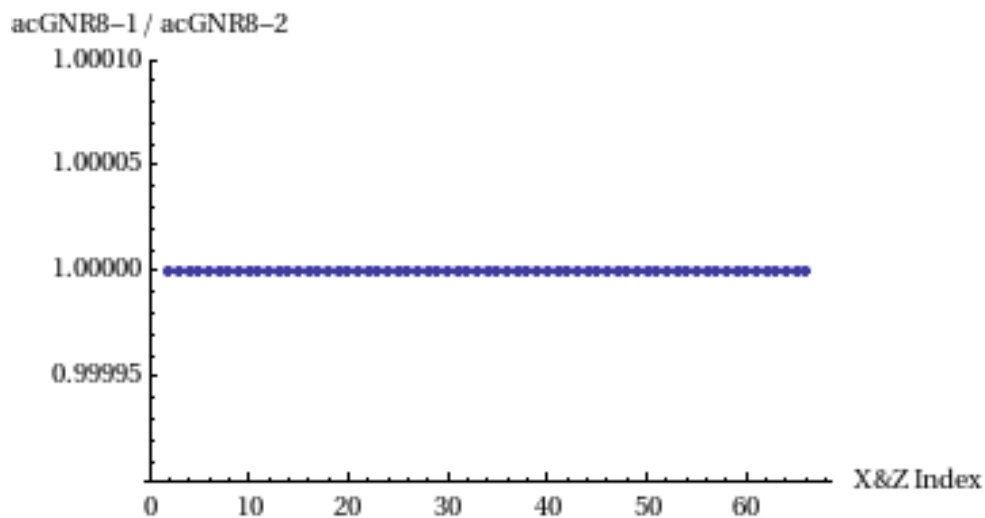


Figure 98 - Plot of acGNR8 Dataset 1 divided by acGNR8 Dataset 41, holding the Y axis constant at 20.

The above plot shows that there is no difference in the acGNR8 potentials, from one Dataset to another. The following plot is the acGNR8 Dataset 1 dataset, ϕ holding the X axis constant at 20.

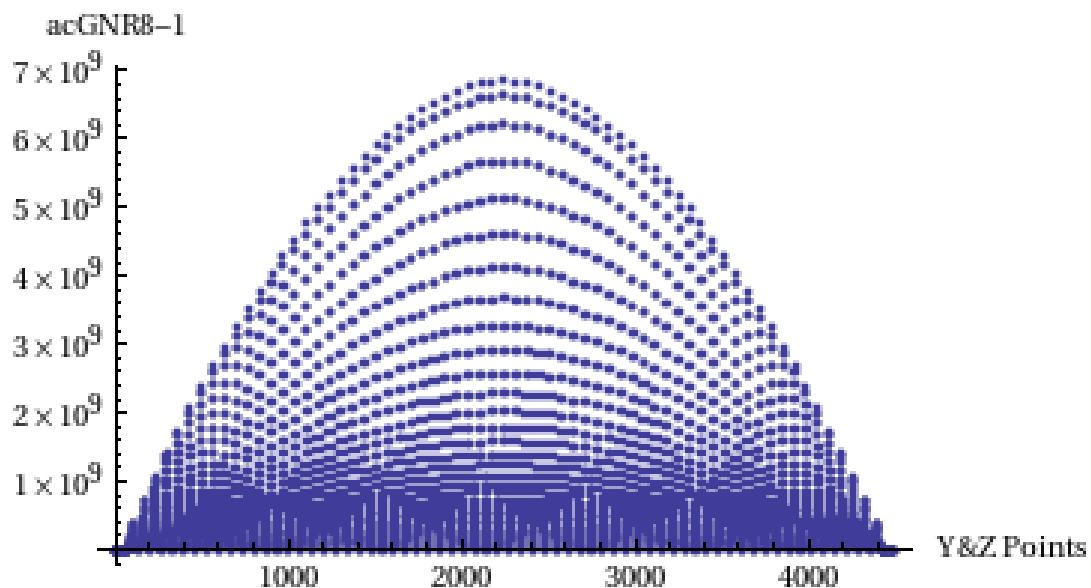


Figure 99 – Plot of potentials for the entire set of N=8 Dataset 1 for Y & Z.

This plot is consistent with the values entered into the nanoribbon. The maximum occurs in the middle of the problem set, and then dampens symmetrically towards the outside edges. Looking at 2D slices from acGNR8 shows no differences between the two Datasets.

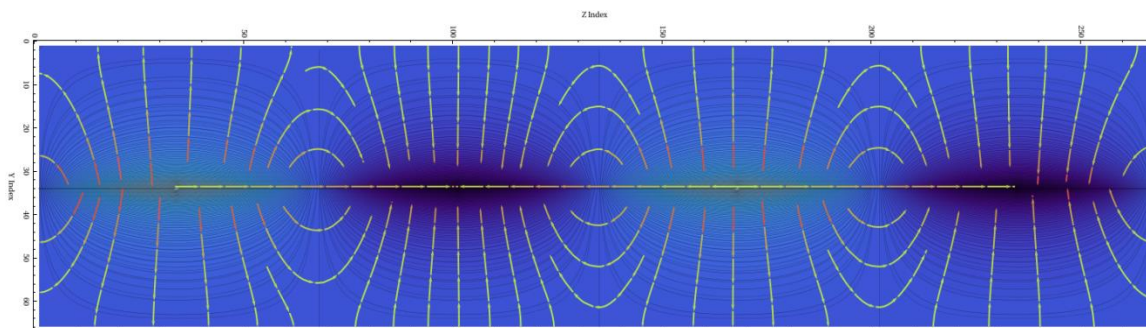


Figure 100 - Voltage potentials and electric field lines associated with Dataset 1 holding the X-Axis constant.

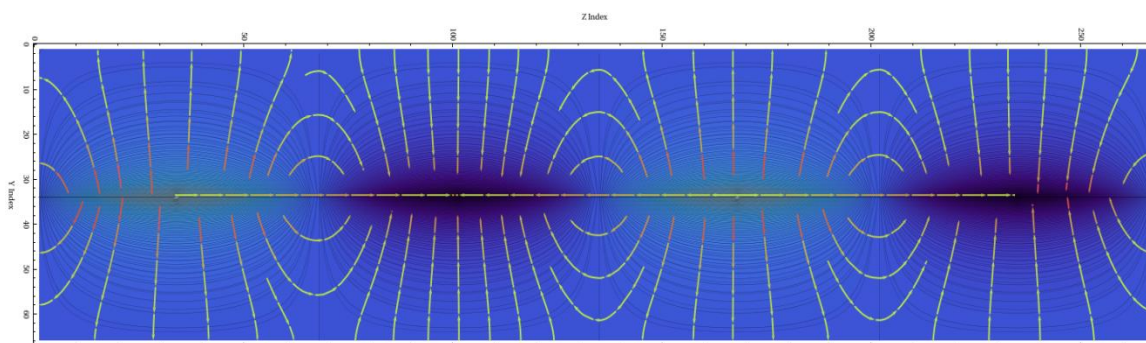


Figure 101 - Voltage potentials and electric Field Lines associated with Dataset 41 holding the X-Axis constant.

Comparing the potentials and the field lines from Dataset 1 and 41 holding the Y-Axis constant is represented in the following.

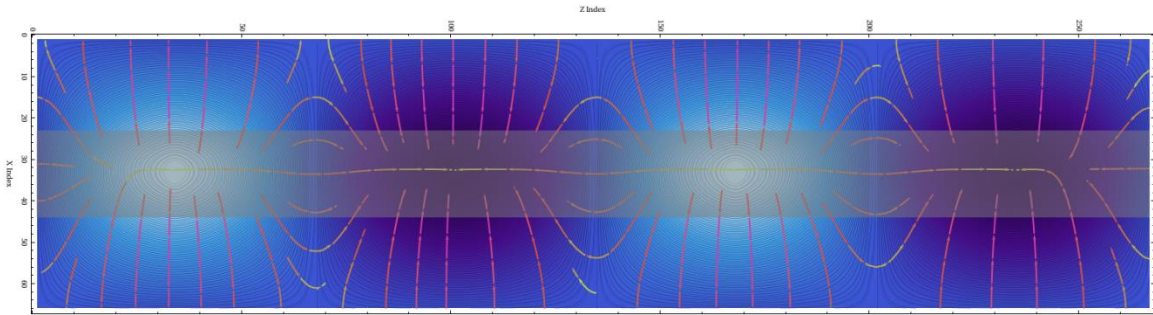


Figure 102 - Voltage potentials and electric Field Lines associated with Dataset 1 holding the Y-Axis constant.

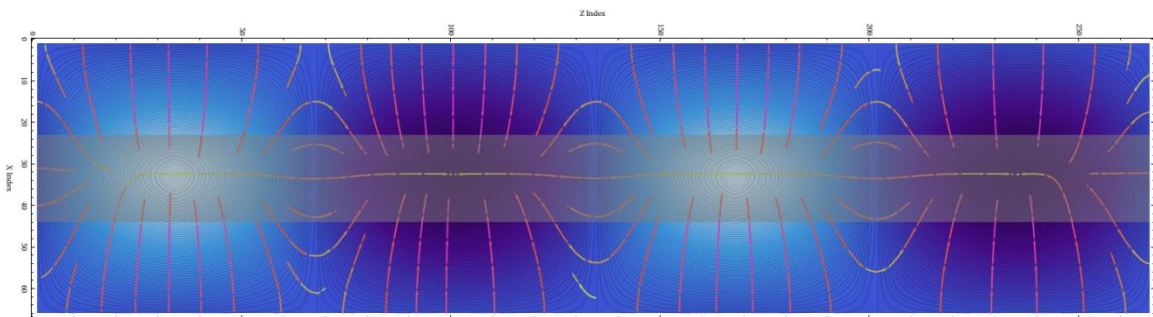


Figure 103 - Voltage potentials and electric field lines associated with Dataset 41 holding the Y-Axis constant.

As expected, there is zero difference visually between the 2 Datasets with respect to the potentials and the field lines. Next, comparing the two Datasets in 3 dimensions results in the same conclusion.

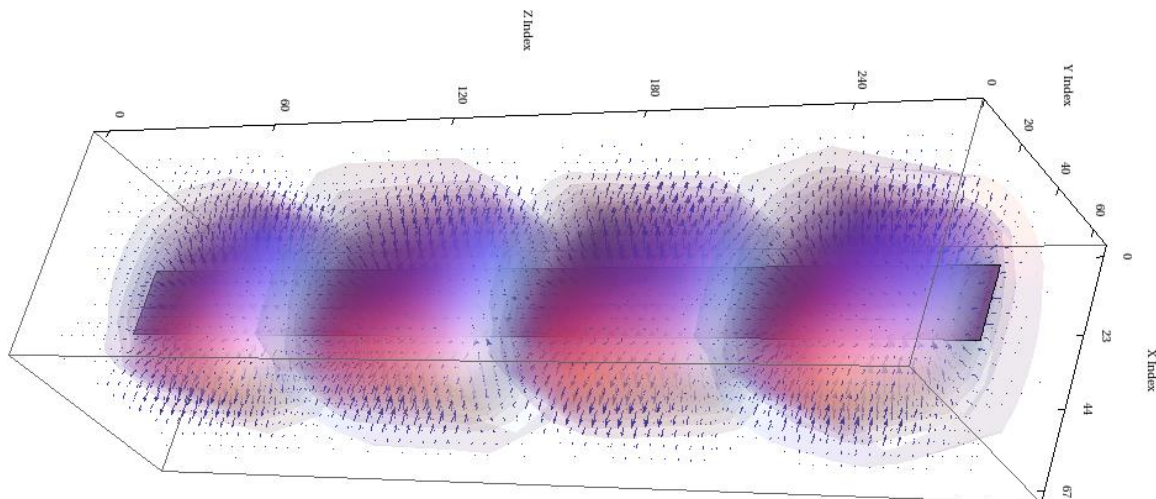


Figure 104 - Voltage Potentials and Field Lines in 3D wrt Dataset 1.

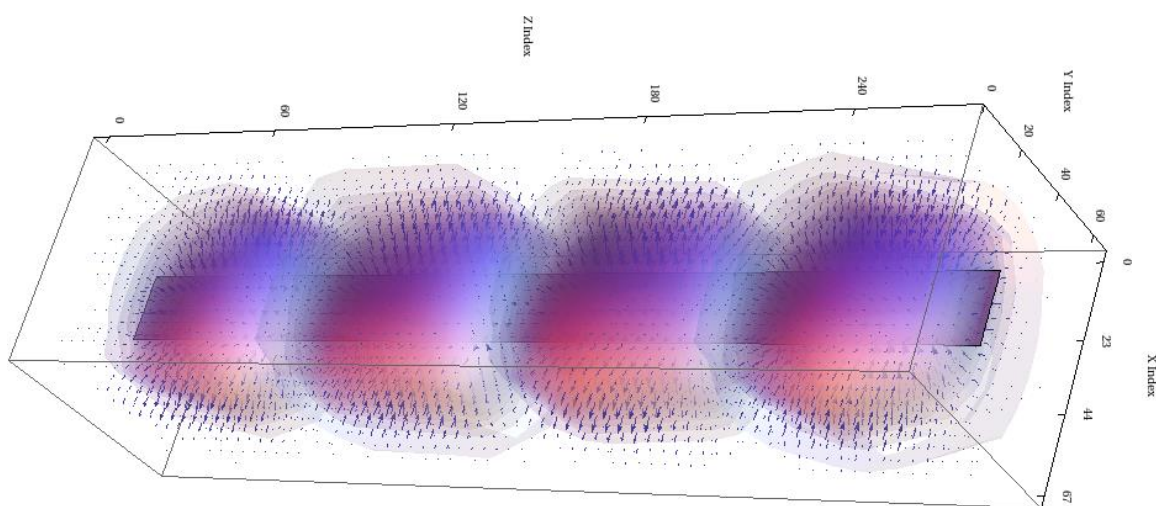


Figure 105 - Voltage Potentials and Field Lines in 3D wrt Dataset 41.

As expected, the potentials and the field lines appear as exact matches, demonstrating the same propagation profile. These figures are indicative of lossless electron transfer.

N=5

Following the N=8 Dataset previous to set-up the illustrations, a sample of the ρ values for N=5 will be given below. For the complete list, refer to Appendix F. The N=5 ρ values for Dataset 2 are listed in the table below.

Position in acGNR {X,Y,Z}	Calculated ρ Values For k= 0.226502274177099
{27,34,34}	0.24661223178846572
{30,34,34}	0.2533575229139936
{33,34,34}	$1.071988224937808 \times 10^{-7}$
{36,34,34}	0.25324070572563334
{39,34,34}	0.24678943237308476

Table 17 – acGNR positions of the ρ values and their associated calculated values for N=5 Dataset 2

Shown again here for reference, note in the table above, that the values increase from the outside in, and then are practically zero in the middle.

The following plot is the Dataset 2, ϕ normalized with ϕ_{\max} for the full Dataset 2 dataset. Using the 67x67x67 array resulted in comparison of 300763 points.

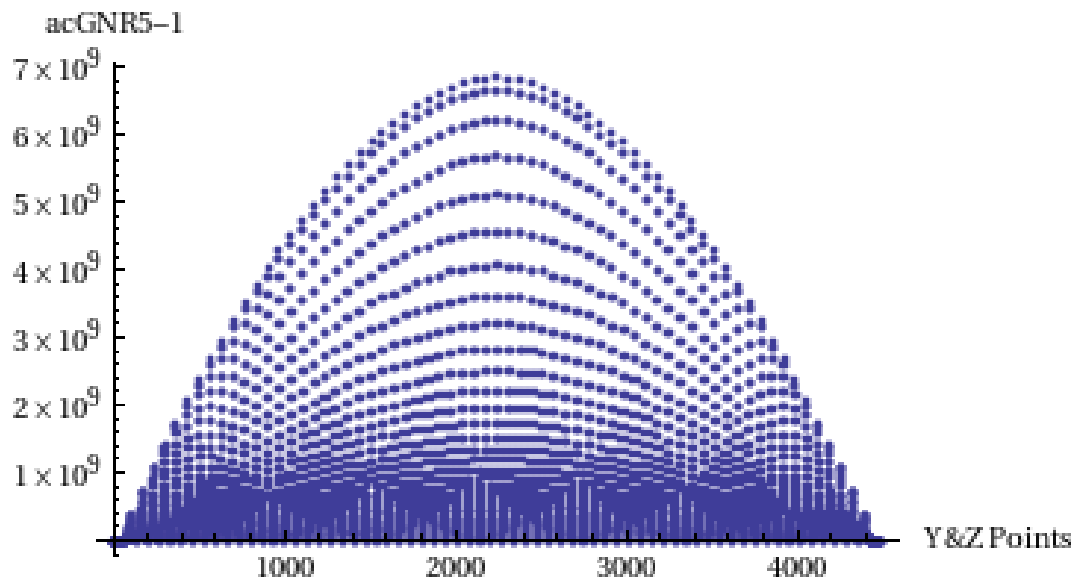


Figure 106 – Plot of potentials for the entire set of N=5 Dataset 1 for Y & Z.

This plot is consistent with the values entered into the nanoribbon. The maximum occurs in the set of values just outside of the middle of the acGNR5, and then dampens towards the outside edges. Since the starting fermion approximation in the center is virtually 0, the Poisson algorithm shows the nearest neighbor contributions and how they fill in the middle accordingly. The symmetry shown above in the potential is consistent with expectations.

As done in the previous Dataset, comparing the first two data Datasets with respect to the X axis shows the following.

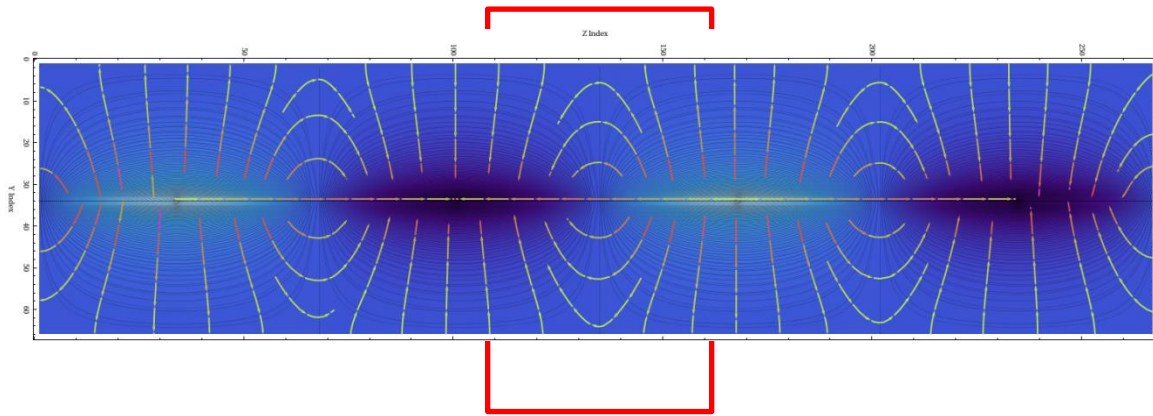


Figure 107 - Voltage potentials and electric Field Lines associated with Dataset 1 holding the X-Axis constant.

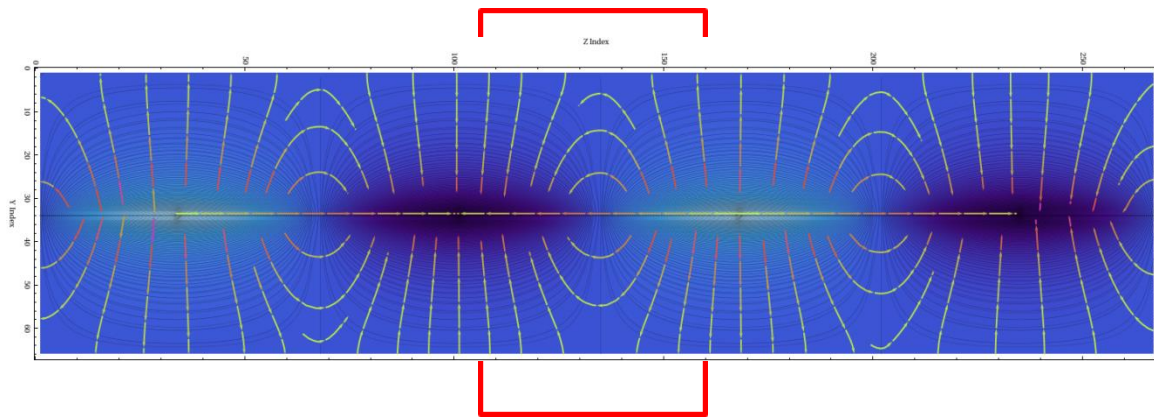


Figure 108 - Voltage potentials and electric Field Lines associated with Dataset 2 holding the X-Axis constant.

There is zero noticeable change in potentials with respect to the X axis, but there is an observable difference in the field lines. The next set of figures will represent the Y axis held constant, with Datasets 3 and 4 respectively.

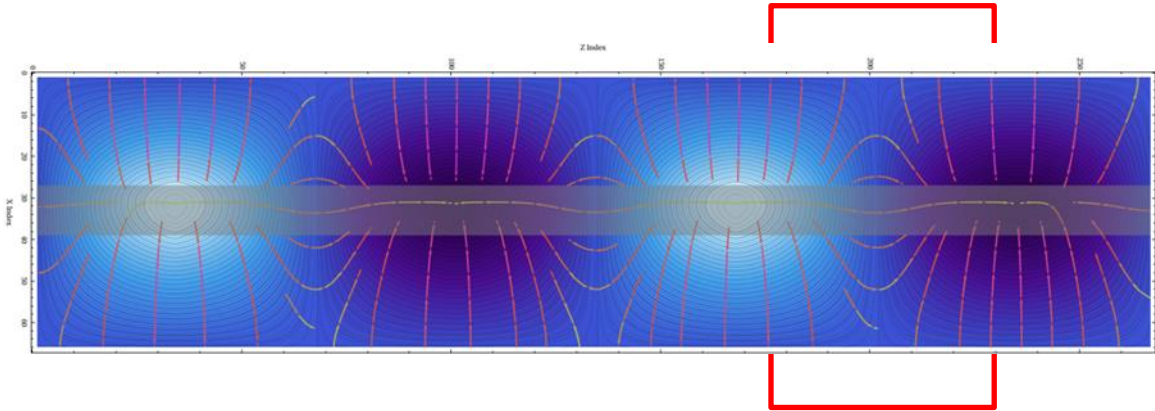


Figure 109 - Voltage potentials and electric Field Lines associated with Dataset 3 holding the Y-Axis constant.

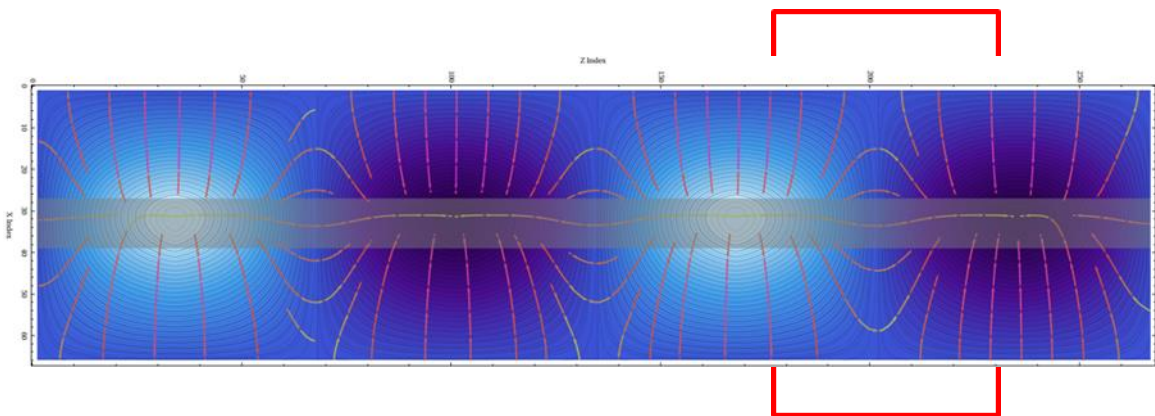


Figure 110 - Voltage potentials and electric Field Lines associated with Dataset 4 holding the Y-Axis constant.

Very noticeable in the figures above is the difference in both the potentials and the field lines between Datasets 3 and 4. These figures are indicative of slight losses in the transport properties of the N=5 ribbon structure. Comparing Datasets 3 and 4 in 3 dimensions is shown below.

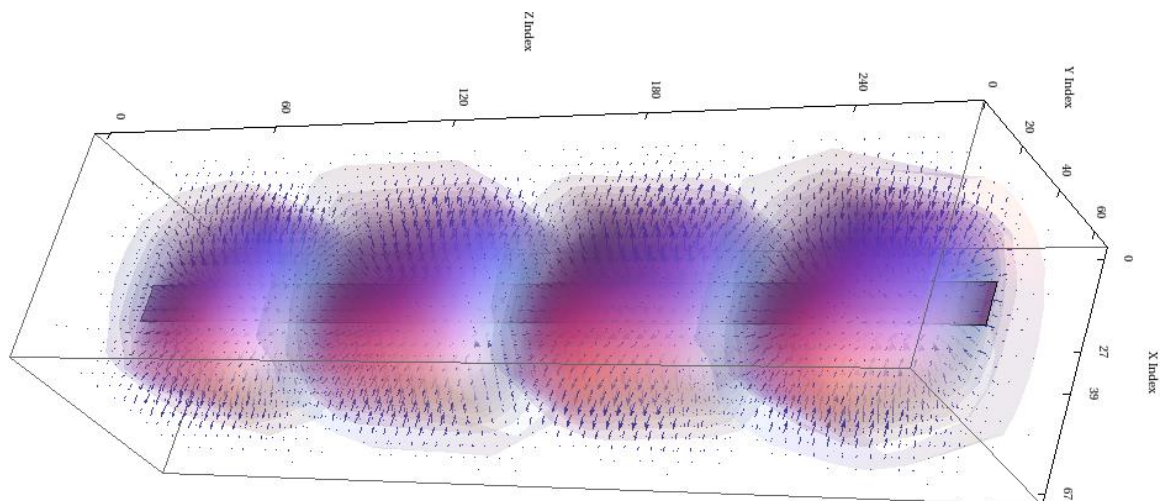


Figure 111 - Voltage Potentials and Field Lines in 3D wrt Dataset 3.

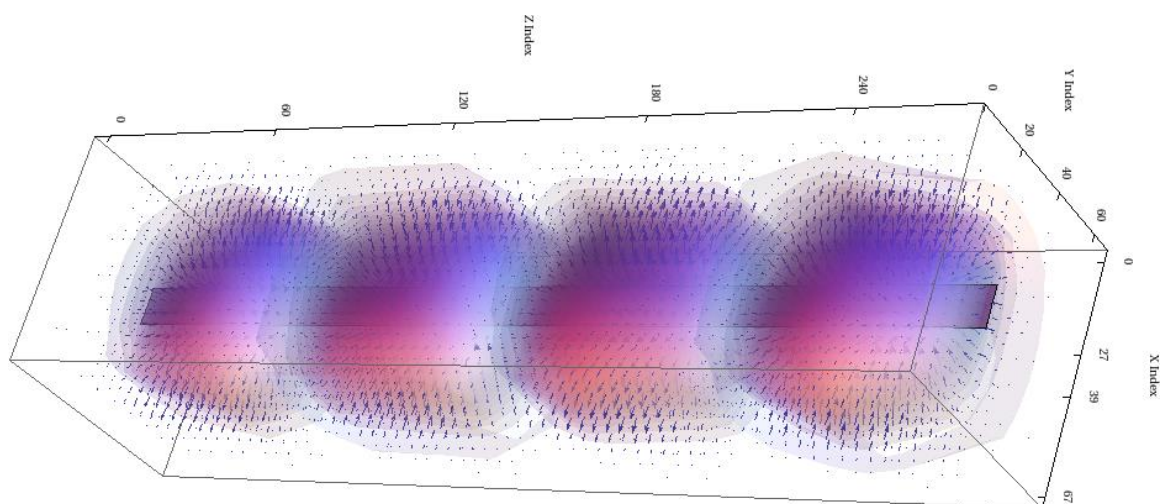


Figure 112 - Voltage Potentials and Field Lines in 3D wrt Dataset 4.

Comparing the two figures above shows that even though the potentials and the field lines are different between Datasets 3 and 4, there is very little, if any, noticeable

change between the two Datasets in the 3 dimension representation. This shows that the changes do not drastically impact the overall magnitudes of the properties.

N=8 vs. N=5

Now that comparisons have been made between each nanoribbon with respect to itself, it is important to see if any differences exist between N=8 and N=5. Comparing the potentials and field lines from N=8 to N=5 is shown below.

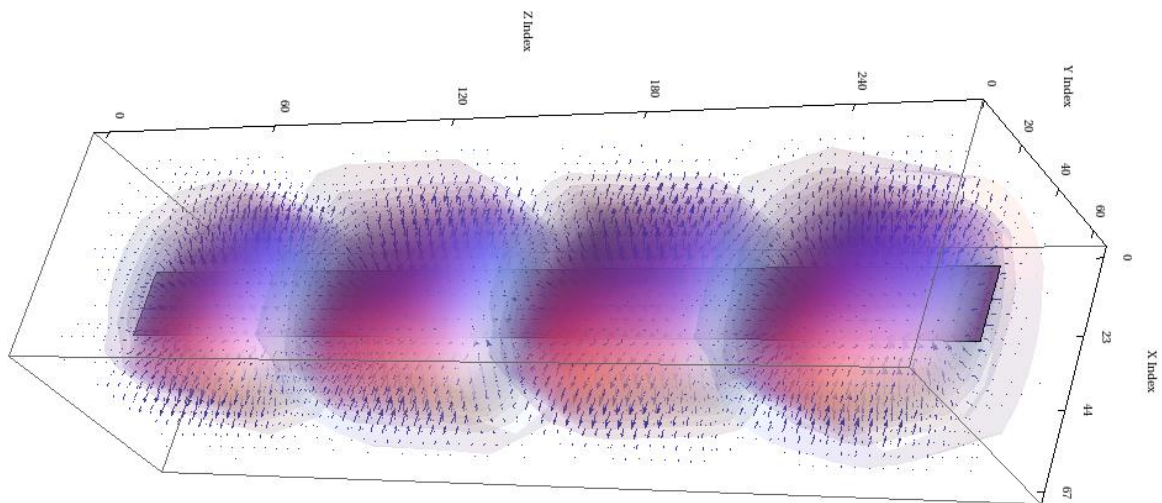


Figure 113 - Voltage Potentials and Field Lines in 3D wrt Dataset 1 from N=8.

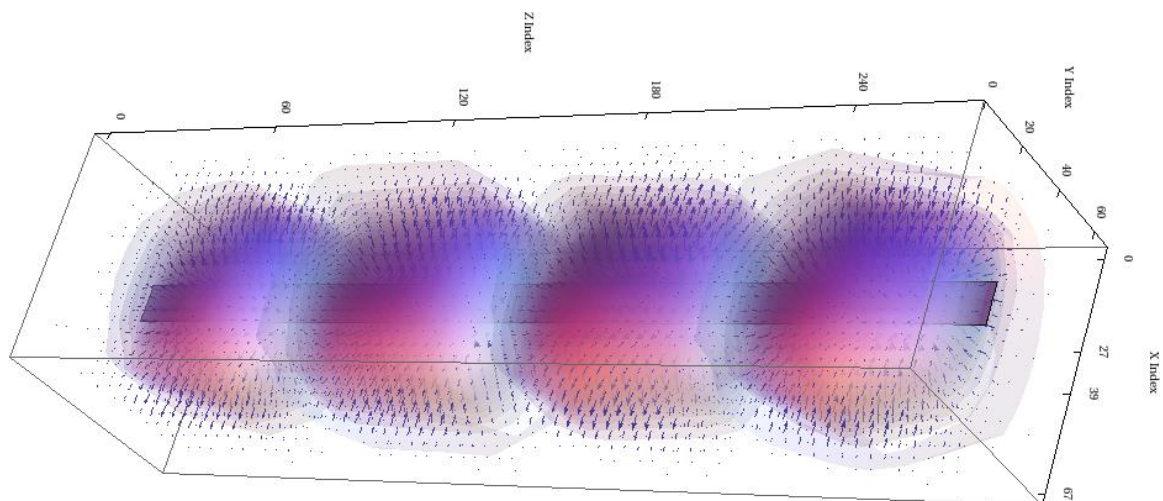


Figure 114 - Voltage Potentials and Field Lines in 3D wrt Dataset 4 from $N=5$.

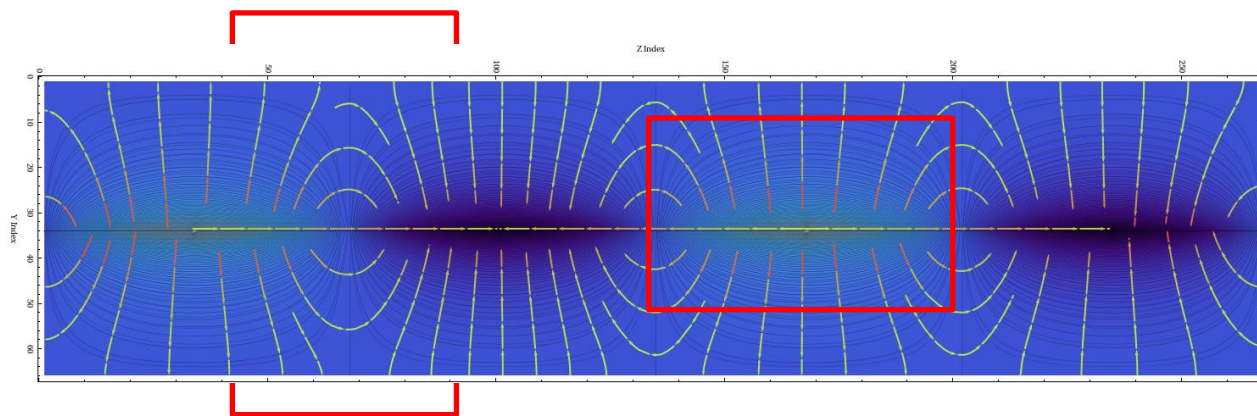


Figure 115 - 2D Y-Z plane slice showing the potential and field lines for acGNR8

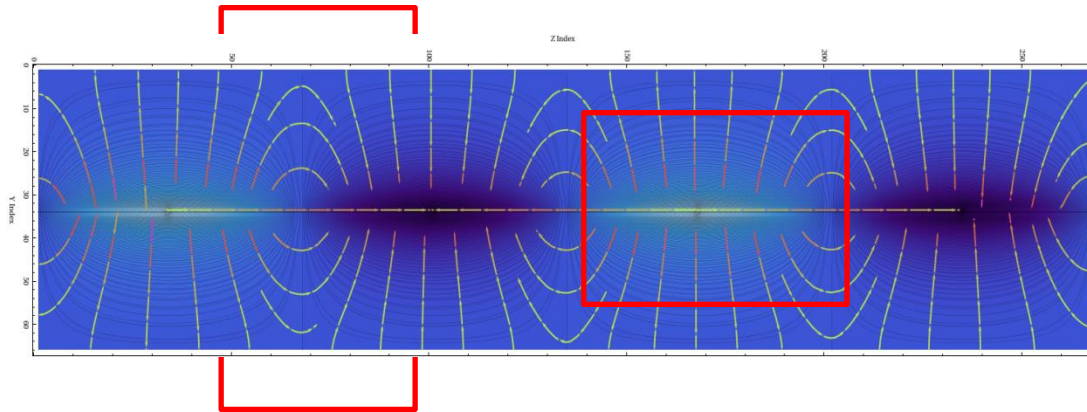


Figure 116 - 2D Y-Z plane slice showing the potential and field lines for acGNR5

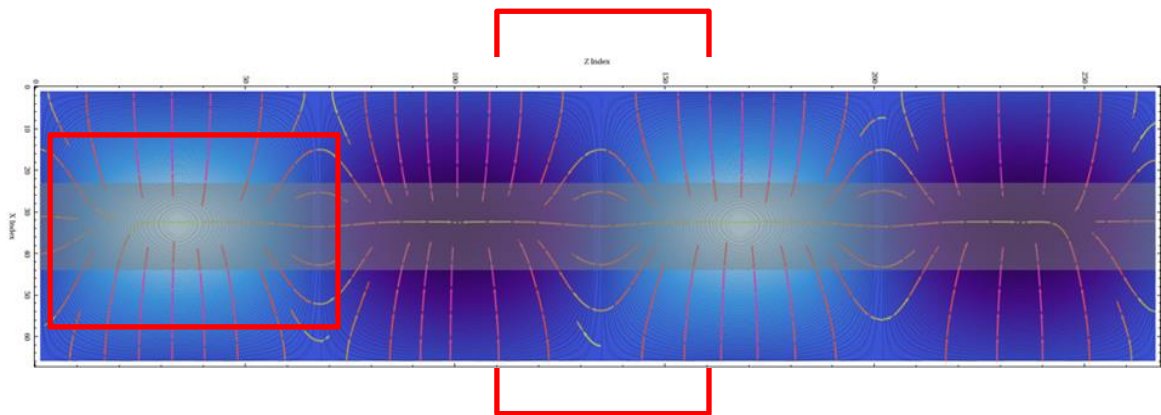


Figure 117 - 2D X-Z plane slice showing the potential and field lines for acGNR8.

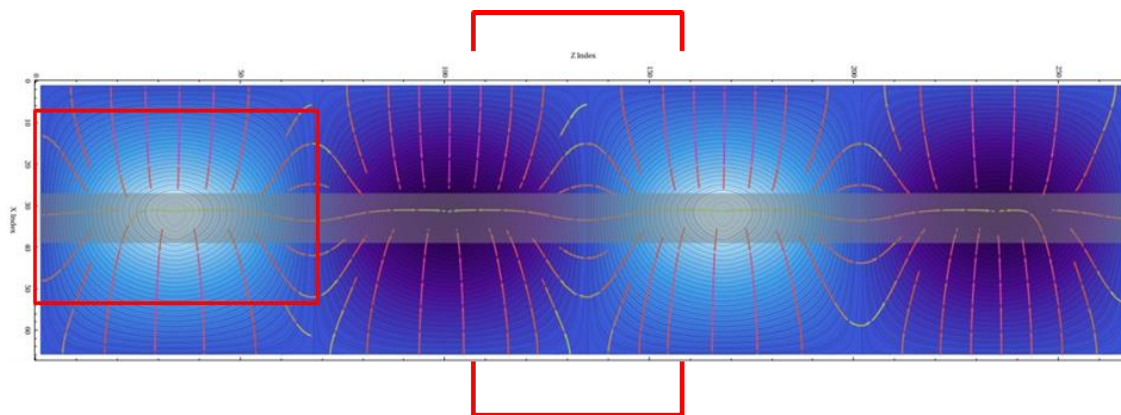


Figure 118 - 2D X-Z plane slice showing the potential and field lines for acGNR5.

It is evident here that the potentials are larger, in terms of magnitude, with the acGNR8 than they are with the acGNR5. Part of this should be contributed to the fact that the N=8 nanoribbon itself is slightly larger in size than the N=5 nanoribbon. The second contributor to the difference in potential magnitude is attributed to the number of electrons per unit cell, and the fact that the electrons are allowed to move more freely in the acGNR8 nanoribbon. A second graphical comparison of the voltage potentials can be seen below. These figures are 2 dimensional plots of the voltage potentials associated from acGNR5 by acGNR8.

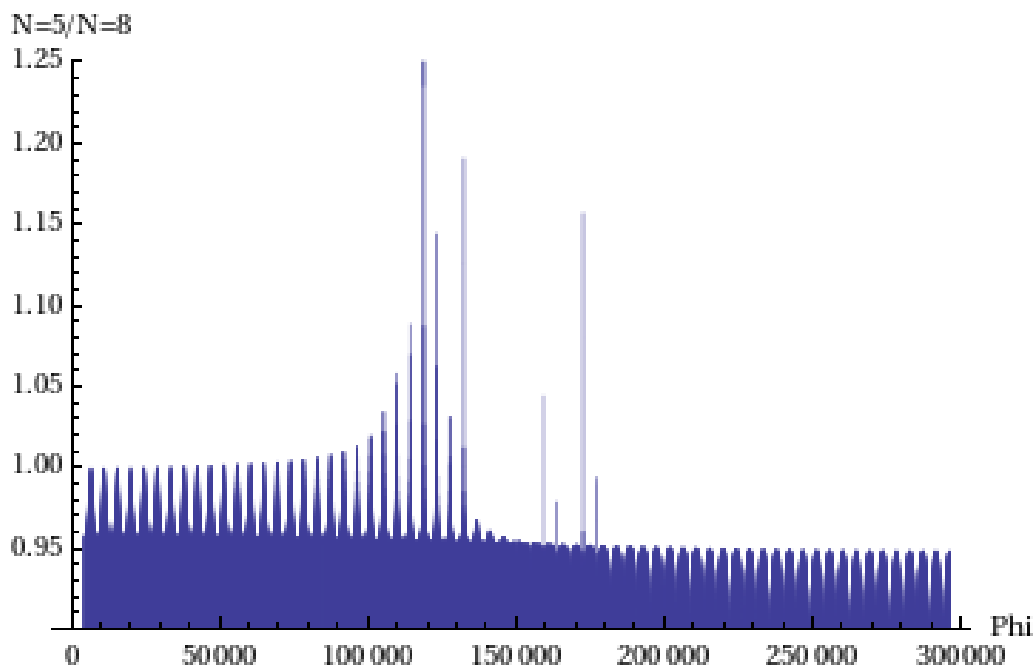


Figure 119 - 2D plot of N=5 by N=8. This plot shows that rate of change in the voltage potentials between the two acGNR datasets.

The figure above shows the voltage potentials plotted as a comparison to one another. What this plot demonstrates is that the potentials are as expected, different between the two acGNR cases. This can be attributed to the physical size differences in the graphene nanoribbon itself, but it should also be attributed to the differences in the massless versus massive Dirac fermion approximations. The latter is directly tied to the 64meV band gap found in the acGNR5.

CHAPTER 8

SUMMARY

Graphene has potential for use as an interconnect for electrical circuitry. With practically zero bandgap, depending on atomic structure, the electron movement within graphene is lossless. Graphene's ballistic transport properties, along with its diamond like strength, make it a front-runner to dethrone silicon as the next revolutionary substrate.

It is possible to calculate and render graphene's 3 dimensional electrical properties. When given the eigenvectors from the pzTB $2N \times 2N$ Hamiltonian, or electron wave functions associated with the varying Fermi energies, the voltage potentials are calculated using Poisson's equation and the electric field lines are calculated by taking the gradient of those potentials. The keys are to set the boundary conditions properly with $\phi = 0$ at the edges of the problem space, and expanding the problem set to allow for complete nearest neighbor contributions.

Computing the derivatives discretely was straight-forward using the central difference method. Writing a software program to solve Poisson's equation and the field gradient iteratively in Mathematica proved extremely useful. It was critical to set the convergence threshold appropriately to allow the nearest neighbor contributions to fully mature.

Rendering the potentials and the field lines provided a visual representation to the propagation profiles throughout the Brillouin zone. The illustrations provided insight into the electrical properties, and how they are influenced by adjusting the nanoribbon structure and ultimately, the bandgap. There is zero observable dependence in the

potentials and field lines with the wave number in the acGNR8 case. There is observable dependence between the potentials and the field lines and the wave number in acGNR5 case. However, due to the ballistic transport properties, there appears to be a very negligible effect on the overall magnitude of the potentials and the field lines. Be it massless Dirac fermions or massive Dirac fermions, the voltage potentials and electric field lines are affected, but not enough to negate graphene's super-conductor qualities.

APPENDIX A

 Ψ (PSI) EDITOR IN MATHEMATICA FORMAT

The electron approximations were provided by way of a data list titled **vecval**.

The vecval reference below will refer to that original dataset.

Line 1 (Input) `vecval[[1]][[1]]`

(Output) {6.70352, {0.114007 - 1.72631*10⁻¹⁷ I, -0.21426 - 0.00108508 I,
0.288675 - 1.34485*10⁻¹⁷ I, -0.328265 - 0.00166244 I,
0.328269 + 0. I, -0.288671 - 0.00146192 I, 0.214263 + 2.41946*10⁻¹⁷ I,
-0.114005 - 0.000577358 I, -0.114005 - 0.000577358 I,
0.214263 - 1.48583*10⁻¹⁷ I, -0.288671 - 0.00146192 I,
0.328269 + 1.49793*10⁻¹⁷ I, -0.328265 - 0.00166244 I,
0.288675 + 1.07626*10⁻¹⁶ I, -0.21426 - 0.00108508 I,
0.114007 + 7.03801*10⁻¹⁷ I}}

Line 10 (Input) `vecval[[1]][[1]][[2]]`

(Output) {0.114007 - 1.72631*10⁻¹⁷ I, -0.21426 - 0.00108508 I,
0.288675 - 1.34485*10⁻¹⁷ I, -0.328265 - 0.00166244 I,
0.328269 + 0. I, -0.288671 - 0.00146192 I,
0.214263 + 2.41946*10⁻¹⁷ I, -0.114005 - 0.000577358 I,
-0.114005 - 0.000577358 I,
0.214263 - 1.48583*10⁻¹⁷ I, -0.288671 - 0.00146192 I,
0.328269 + 1.49793*10⁻¹⁷ I, -0.328265 - 0.00166244 I,
0.288675 + 1.07626*10⁻¹⁶ I, -0.21426 - 0.00108508 I,
0.114007 + 7.03801*10⁻¹⁷ I}

Line 20 (Input) `a = evecval[[1]][[1]][[2]] Conjugate[evecval[[1]][[1]][[2]]]`

(Output) {0.0129975 + 0. I, 0.0459084 + 0. I, 0.0833333 + 0. I,
 0.107761 + 0. I, 0.107761 + 0. I, 0.0833333 + 0. I, 0.0459084 + 0. I,
 0.0129975 + 0. I, 0.0129975 + 0. I, 0.0459084 + 0. I,
 0.0833333 + 0. I, 0.107761 + 0. I, 0.107761 + 0. I, 0.0833333 + 0. I,
 0.0459084 + 0. I, 0.0129975 + 0. I}

(Input) `aa = Table[0, {8}];`

`Do[aa[[i]] = (a[[i]] + a[[i+8]]), {i, 1, 8}];`

`Print[Chop[aa]];`

(Output) {0.058906, 0.191094, 0.191094, 0.058906, 0.058906, 0.191094,

Line 30 0.191094, 0.058906}

APPENDIX B

P (RHO) EDITOR IN MATHEMATICA FORMAT

Line 1 (Input) rho = Table[0, {67}, {67}, {67}];

$$\text{rho}[[23]][[34]][[34]] = 0.0589059741807697$$

$$\text{rho}[[26]][[34]][[34]] = 0.191136209718213$$

$$\text{rho}[[29]][[34]][[34]] = 0.191094034488106$$

$$\text{rho}[[32]][[34]][[34]] = 0.0589059655119839$$

$$\text{rho}[[35]][[34]][[34]] = 0.0589073878770326$$

$$\text{rho}[[38]][[34]][[34]] = 0.191095114260127$$

$$\text{rho}[[41]][[34]][[34]] = 0.286306491843393$$

$$\text{rho}[[44]][[34]][[34]] = 0.0589059655118936$$

The following lines use the sinusoidal modifier mentioned in the narrative to create the remainder of the ρ values scaled sinusoidally along the nanoribbon.

Line 10 Do[rho[[23]][[34]][[k]] = rho[[23]][[34]][[34]] Sin[(Pi/2) k/34], {k, 1, 33}];

$$\text{Do}[\text{rho}[[23]][[34]][[k]] = \text{rho}[[23]][[34]][[34]] \text{Sin}[(\text{Pi}/2) k/34], \{k, 35, 67\}];$$

$$\text{Do}[\text{rho}[[26]][[34]][[k]] = \text{rho}[[26]][[34]][[34]] \text{Sin}[(\text{Pi}/2) k/34], \{k, 1, 33\}];$$

$$\text{Do}[\text{rho}[[26]][[34]][[k]] = \text{rho}[[26]][[34]][[34]] \text{Sin}[(\text{Pi}/2) k/34], \{k, 35, 67\}];$$

$$\text{Do}[\text{rho}[[29]][[34]][[k]] = \text{rho}[[29]][[34]][[34]] \text{Sin}[(\text{Pi}/2) k/34], \{k, 1, 33\}];$$

$$\text{Do}[\text{rho}[[29]][[34]][[k]] = \text{rho}[[29]][[34]][[34]] \text{Sin}[(\text{Pi}/2) k/34], \{k, 35, 67\}];$$

$$\text{Do}[\text{rho}[[32]][[34]][[k]] = \text{rho}[[32]][[34]][[34]] \text{Sin}[(\text{Pi}/2) k/34], \{k, 1, 33\}];$$

$$\text{Do}[\text{rho}[[32]][[34]][[k]] = \text{rho}[[32]][[34]][[34]] \text{Sin}[(\text{Pi}/2) k/34], \{k, 35, 67\}];$$

$$\text{Do}[\text{rho}[[35]][[34]][[k]] = \text{rho}[[35]][[34]][[67]] \text{Sin}[(\text{Pi}/2) k/34], \{k, 1, 33\}];$$

```
Do[rho[[35]][[34]][[k]] = rho[[35]][[34]][[67]] Sin[(Pi/2) k/34], {k, 35, 67}];
```

```
Line 20 Do[rho[[38]][[34]][[k]] = rho[[38]][[34]][[34]] Sin[(Pi/2) k/34], {k, 1, 33}];
```

```
Do[rho[[38]][[34]][[k]] = rho[[38]][[34]][[34]] Sin[(Pi/2) k/34], {k, 35, 67}];
```

```
Do[rho[[41]][[34]][[k]] = rho[[41]][[34]][[34]] Sin[(Pi/2) k/34], {k, 1, 33}];
```

```
Do[rho[[41]][[34]][[k]] = rho[[41]][[34]][[34]] Sin[(Pi/2) k/34], {k, 35, 67}];
```

```
Do[rho[[44]][[34]][[k]] = rho[[44]][[34]][[34]] Sin[(Pi/2) k/34], {k, 1, 33}];
```

```
Do[rho[[44]][[34]][[k]] = rho[[44]][[34]][[34]] Sin[(Pi/2) k/34], {k, 35, 67}];
```

The next line writes the array to a file for input into the Poisson algorithm.

```
rho >> "/directory/Rho_67x67x67_1.mat";
```

APPENDIX C

THE POISSON SOLVER WITH NOTES ADDED

Actual code denoted in **bold** text.

Initialize Constants mentioned in the opening of this chapter

Line 1 **deltaX = 1.23/3;**

deltaY = 3/3;

deltaZ = 4.26/3;

Epsilon=8.854187812620*10^-12;

Initialize Arrays

Vold = ConstantArray[0, {67, 67, 67}];

Vnew = ConstantArray[0, {67, 67, 67}];

Enew = Table[0, {67}, {67}, {67}];

Next line is Diagnostics for loading the Rho file created from the rho editor

Print[" Loading Rho "];

Next line gets the Rho file

Line 10 << **"/directory/Rho_67x67x67_1.mat"**

Diagnostics

Print[Dimensions[Rho]];

Print[" Loading Rho Complete "];

Initialize ConvergenceLoop to 0 - This will serve as a fail-safe to kick out of the

loop if necessary

ConvergenceLoop = 0;

Initialize Convergence to zero

Convergence = 0;

This begins the computation loop

While[Convergence == 0 && ConvergenceLoop < 100000,

The following nested DO Loop will calculate ϕ using Poisson's Equation

Do[Vnew[[i]][[j]][[k]] =

(1/(2/deltaX^2 + 2/deltaY^2 + 2/deltaZ^2)) *

((Vold[[i + 1]][[j]][[k]] + Vold[[i - 1]][[j]][[k]])/(deltaX^2)) +

((Vold[[i]][[j + 1]][[k]] + Vold[[i]][[j - 1]][[k]])/(deltaY^2)) +

Line 20 ((Vold[[i]][[j]][[k + 1]] + Vold[[i]][[j]][[k -

1]))/(deltaZ^2)) + ((Rho[[i]][[j]][[k]]/ Epsilon))),

{i, 2, 66}, {j, 2, 66}, {k, 2, 66}];

Next line assumes all points have converged so the next iteration is invoked when the test hits the first value exceeding the defined convergence threshold

Convergence = 1;

This is the convergence test. User defined Convergence threshold for 1^{-7} .

Note that this test is performed for all data points within the array

Do[

If[

Vold[[i]][[j]][[k]] == 0, Null,

If[

(Vnew[[i]][[j]][[k]] - Vold[[i]][[j]][[k]])/ Vold[[i]][[j]][[k]] > (1*^-7),

Convergence = 0, Null

] Line 30

```
],
{i, 2, 66}, {j, 2, 66}, {k, 2, 66}];
```

This line Ignores the first iteration until V_{new} and V_{old} are nonzero

```
If[ConvergenceLoop < 2, Convergence = 0, Null];
```

Added for visual diagnostics, the following lines capture the current status of the loop with respect to the iteration loop number, memory usage, and the current session time. Memory usage is helpful for running simultaneous jobs, so you can track RAM usage for your machine.

```
If[ConvergenceLoop == 1, Print[ConvergenceLoop ];
```

```
Print[MemoryInUse[]]; Print[(SessionTime[]/3600), Null];
```

```
If[ConvergenceLoop == 2, Print[ConvergenceLoop ];
```

```
Print[MemoryInUse[]]; Print[(SessionTime[]/3600), Null];
```

```
If[ConvergenceLoop == 3, Print[ConvergenceLoop ];
```

```
Print[MemoryInUse[]]; Print[(SessionTime[]/3600), Null];
```

```
If[ConvergenceLoop == 4, Print[ConvergenceLoop ];
```

```
Line 40 Print[MemoryInUse[]]; Print[(SessionTime[]/3600), Null];
```

```
If[ConvergenceLoop == 10, Print[ConvergenceLoop ];
```

```
Print[MemoryInUse[]]; Print[(SessionTime[]/3600), Null];
```

```
If[ConvergenceLoop == 50, Print[ConvergenceLoop ];
```

```
Print[MemoryInUse[]]; Print[(SessionTime[]/3600), Null];
```

```
If[ConvergenceLoop == 100, Print[ConvergenceLoop ];
```

```

Print[MemoryInUse[]]; Print[(SessionTime[]/3600), Null];
If[ConvergenceLoop == 250, Print[ConvergenceLoop ];
Print[MemoryInUse[]]; Print[(SessionTime[]/3600), Null];
If[ConvergenceLoop == 500, Print[ConvergenceLoop ];
Line 50 Print[MemoryInUse[]]; Print[(SessionTime[]/3600),
If[ConvergenceLoop == 750, Print[ConvergenceLoop ];
Print[MemoryInUse[]]; Print[(SessionTime[]/3600), Null];
If[ConvergenceLoop == 1000, Print[ConvergenceLoop ];
Print[MemoryInUse[]]; Print[(SessionTime[]/3600), Null];
If[ConvergenceLoop == 2000, Print[ConvergenceLoop ];
Print[MemoryInUse[]]; Print[(SessionTime[]/3600), Null];
If[ConvergenceLoop == 3000, Print[ConvergenceLoop ];
Print[MemoryInUse[]]; Print[(SessionTime[]/3600), Null];
If[ConvergenceLoop == 5000, Print[ConvergenceLoop ];
Line 60 Print[MemoryInUse[]]; Print[(SessionTime[]/3600), Null];
If[ConvergenceLoop == 10000, Print[ConvergenceLoop ];
Print[MemoryInUse[]]; Print[(SessionTime[]/3600), Null];
If[ConvergenceLoop == 15000, Print[ConvergenceLoop ];
Print[MemoryInUse[]]; Print[(SessionTime[]/3600), Null];
If[ConvergenceLoop == 15000, Vnew >> "/directory/Vnew^-7_15000.mat",
Null];
If[ConvergenceLoop == 20000, Print[ConvergenceLoop ];
Print[MemoryInUse[]]; Print[(SessionTime[]/3600), Null];

```

```
If[ConvergenceLoop == 25000, Print[ConvergenceLoop ];
```

```
Line 70 Print[MemoryInUse[]]; Print[(SessionTime[]/3600), Null];
```

```
If[ConvergenceLoop == 50000, Print[ConvergenceLoop ];
```

```
Print[MemoryInUse[]]; Print[(SessionTime[]/3600), Null];
```

```
If[ConvergenceLoop == 75000, Print[ConvergenceLoop ];
```

```
Print[MemoryInUse[]]; Print[(SessionTime[]/3600), Null];
```

These put statements were added in the event that the algorithm is physically interrupted. The job can be run again where it left off instead of starting over from scratch.

```
If[ConvergenceLoop == 500, Vnew >> "/directory/Vnew^-  
7_500.mat", Null];
```

```
If[ConvergenceLoop == 1000, Vnew >> "/directory/Vnew^-  
7_1000.mat", Null];
```

```
If[ConvergenceLoop == 5000, Vnew >> "/directory/Vnew^-  
7_5000.mat", Line 80 Null];
```

```
If[ConvergenceLoop == 10000, Vnew >> "/directory/Vnew^-  
7_10000.mat", Null];
```

```
If[ConvergenceLoop == 20000 Vnew >> "/directory/Vnew^-  
7_20000.mat", Null];
```

```
If[ConvergenceLoop == 25000, Vnew >> "/directory/Vnew^-  
7_25000.mat", Null];
```

Next line Forces V_{old} to evolve 1 iteration behind V_{new} for the convergence test.

```
Vold = Vnew;
```

Next line maximizes algorithm execution speed

```
ClearSystemCache[];
```

Counter for the loop

```
ConvergenceLoop ++;
```

This statement will kick out of the loop if not converged within 100000 iterations.

```
Line 80 If[ConvergenceLoop == 100000,
```

```
  Print["Convergence Loop Limit Reached. " (SessionTime[]/3600) ],
```

```
  Print["Convergence Loop Limit Not Reached."];
```

When the convergence threshold is met, the loop is exited.

```
If[Convergence == 1, Print[ ConvergenceLoop];
```

```
  Print[" Converged! "] (*; Print[Vnew]);
```

```
  Print["Did Not Converge!"];
```

Now that ϕ has been successfully calculated down to convergence limit of 1^{-7} , it

is time to calculate the gradient for the electric field.

The following calculates the electric field using ϕ .

```
Enew = Table[
```

```
  {{i, j, k},
```

```
  {-((Vnew [[i + 1]][j][k]) - Vnew [[i]][j][k]) / deltaX),
```

```
  - ((Vnew [[i]][j + 1][k]) - Vnew [[i]][j][k]) / deltaY),
```

```
Line 90  - ((Vnew [[i]][j][k + 1]) - Vnew [[i]][j][k]) / deltaZ}} ,
```

```
{i, 1, 66}, {j, 1, 66}, {k, 1, 66}
```

```
];
```

```
Print [Min[Enew];
```

Print [Max[Enew]];

This put statement writes V_{new} , (φ) to a file.

Vnew >> "/directory/67x67x67_1_Vnew^-7.mat";

The Export writes the Rendering of the Electric Field to a file in vector format.

Export["/directory/67x67x67_1_Efield^-7.png", ListVectorPlot3D[{Enew}]];

This put statement writes E_{new} to a file.

Enew >> "/directory/67x67x67_1_EfieldTable^-7.mat";

MemoryInUse[];

This print statement concludes the job and prints the total runtime

Print[" Job Complete! - " (SessionTime[]/3600)];

APPENDIX D

POISSON SOLVER AFTER EXECUTION, WITHOUT NOTES.

```
deltaX=1.23/3;
```

```
deltaY=3/3;
```

```
deltaZ=4.26/3;
```

```
Epsilon=8.854187812620*10^-12;
```

```
Vold=ConstantArray[0,{67,67,67}];
```

```
Vnew=ConstantArray[0,{67,67,67}];
```

```
Enew =Table[0,{67},{67},{67}];
```

```
Print[" Loading Rho "];
```

```
<<"/home/jkdale/Thesis/1st Run/Rho_67.mat"
```

```
Print[Dimensions[Rho]];
```

```
Print[" Loading Rho Complete "];
```

```
ConvergenceLoop =0;
```

Convergence=0;

While[Convergence \square 0 && ConvergenceLoop< 100000,

Do[Vnew[[i]][[j]][[k]]=(1/(2/deltaX^2+2/deltaY^2+2/deltaZ^2))
 *(((Vold[[i+1]][[j]][[k]]+Vold[[i-1]][[j]][[k]])/(deltaX^2))+((Vold[[i]][[j+1]][[k]]+
 Vold[[i]][[j-1]][[k]])/(deltaY^2))+((Vold[[i]][[j]][[k+1]]+
 Vold[[i]][[j]][[k-1]])/(deltaZ^2))+((Rho[[i]][[j]][[k]]/Epsilon))),
 {i,2,66},{j,2,66},{k,2,66}];

Convergence=1;

Do[If[Vold[[i]][[j]][[k]] \square 0,Null, If[
 (Vnew[[i]][[j]][[k]]-Vold[[i]][[j]][[k]])/Vold[[i]][[j]][[k]]>(1*^-7),Convergence
 =0, Null]],{i,2,66},{j,2,66},{k,2,66}];

If[ConvergenceLoop < 2, Convergence = 0, Null];

If[ConvergenceLoop == 1, Print[ConvergenceLoop];Print[MemoryInUse[]];
 Print[(SessionTime[]/3600), Null];

If[ConvergenceLoop == 2, Print[ConvergenceLoop];Print[MemoryInUse[]];
 Print[(SessionTime[]/3600), Null];

If[ConvergenceLoop == 3, Print[ConvergenceLoop];Print[MemoryInUse[]];
 Print[(SessionTime[]/3600), Null];


```

    If[ConvergenceLoop == 4, Print[ConvergenceLoop ];Print[MemoryInUse[]];
Print[(SessionTime[]/3600), Null];

    If[ConvergenceLoop == 10, Print[ConvergenceLoop ];Print[MemoryInUse[]];
Print[(SessionTime[]/3600), Null];

    If[ConvergenceLoop == 50, Print[ConvergenceLoop ];Print[MemoryInUse[]];
Print[(SessionTime[]/3600), Null];

    If[ConvergenceLoop == 100, Print[ConvergenceLoop ];Print[MemoryInUse[]];
Print[(SessionTime[]/3600), Null];

    If[ConvergenceLoop == 250, Print[ConvergenceLoop ];Print[MemoryInUse[]];
Print[(SessionTime[]/3600), Null];

    If[ConvergenceLoop == 500, Print[ConvergenceLoop ];Print[MemoryInUse[]];
Print[(SessionTime[]/3600), Null];

    If[ConvergenceLoop == 750, Print[ConvergenceLoop ];Print[MemoryInUse[]];
Print[(SessionTime[]/3600), Null];

    If[ConvergenceLoop == 1000, Print[ConvergenceLoop ];Print[MemoryInUse[]];
Print[(SessionTime[]/3600),Null];

    If[ConvergenceLoop == 2000, Print[ConvergenceLoop ];Print[MemoryInUse[]];
Print[(SessionTime[]/3600), Null];

    If[ConvergenceLoop == 3000, Print[ConvergenceLoop ];Print[MemoryInUse[]];
Print[(SessionTime[]/3600), Null];

    If[ConvergenceLoop == 5000, Print[ConvergenceLoop ];Print[MemoryInUse[]];
Print[(SessionTime[]/3600),Null];

```

```
If[ConvergenceLoop == 10000, Print[ConvergenceLoop
];Print[MemoryInUse[]]; Print[(SessionTime[]/3600),Null];
```

```
If[ConvergenceLoop == 15000, Print[ConvergenceLoop
];Print[MemoryInUse[]]; Print[(SessionTime[]/3600),Null];
```

```
If[ConvergenceLoop == 20000, Print[ConvergenceLoop
];Print[MemoryInUse[]]; Print[(SessionTime[]/3600),Null];
```

```
If[ConvergenceLoop == 25000, Print[ConvergenceLoop
];Print[MemoryInUse[]]; Print[(SessionTime[]/3600),Null];
```

```
If[ConvergenceLoop == 50000, Print[ConvergenceLoop
];Print[MemoryInUse[]]; Print[(SessionTime[]/3600), Null];
```

```
If[ConvergenceLoop == 75000, Print[ConvergenceLoop
];Print[MemoryInUse[]]; Print[(SessionTime[]/3600), Null];
```

```
If[ConvergenceLoop == 500,Vnew>> "/home/jkdale/Thesis/1st
Run/Input/67x500.mat",Null];
```

```
If[ConvergenceLoop == 1000,Vnew>> "/home/jkdale/Thesis/1st
Run/Input/67x1000.mat",Null];
```

```
If[ConvergenceLoop == 1500,Vnew>> "/home/jkdale/Thesis/1st
Run/Input/67x1500.mat",Null];
```

```
If[ConvergenceLoop == 2000,Vnew>> "/home/jkdale/Thesis/1st
Run/Input/67x2000.mat",Null];
```

```
If[ConvergenceLoop == 2500,Vnew>> "/home/jkdale/Thesis/1st
Run/Input/67x2500.mat",Null];
```

```
Vold=Vnew;
```

```
ClearSystemCache[];
```

```
ConvergenceLoop ++;]
```

```
If[ConvergenceLoop <= 100000, Print["Convergence Loop Limit Reached. "
(SessionTime[]/3600) ],Print["Convergence Loop Limit Not Reached."]];
```

```
If[Convergence <= 1, Print[ ConvergenceLoop]; Print[" Converged! "],Print["Did
Not Converge!"]];
```

```
Enew=Table[{ {i,j,k},{-((Vnew [[i+1]][j][k]- Vnew [[i]][j][k]) / deltaX) , -
((Vnew [[i]][j+1][k]- Vnew [[i]][j][k]) / deltaY) ,- ((Vnew [[i]][j][k+1]- Vnew
[[i]][j][k]) / deltaZ)} } ,{i,1,66},{j,1,66},{k,1,66}];
```

```
Print [Min[Enew]];
```

```
Print [Max[Enew]];
```

```
Vnew>> "/home/jkdale/Thesis/1st Run/Input/67_Vnew^-7.mat";  
Export["/home/jkdale/Thesis/1st Run/Output/67_Efield^-7.png",  
ListVectorPlot3D[{Enew}]];  
  
Enew>>"/home/jkdale/Thesis/1st Run/Input/67_EfieldTable^-7.mat";  
MemoryInUse[];  
Print[" Job Complete! - " (SessionTime[]/3600)];
```

Loading Rho

{67,67,67}

Loading Rho Complete

1

25789048

0.1032524417

2

25866520

0.1039582667

3

25969720

0.1046657503

4

26085256

0.1053767536

10

26958856

0.1097101397

50

34448232

0.1431951431

100

34533512

0.1888005531

250

34533512

0.3255416950

500

34533512

0.5535843883

750

34539720

0.7817216892

1000

34539720

1.0097472731

2000

34540000

1.9225630056

3000

34540000

2.8351556022

5000

34540016

4.6607327025

Convergence Loop Limit Not Reached.

7562

Converged!

-4.84096×10^9

6.35838×10^9

6.9886794261 Job Complete! -

APPENDIX E
RENDERING CODE

```

<<"/home/jkdale/Thesis/N=5/N57/N57.mat"
<<"/home/jkdale/Thesis/N=5/N57/N57ETable.mat"
Dimensions[Efield67]
Dimensions[Vpot67]
y=ListContourPlot3D[Vpot67,Contours→50,ContourStyle→Opacity[0.2],Mesh→
None,Boxed→False,AxesLabel→{"X","Y","Z"}]
z=ListVectorPlot3D[Efield67, Boxed→ False, AxesLabel→{"X","Y","Z"} ]
x = Show[z,y]
Export["/home/jkdale/Thesis/N=5/N57/Output/3DV2.png",y]
Export["/home/jkdale/Thesis/N=5/N57/Output/3DE2.png",z]
Export["/home/jkdale/Thesis/N=5/N57/Output/3DB2.png",x]

a = Table[{ { Efield67[[i]][j][k][1][1],Efield67[[i]][j][k][1][2],
Efield67[[i]][j][k][1][3]},{ Efield67[[i]][j][k][2][1],Efield67[[i]][j][k][2]
][2],
Efield67[[i]][j][k][2][3]},{i,1,66},{j,1,66},{k,1,66}}];
b=Table[{ { Efield67[[i]][j][k][1][1],Efield67[[i]][j][k][1][2],
Efield67[[i]][j][k][1][3]+67},{ -Efield67[[i]][j][k][2][1],-
Efield67[[i]][j][k][2][2],
-Efield67[[i]][j][k][2][3]},{i,1,66},{j,1,66},{k,1,66}}];
c = Table[{ { Efield67[[i]][j][k][1][1],Efield67[[i]][j][k][1][2],

```

Efield67[[i]][[j]][[k]][[1]][[3]]+134},{Efield67[[i]][[j]][[k]][[2]][[1]],Efield67[[i]][[j]][[k]][[2]][[2]],

Efield67[[i]][[j]][[k]][[2]][[3]]},{i,1,66},{j,1,66},{k,1,66}};

d = Table[{{Efield67[[i]][[j]][[k]][[1]][[1]],Efield67[[i]][[j]][[k]][[1]][[2]],

Efield67[[i]][[j]][[k]][[1]][[3]]+201},{-Efield67[[i]][[j]][[k]][[2]][[1]],-

Efield67[[i]][[j]][[k]][[2]][[2]],

-Efield67[[i]][[j]][[k]][[2]][[3]]},{i,1,66},{j,1,66},{k,1,66}};

e = Table[{i, j, k,Vpot67[[i]][[j]][[k]]},{i, 1, 66}, {j, 1, 66}, {k, 1, 66}};

f=Table[{i, j, k+66,- Vpot67[[i]][[j]][[k]]},{i, 1, 66}, {j, 1, 66}, {k, 1, 66}};

g=Table[{i, j, k+132, Vpot67[[i]][[j]][[k]]},{i, 1, 66}, {j, 1, 66}, {k, 1, 66}};

h=Table[{i, j, k+198,- Vpot67[[i]][[j]][[k]]},{i, 1, 66}, {j, 1, 66}, {k, 1, 66}};

Rib=Graphics3D[{LightGray,BoxRatios→ {.4, 1,

1.42},Opacity[1],Polygon[{{27,34,1},{27,34,67},{39,34,67},{39,34,1}}]}, Boxed→

False];

Rib2=Graphics3D[{LightGray,BoxRatios→ {.4, 1,

1.42},Opacity[1],Polygon[{{27,34,67},{27,34,134},{39,34,134},{39,34,67}}]},

Boxed→ False];

Rib3=Graphics3D[{LightGray,BoxRatios→ {.4, 1,

1.42},Opacity[1],Polygon[{{27,34,135},{27,34,201},{39,34,201},{39,34,135}}]},

Boxed→ False];

Rib4=Graphics3D[{LightGray,BoxRatios→ {.4, 1,

1.42},Opacity[1],Polygon[{{27,34,202},{27,34,269},{39,34,269},{39,34,202}}]},

Boxed→ False];

(*2D Dataset*) (*2D Dataset*) (*2D Dataset*) (*2D Dataset*) (*2D Dataset*)
 (*2D Dataset*) (*2D Dataset*)

```
ee = Table[{j,k,Vpot67[[31]][[j]][[k]]},{j, 1, 66}, {k, 1, 66}];
ff =Table[{j,k+66,- Vpot67[[31]][[j]][[k]]},{j, 1, 66}, {k, 1, 66}];
gg =Table[{j,k+132, Vpot67[[31]][[j]][[k]]},{j, 1, 66}, {k, 1, 66}];
hh =Table[{j,k+198,- Vpot67[[31]][[j]][[k]]},{j, 1, 66}, {k, 1, 66}];
```

```
e1 = Table[{i,k,Vpot67[[i]][[30]][[k]]},{i, 1, 66}, {k, 1, 66}];
f1 =Table[{i,k+66,- Vpot67[[i]][[30]][[k]]},{i, 1, 66}, {k, 1, 66}];
g1 =Table[{i,k+132, Vpot67[[i]][[30]][[k]]},{i, 1, 66}, {k, 1, 66}];
h1 =Table[{i,k+198,- Vpot67[[i]][[30]][[k]]},{i, 1, 66}, {k, 1, 66}];
```

```
V2DI = Join[ee,ff,gg,hh];
```

```
V2DJ = Join[e1,f1,g1,h1];
```

```
V2Dk = Table[{i, j, Vpot67[[i]][[j]][[34]]},{i, 1, 66}, {j, 1, 66}];
```

```
V2DI >> "/home/jkdale/Thesis/N=5/N57/Output/67_V2D_I31.mat"
```

```
V2DJ >> "/home/jkdale/Thesis/N=5/N57/Output/67_V2D_J30.mat"
```

```
V2Dk >> "/home/jkdale/Thesis/N=5/N57/Output/67_V2D_K34.mat"
```

```
<<"/home/jkdale/Thesis/N=5/N57/Output/67_V2D_I31.mat"
```

```
<<"/home/jkdale/Thesis/N=5/N57/Output/67_V2D_J30.mat"
```

```
<<"/home/jkdale/Thesis/N=5/N57/Output/67_V2D_K34.mat"
```

```
C2DI =ListContourPlot[V2DI,
```

```
ColorFunction->"DeepSeaColors",ContourStyle->Dashed, FrameLabel-> {"Y",
"Z"},ImageSize-> 400,AspectRatio-> 4]
```

```
C2DJ =ListContourPlot[V2DJ,
```

```
ColorFunction->"DeepSeaColors",ContourStyle->Dashed, FrameLabel->
{"X","Z"},ImageSize-> 400,AspectRatio-> 4]
```

C2DK

```
=ListContourPlot[V2DK,ColorFunction->"DeepSeaColors",ContourStyle->Dashed,
FrameLabel-> {"X","Y"},ImageSize-> 400, AspectRatio-> 1]
```

a4 =

```
Table[{{Efield67[[36]][[j]][[k]][[1]][[2]],Efield67[[36]][[j]][[k]][[1]][[3]]},{Efield67[[36]][[j]][[k]][[2]][[2]],Efield67[[36]][[j]][[k]][[2]][[3]]},{j,1,66},{k,1,66}}];
```

```
b4=Table[{{Efield67[[36]][[j]][[k]][[1]][[2]],Efield67[[36]][[j]][[k]][[1]][[3]]+67},{-1*Efield67[[36]][[j]][[k]][[2]][[2]],-1*Efield67[[36]][[j]][[k]][[2]][[3]]},{j,1,66},{k,1,66}}];
```

c4

```
=Table[{{Efield67[[36]][[j]][[k]][[1]][[2]],Efield67[[36]][[j]][[k]][[1]][[3]]+134},{Efield67[[36]][[j]][[k]][[2]][[2]],Efield67[[36]][[j]][[k]][[2]][[3]]},{j,1,66},{k,1,66}}];
```

d4 =

```
Table[{{Efield67[[36]][[j]][[k]][[1]][[2]],Efield67[[36]][[j]][[k]][[1]][[3]]+201},{-1*Efield67[[36]][[j]][[k]][[2]][[2]],-1*Efield67[[36]][[j]][[k]][[2]][[3]]},{j,1,66},{k,1,66}}];
```

aaa =

```
Table[{{Efield67[[i]][[36]][[k]][[1]][[1]],Efield67[[i]][[36]][[k]][[1]][[3]]},{Efield67[[i]][[36]][[k]][[2]][[1]],Efield67[[i]][[36]][[k]][[2]][[3]]},{i,1,66},{k,1,66}}];
```

```
bbb=Table[{{Efield67[[i]][[36]][[k]][[1]][[1]],Efield67[[i]][[36]][[k]][[1]][[3]]+67},{-1*Efield67[[i]][[36]][[k]][[2]][[1]],-1*Efield67[[i]][[36]][[k]][[2]][[3]]},{i,1,66},{k,1,66}}];
```

ccc

```
=Table[{{Efield67[[i]][[36]][[k]][[1]][[1]],Efield67[[i]][[36]][[k]][[1]][[3]]+134},{Efield67[[i]][[36]][[k]][[2]][[1]],Efield67[[i]][[36]][[k]][[2]][[3]]},{i,1,66},{k,1,66}}];
```

```

ddd =
Table[{{Efield67[[i]][[36]][[k]][[1]][[1]],Efield67[[i]][[36]][[k]][[1]][[3]]+201},{-
1*Efield67[[i]][[36]][[k]][[2]][[1]],-
1*Efield67[[i]][[36]][[k]][[2]][[3]]},{i,1,66},{k,1,66}];

efJ = Join[aaa,bbb,ccc,ddd];
efI = Join[a4,b4,c4,d4];
efk =
Table[{{Efield67[[i]][[j]][[34]][[1]][[1]],Efield67[[i]][[j]][[34]][[1]][[2]]},{Efield67[[i]][[j]][[34]][[2]][[1]],Efield67[[i]][[j]][[34]][[2]][[2]]},{i,1,66},{j,1,66}];

efI2=ListStreamPlot[efI,StreamColorFunction->"NeonColors",StreamStyle->Thick, FrameLabel-> {"Y","Z"}, AspectRatio-> 4, ImageSize -> 400]

efJ2
=ListStreamPlot[efJ,StreamColorFunction->"NeonColors",StreamStyle->Thick,FrameLabel-> {"X","Z"}, AspectRatio-> 4, ImageSize -> 400]

efK2=ListStreamPlot[efk,StreamColorFunction->"NeonColors",StreamStyle->Thick, FrameLabel-> {"X","Y"},AspectRatio-> 1, ImageSize -> 400]

Show[C2DI, efI2]
Show[C2DJ, efJ2]
Show[C2DK, efK2]

Export["/home/jkdale/Thesis/N=5/N57/Output/I34.png",C2DI]
Export["/home/jkdale/Thesis/N=5/N57/Output/J33.png",C2DJ]
Export["/home/jkdale/Thesis/N=5/N57/Output/K34.png",C2DK]
Export["/home/jkdale/Thesis/N=5/N57/Output/IE34.png",efI2]
Export["/home/jkdale/Thesis/N=5/N57/Output/JE33.png",efJ2]
Export["/home/jkdale/Thesis/N=5/N57/Output/KE34.png",efK2]
Export["/home/jkdale/Thesis/N=5/N57/Output/BI34.png",Show[C2DI, efI2]]

```

```
Export["/home/jkdale/Thesis/N=5/N57/Output/BJ33.png",Show[C2DJ, efJ2]]
```

```
Export["/home/jkdale/Thesis/N=5/N57/Output/BK342.png",Show[C2DK, efK2]]
```

```
(* 3D DATASET*) (* 3D DATASET*)(* 3D DATASET*)(* 3D DATASET*)(*
3D DATASET*)(* 3D DATASET*)(* 3D DATASET*)(* 3D DATASET*)
```

```
L = Join[a,b, c, d];
```

```
L>>"/home/jkdale/Thesis/N=5/N57/Output/67_Efield_Join.mat"
```

```
M = Join[e,f,g,h];
```

```
M >>"/home/jkdale/Thesis/N=5/N57/Output/67_Vpot_Join.mat"
```

```
<<"/home/jkdale/Thesis/N=5/N57/Output/67_Efield_Join.mat"
```

```
<<"/home/jkdale/Thesis/N=5/N57/Output/67_Vpot_Join.mat"
```

```
Dimensions[Ejoin67]
```

```
Dimensions[Vjoin67]
```

```
PP=ListVectorPlot3D[Ejoin67, AxesLabel→ {"X","Y","Z"}, Axes→ {True, False,
True}, Boxed→ False, BoxRatios→ {.4,1,4}, VectorScale→ Small, (*VectorColorFunction
→ "DeepSeaColors",*)VectorPoints→ {10,10,67}, ImageSize→ 400]
```

```
Q =ListContourPlot3D[Vjoin67,ContourStyle→ Opacity[0.03], ColorFunction→
"SunsetColors", Contours→ 300,Boxed→ False,Mesh→ None, Axes→ {True, False, True},
AxesLabel→ {"X","Y","Z"},BoxRatios→ {.4,1,4} , ImageSize→ 400]
```

```
Show[PP,Q, Rib, Rib2, Rib3, Rib4]
```

```
Show[Q, Rib, Rib2, Rib3, Rib4]
```

```
Show[PP, Rib, Rib2, Rib3, Rib4]
```

```
Export["/home/jkdale/Thesis/N=5/N57/Output/67Efield.png",Show[PP]]
```

```
Export["/home/jkdale/Thesis/N=5/N57/Output/67VCont.png",Show[Q]]
```

Export["/home/jkdale/Thesis/N=5/N57/Output/67E&R.png",Show[PP,Rib, Rib2,
Rib3, Rib4]]

Export["/home/jkdale/Thesis/N=5/N57/Output/67C&R.png",Show[Q, Rib, Rib2,
Rib3, Rib4]]

Export["/home/jkdale/Thesis/N=5/N57/Output/67All.png",Show[PP,Q, Rib, Rib2,
Rib3, Rib4]]

APPENDIX F
CALCULATED RHO (P) VALUES FROM GIVEN FERMION
PROBABILITIES.

<u>acGNR8 ρ Values</u>	
Dataset 1	0.02599506187566887, 0.09181686914811862, 0.16666666666666635, 0.2155214023095454, 0.2155214023095458, 0.16666666666666696, 0.09181686914811915, 0.025995061875669113
Dataset 41	0.025995061875669304, 0.09181686914811957, 0.16666666666666671, 0.21552140230954528, 0.2155214023095457, 0.166666666666666596, 0.09181686914811867, 0.02599506187566893

Dataset 81	0.025995061875669256, 0.0918168691481191, 0.16666666666666682, 0.21552140230954564, 0.21552140230954525, 0.16666666666666657, 0.09181686914811876, 0.025995061875669034
Dataset 121	0.02599506187566914, 0.09181686914811926, 0.16666666666666755, 0.21552140230954608, 0.21552140230954522, 0.16666666666666596, 0.09181686914811818, 0.02599506187566894
Dataset 161	0.025995061875669842, 0.09181686914812083, 0.16666666666666896, 0.21552140230954592, 0.21552140230954447, 0.16666666666666643, 0.09181686914811701, 0.025995061875668482

Dataset 201	0.02599506187566986, 0.09181686914812087, 0.16666666666666868, 0.21552140230954636, 0.21552140230954547, 0.16666666666666427, 0.09181686914811601, 0.025995061875667996
-------------	--

Table F1 - N=8 Calculated Rho Values – This table shows the unique ρ values used to calculate the potentials and the field lines.

<u>acGNR5 ρ Values</u>	
Dataset 1	0.2440934700590991, 0.2538018427644523, 1.2396576538570847*10 ⁻⁸ , 0.25595087934816363, 0.24615379543170846
Dataset 2	0.24661223178846572, 0.2533575229139936, 1.0719882249378084*10 ⁻⁷ , 0.25324070572563334, 0.24678943237308476
Dataset 3	0.246805772087055, 0.2535912571939378,

	4.143083154085276*10 ⁻⁷ , 0.25287642583515113, 0.24672613057554033
Dataset 4	0.246185, 0.2533317467170475, 3.284342581334505*10 ⁻⁸ , 0.25375918559809657, 0.2467241764592481
Dataset 5	0.2468055480210266, 0.253861957845413, 9.046884173404786*10 ⁻⁷ , 0.2527136070496206, 0.24661798239552246
Dataset 6	0.250082229246683, 0.25205536323516947, 1.990616704563155*10 ⁻⁸ , 0.249909489167656, 0.24795289844432453
Dataset 7	0.247986734498357, 0.2525295211809991, 5.719688545090018*10 ⁻⁸ , 0.25210531017401683, 0.24737837694974155

Table F2 - N=5 Calculated Rho Values – This table shows the unique ρ values used to calculate the potentials and the field lines.

BIBLIOGRAPHY

- "MECHANICAL ENGINEERING: A Complete Online Guide For Every Mechanical Engineer," [Online]. Available: <http://www.mechanicalengineeringblog.com/tag/graphene-vs-silicon/>. [Accessed 3 March 2013].
- Palmer, "How and Why: Graphene seems valuable for computers, batteries and other uses," 25 October 2010. [Online]. Available: <http://www.washingtonpost.com/wp-dyn/content/article/2010/10/25/AR2010102503505.html>. [Accessed 15 11 2012].
- "Graphite," Amethyst Galleries, Inc., [Online]. Available: <http://www.galleries.com/Graphite>. [Accessed 12 January 2013].
- L. Sherriff, "What is graphene?," 6 June 2011. [Online]. Available: <http://www.zdnet.com/what-is-graphene-3040092971/>. [Accessed 7 October 2012].
- D. Andersen and R. Hassan, "Plasmon dispersion in semimetallic armchair graphene nanoribbons," *Department of Electrical and Computer Engineering The University of Iowa, Iowa City, IA 52242, USA*, 2012.
- D. R. Andersen and R. Hassan, "Collective modes of massive Dirac fermions in armchair graphene nanoribbons," *Journal Of Physics: Condensed Matter*, vol. 25, no. 045303, pp. 1-4, 2012.
- A. J. Leggett, "Cuprate Superconductivity: The Current State Of Play," 2010. [Online]. Available: <http://media.iqc.ca/lectures/Leggett-2010/notes/lecture-12.pdf>. [Accessed 12 February 2013].
- "The Free Dictionary," [Online]. Available: <http://www.thefreedictionary.com/charge+densities>. [Accessed 30 October 2012].
- "Electric Field," 7 July 1999. [Online]. Available: <http://physics.bu.edu/~duffy/PY106/Electricfield.html>. [Accessed 30 October 2012].
- "The Particle Adventure: The Fundamentals of Matter and Force," [Online].

- 10] Available: <http://www.particleadventure.org/fermibos.html>. [Accessed 7 January 2013].
- J. O. Smith, "Physical Audio Signal Processing," W3K Publishing, 2010.
- 11]
- "Planet Math.Org," [Online]. Available:
- 12] <http://planetmath.org/search/site/matrix%20complex%20conjugate>. [Accessed 16 February 2013].
- "Physics-Help Info," [Online]. Available: http://physics-help.info/physicsguide/appendices/si_units.shtml. [Accessed 15 October 2012].
- 13]
- K. E. Lonngren, S. V. Savov and R. J. Jost, Fundamentals of
- 14] Electromagnetics with MATLAB, Raleigh: SciTech, 2007.
- "Electric Potential: Voltage," [Online]. Available:
- 15] <http://faculty.wvu.edu/vawter/PhysicsNet/Topics/ElectricPotential/Potential.html>. [Accessed 26 October 2012].
- "Wolfram Mathematica Home Page," [Online]. Available:
- 16] <http://www.wolfram.com/mathematica/>. [Accessed 10 February 2012].
- J. H. a. K. K. F. Mathews, "Numerical Methods Using Matlab, 4th Edition,
- 17] 2004," Prentice Hall, Upper Saddle River, 2004.
- "Permittivity," [Online]. Available:
- 18] <http://www.britannica.com/EBchecked/topic/452314/permittivity> .
- K. S. Novoselov, A. K. Geim, S. V. Morozov and D. Jiang, "Electric Field
- 19] Effect in Atomically Thin Carbon Films," *Science*, vol. 306, pp. 666-669, 2004.
- "Brillouin Zones," [Online]. Available:
- 20] <http://www.phy.iitb.ac.in/~tomy/brillouin.pdf>. [Accessed 1 February 2013].
- C. A. H. Neto, F. Guinea, N. M. R. Peres and K. S. a. A. K. G. Novoselov,
- 21] "The electronic properties of graphene," *REVIEWS OF MODERN PHYSICS*, vol.

81, 2009.

22] "Mathematica edition 7," Wolfram, Champaign, 2013.